1-1-2013

Meta-Heuristic Optimization of Antennas for Biomedical Applications

Aaron Zachary Hood

Meta-heuristic optimization of antennas for biomedical applications

By

Aaron Zachary Hood

A Dissertation
Submitted to the Faculty of
Mississippi State University
in Partial Fulfillment of the Requirements
for the Degree of Doctor of Philosophy
in Electrical and Computer Engineering
in the Department of Electrical and Computer Engineering

Mississippi State, Mississippi

December 2013

Meta-heuristic optimization of antennas for biomedical applications

By

Aaron Zachary Hood

Approved:

_____

Erdem Topsakal
(Major Professor)

_____

J. Patrick Donohoe
(Committee Member)

_____

Burak Eksioglu
(Committee Member)

_____

Pan Li
(Committee Member)

_____

James E. Fowler
(Graduate Coordinator)

_____

Achille Messac
Dean
James Worth Bagley College of Engineering

Name: Aaron Zachary Hood

Date of Degree: December 14, 2013

Institution: Mississippi State University

Major Field: Electrical and Computer Engineering

Major Professor: Erdem Topsakal

Title of Study: Meta-heuristic optimization of antennas for biomedical applications

Pages in Study: 159

Candidate for Degree of Doctor of Philosophy

Given the proper conditions, antennas applied in medicine can offer improved quality of life to patients. However the human body proves hostile to typical, analytical antenna design techniques as it is composed entirely of frequency- and temperature-dependent lossy media. By combining optimization techniques with numerical methods, many of these challenges may be overcome. Particle swarm optimization (PSO) models the solution process after the natural movement of groups such as swarms of bees as they search for food sources. This meta-heuristic procedure has proven adept at overcoming many challenging problems in the electromagnetics literature. Therefore, this dissertation explores PSO and some of its variants in the solution of two biomedical antenna problems.

Recent advances in biosensor technology have led to miniaturized devices that are suitable for *in vivo* operation. While these sensors hold great promise for medical treatment, they demand a wireless installation for maximum patient benefit, which in turn demands quite specific antenna requirements. The antennas must be composed of biocompatible materials, and must be very small (no more than a few square centimeters)

to minimize invasiveness. Here PSO is applied to design a 22.5 mm × 22.5 mm × 2.5 mm implantable serpentine planar inverted-F antenna for dual-band MedRadio and ISM operation. Measurements reveal the accuracy of the models.

Hyperthermia is the process of elevating a patient's temperature for therapeutic gain. Since the ancient Egyptians, physicians have employed hyperthermia in the destruction of cancerous tumors. Modern implementations typically apply electromagnetic radiation at radio and microwave frequencies to induce local or regional heating. In this dissertation PSO is used to evaluate candidate antennas for inclusion in an array of antennas with the aim of local adjuvant hyperthermia for breast cancer treatment. The near-field of the array is then optimized to induce a uniform specific absorption rate throughout the breast.

DEDICATION

To my longsuffering wife and to my parents who always let me assume I could accomplish anything

ACKNOWLEDGEMENTS

I believe that many advisors would not wait eight years for a student to complete a single dissertation, so I would like to first thank Dr. Erdem Topsakal for his patience and encouragement on this journey.

Though we have not spoken in several years, I was constantly reminded during the compilation of this dissertation of the contributions that Tutku Karaçolak made to our collaboration, and I am deeply appreciative of his assistance.

I would also like to thank Dr. J. Patrick Donohoe, Dr. Burak Eksioglu, and Dr. Pan Li for serving on my committee.

Finally, I must acknowledge the enormous support of my family: my wife, Brandy, who allowed me to pursue this goal without worrying too much about where we end up; my father, Harry, who never let me get overstressed; my mother, Sandra, who gave up countless hours watching my daughter in the hope that I might someday complete this work; and my beautiful baby girl, Fiona, who provided enough distraction to remind me that I needed to finish my work, so that I can always be available for distraction.

TABLE OF CONTENTS

LIST OF TABLES

LIST OF FIGURES

CHAPTER I

INTRODUCTION

1.1 A Brief Overview

For several decades scientists have sought methods that allow more direct observations and manipulations inside live bodies. Electromagnetics has played an essential role in medicine for many years, and current advances point to promising solutions for these problems. Radio frequency waves enable communication with implanted sensors to permit real-time monitoring. Similarly, directed radio frequency waves can alter physiological mechanisms by disrupting normal electrical signals and by heating exposed tissue. In this paper, I explore the antennas that enable these therapeutic technologies.

1.2 Electromagnetics in Medicine

Technologies with fundamental roots in electromagnetics have been applied in many areas of medicine including imaging, tissue dissection, monitoring, and therapy. Two growing areas of interest are implantable medical devices and adjuvant hyperthermia for cancer treatment. Both of these applications benefit from well-designed antennas.

1.2.1 Implantable Medical Devices

Implantable medical devices (IMDs) offer great promise in an array of applications, but possess the distinct disadvantage of being implanted inside the body. Each access to retrieve data or modify functionality requires invasive surgeries that greatly increase the inconvenience, discomfort, and risk to the subject. Therefore, techniques that rely on IMDs must include some noninvasive means of data in- and exfiltration. Electromagnetics has a long history in medicine and offers the obvious solution here – a wireless link. In the earliest years of the research, sophisticated radio electronics occupied too much volume for long-term implantation, so simple antenna configurations were necessary. Since the late 1950s, IMDs have relied on inductive coupling, which requires very short distances (less than 10 cm) and only permits very low data rates [1], [2]. In 1999, the United States Federal Communications Commission (FCC) allocated spectrum for the Medical Implant Communication Service (MICS) band, which sets rules regarding radio communication with IMDs [3]. The regulations allow greater range of up to a few meters. Coupled with the unyielding march to miniaturization of electronics, this has opened new avenues for advanced implant communication to support increasing telemetry requirements. As early as 2004, papers describing implantable patch antennas begin to appear [4], [5]. Patch antennas have an advantage for implantation as the ground plane reduces undesirable radiation towards the body. The unique dielectric properties of living tissue create interesting problems for antenna design, and regulations governing live testing make frequent *in vivo* measurements impractical. Therefore, many researchers have expended significant effort to create realistic models. In 1996, scientists with the Air Force Research Laboratory

published measurements of the dielectric properties of human tissue over a large spectrum [6]-[8]. While this resource provides valuable information for developing models, barriers to human testing remain high, so it is important to understand the properties of typical laboratory animals as well. To this end, the electromagnetics research group at Mississippi State University (MSU) performed measurements of rat skin in 2008 and created tissue-mimicking materials for prototyping [9]-[11]. Availability of these resources and publications has allowed vast improvement over early work in the field.

1.2.2 Therapeutic Hyperthermia

Electromagnetics offers another therapeutic use in radiation hyperthermia, which theoretically allows noninvasive, targeted destruction by elevated temperature of cancerous growths. Three basic types of hyperthermia (or thermotherapy) exist: local, regional, and whole-body [12]-[14]. Local hyperthermia heats a small group of cells by carefully directing energy, while regional hyperthermia heats a large portion of the body. Both varieties generally deposit energy into tumors via antennas operating at radio or microwave frequencies placed in, on, or near the tumor. Typically used in treatment of metastatic cancers, whole-body hyperthermia (WBH) raises the temperature of the entire body; commercial systems such as the Aquatherm and IRATHERM®2000 employ water and infrared radiation in this task [12], [14]. According to [13], hyperthermia as a tumor treatment first appears circa 3000 BCE in the *Edwin Smith Papyrus* [15]. While less toxic than radiotherapy or chemotherapy, the other benefits of hyperthermia alone pale in comparison to those better known treatments [14]. However, many studies have found that adjuvant thermotherapy greatly enhances the cytotoxicity of both radio- and

chemotherapy [14], [16] in cancers of the bladder [17]-[21], blood [22], brain [23], [24], breast [25]-[34], cervix [18], [35]-[37], connective tissue [38], head/neck [39], lung [40], prostate [41], rectum [18], [42], skin [43], [44], and vagina [45]. The earliest clinical applications of hyperthermia with radiotherapy date to 1910 by Müller [46] according to [44] or Warren in 1935 [47] according to [13]. Despite extensive clinical experience and numerical modeling [48]-[56], uniform regional heating remains elusive [44]. Therefore, more antenna arrangements must be studied to improve treatment by local and regional hyperthermia.

1.3 Optimization in Electromagnetics

Given the complexities of the antennas involved and heavy reliance on numerical methods, these problems benefit greatly from optimization procedures. Many methods exist, but a few that have proven useful in electromagnetics literature for generalized antenna problems are genetic algorithms (GA) and particle swarm optimization (PSO) [57]-[61]. Based on Mendelian genetics, GA incorporates principles such as selection, crossover, and mutation. PSO mimics the behavior of groups of animals like bees, birds, and fish as they work toward a common goal.

Many variations of these heuristics have shown improvement over the standard implementations, but authors in the electromagnetics literature tend to overlook their efficacy [61]-[65]. This paper proposes a more thorough exploration of optimization in refining solutions to the problems described above. Improvements in implantable antennas require further miniaturization while maintaining or increasing performance. A successful hyperthermia optimization will create an array with uniform near-field heating throughout the female breast.

1.4 Organization of the Dissertation

The dissertation begins with a review of the pertinent motivations and concepts, and follows those with two applications of optimization in biomedical antenna design. Chapter II describes the relevant background of electromagnetics in implantable medical devices and adjuvant cancer therapies. Chapter III reviews a few optimization techniques often found in the literature, and explains the methods as implemented for use in this project. Chapter IV presents an optimized implantable antenna with dual-band characteristics, and Chapter V demonstrates the application of PSO in hyperthermia treatment.

CHAPTER II

REVIEW OF ELECTROMAGNETICS IN MEDICINE

One of the most common applications of electromagnetics in medicine is the use of antennas to interact with the human body. Antennas may act in the relay of data from devices that are implanted to assist patients, or the antenna's response to a patient may be the primary interface as in the case of imaging. This chapter explores the motivation for optimizing antennas to improve the capabilities of IMDs and to assist in treating cancer.

2.1 Implantable Antennas

Medical practitioners have long recognized the potential benefits of implanted devices. One of the earliest implants deployed on a large scale is the artificial cardiac pacemaker. In their infancy, pacemakers were large, tabletop contraptions that used a standard wall outlet to provide transcutaneous pacing [66]. Development of the silicon transistor enabled shrinking designs, and in 1958, a Swedish team installed the first fully implantable pacemaker in a human [67]. This device employed an internal coil that inductively coupled with an external coil to recharge batteries and provide communication. Conceived of in the late 1960s, surgeons implanted the first automatic implantable cardioverter defibrillator (AICD) in February 1980 [68]. Even today communication between the AICD and external programmer/recorder/monitor (PRM) unit occurs via an inductive link established from the PRM wand's coil and the AICD's

internal coil. Many modern applications continue to rely on resonant inductive coupling. In [69], engineers from the University of Michigan consider the feasibility of a "stentenna" for implant monitoring in 2003. The authors use micro electro-discharge machining (μDEM) to form a lattice from 50 μm thick planar steel foil, which is then threaded with a deflated angioplasty balloon. On balloon inflation, the lattice breaks strategically to form a 20 nH resonant inductive coil that is 4 mm long with a 3.5 mm diameter. By integrating this "stentenna" with a micromachined pressure sensor, the authors are able to analytically and experimentally correlate changes in liquid pressure in a testing tank. In [70]-[72], NASA scientists investigate an implantable 1mm x 1mm square spiral chip antenna on high resistivity silicon (HR-Si) for monitoring astronauts' physiology during space flight. From approximately 200-700 MHz, the authors find a maximum operational range of 5-10 cm. A group from the University of Tokyo presents an implantable capsule to monitor cardiac behavior in [73]. The authors choose a coil with 6 mm diameter and 5 mm length to communicate at 80 MHz. Even at such a low frequency the implant can only reliably transmit data approximately 4 cm when submerged in water. Since the dielectric properties of plain water vary significantly from some tissue, range would likely suffer with implantation of the capsule. As recently as 2009, [74] presents a 4 mm x 5 mm spiral chip radiator on fused silica operating at 200 MHz. Even though this structure is larger than similar devices, it only demonstrates acceptable transmission up to 20 cm. From the preceding results, a limitation of inductive coupling begins to emerge. Since the primary mechanism for these links is near-field magnetic coupling, their range is limited in experiments to 10-20 cm, and in practice, the external coils often require direct skin contact. This lack of range effectively

tethers patients to their monitoring equipment, and while most find inconvenience superior to death, the confluence of updated spectrum regulation and continual miniaturization of electronic components has enabled opportunities for more sophisticated implants with enhanced capabilities and range.

In 1999, the FCC allocated spectrum from 402-405 MHz for the MICS band to enable and govern radio communication with implants. Devices may occupy 300 kHz at any given time, and must not exceed an effective isotropic radiated power of 25 μW [3]. By using this band, devices gain increased communication range, and, therefore, remove some of the tethered equipment that restricts patients' mobility. Research regarding implanted antennas for MICS operation begins to appear in 2003. Kim and Rahmat-Samii explore the performance of a MICS dipole inside a human head modeled as a sphere [75]. The first patch antennas for medical implant telemetry appear in [4] and [5]. In these papers, the authors compare spiral and serpentine antennas tuned for 402 MHz resonant frequencies, and also address design challenges rising from environmental and material dielectric properties. These issues drive the design because the close contact between tissue and antenna significantly impacts communication. In 1996, Gabriel and Gabriel published a series of papers describing the measured dielectric properties of human and animal tissues across ten frequency decades from 10 Hz to 20 GHz, and showed that the complex permittivity of each tissue is frequency dependent but largely species independent [6]-[8]. Figure 2.1 compares the properties of fatty breast tissue to vitreous humor. Therefore, each antenna design must account for the varying environmental factors across its active bandwidth. To minimize the formation of scar tissue, biocompatible materials (or biomaterials) must constitute any antenna surface in

direct contact with tissue [76]. This often means silicone or some other relatively flexible biomaterial must coat the entire IMD. Soontornpipit, Furse, and Chung target MICS band antennas that can fit on a pacemaker battery and take advantage of its metallization by using it as the antenna's ground [4]. The authors explore a spiral and serpentine planar inverted-F antenna configurations (Figure 2.2) occupying an area of 16.8 mm x 26.6 mm with a variety of sub- and superstrate materials and thicknesses; feed and grounding locations; and non-uniform superstrates. To simplify simulation and measurement, the antenna is embedded in a mimicking material with two-thirds the complex permittivity of muscle. Their conclusions suggest choosing biocompatible sub- and superstrates with large permittivity and low conductivity. Kim and Rahmat-Samii also present 24 mm x 16 mm spiral planar inverted-F antennas (PIFA) in [5].

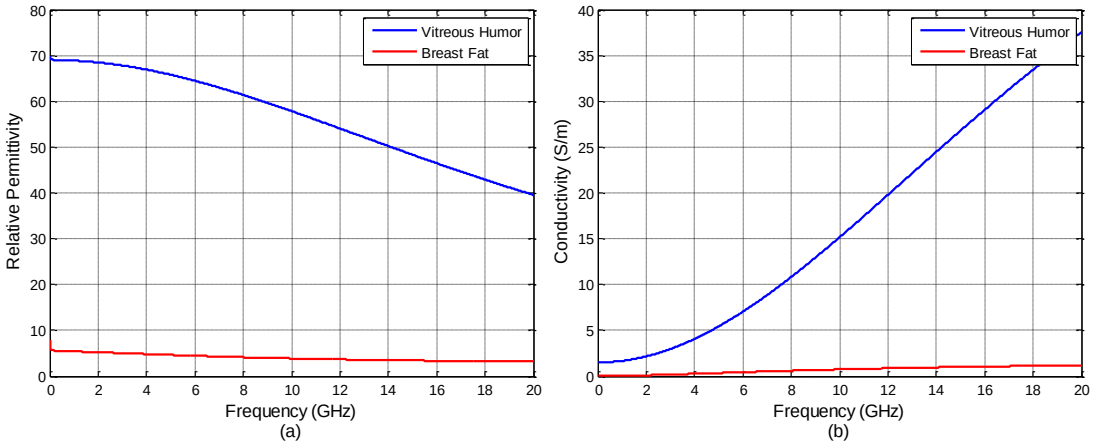

Figure 2.1 Dielectric Properties of Vitreous Humor and Breast Fat

(a) Relative Permittivity as measured in [6]-[8]
(b) Conductivity as measured in [6]-[8]

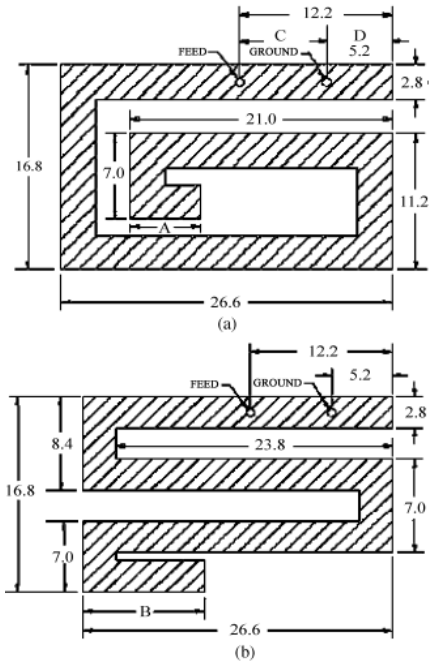

Figure 2.2 PIFA Configurations Reported in [4]

(a) Spiral
(b) Serpentine

2.2 Hyperthermia

Hyperthermia (sometimes called thermotherapy) is the process of elevating a patient's temperature for therapeutic gain. Since the ancient Egyptians [15], physicians have often employed hyperthermia in the destruction of cancerous tumors. Modern implementations of hyperthermia typically use electromagnetic radiation at radio and microwave frequencies to induce local or regional heating. Local hyperthermia encompasses both interstitial and surface treatments that only heat the tumor; regional hyperthermia targets a larger section of the body such as the arm, pelvis, abdomen, or breast. For interstitial applications, antenna probes are inserted into the tumor. Both surface and regional heating typically deposit energy through a waveguide, horn, spiral patch, current sheet, or phased array coupled to the patient through a water bolus [12],

[14]. The commercially available Sigma-60 and Sigma-Eye applicators of the BSD-2000 system employ arrays of 8 or 24 dipoles, respectively, to allow phase-steering to position the beam in three dimensions [12], [14]. Documented EM-induced hyperthermia systems operate from 10-2450 MHz with the most commonly used frequencies residing in the 433 and 915 MHz ISM bands [12], [13], [19], [20], [25], [26], [27], [42], [86], [87], [88], [89], [90]. Applied power ranges from 0-2,100 W [42], [90] to achieve target temperatures of 39-45 °C [12], [14].

During the early twentieth century, scientists discovered that adjuvant application of thermotherapy enhances the efficacy of conventional radiotherapy [46], [47]. A range of more recent studies has confirmed this behavior and shown that hyperthermia also improves patients' response to chemotherapy for a variety of cancers [17]-[45]. The Dutch Deep Hyperthermia Trial (DDHT) represents one of the most successful thermotherapy experiments to date [18], [36]. Between 1990 and 1996, researchers randomly assigned 114 women with locoregionally advanced cervical carcinoma to groups receiving radiotherapy (RT) alone or RT combined with hyperthermia (RT+HT). Three-year local control rates of 41% for RT alone improved to 61% with the addition of HT. After 12 years, patients who received RT+HT showed local control of 56% and survival of 37% compared to 37% and 20% for RT alone. These results have prompted many institutes to recommend RT+HT as the standard treatment for cervical carcinoma [36]. Adjuvant HT also shows promise for treating breast cancer (the second leading cause of cancer death for women in the United States [91], [92]). From 1984 to 1987, physicians at Henry Ford Hospital treated 30 patients with recurrent breast carcinoma using a regimen of HT and low-dose RT [25]. After each twice-weekly RT session,

patients received 60 minutes of 43 °C HT from 200-700 MHz sources. The authors report a 57% complete response (CR) and 36% partial response (PR). From 1992 to 1998, 25 patients with inoperable breast cancer received daily RT and weekly HT combined with chemotherapy (CT) at the Medical University of Lübeck [30]. HT was applied with BSD-500 and 2000 systems with standard 43 °C, 60 minute targets. This triple-modality therapy achieved 44% CR and 80% remission rate. [26] presents the combined results of five European and Canadian clinical trials involving 306 patients treated with RT or RT+HT. Although the exact methods varied among facilities, 41% of RT alone and 59% of RT+HT patients achieved CR. 27 patients at Duke University Medical Center received RT and CT combined with HT to treat recurrent breast cancer between 1994 and 2007 [26]. From the group of 20 patients that returned for their 1 month follow-up, 80% showed CR, and 20% had PR. Only four patients presented with disease progression or recurrence after one year.

Based on these and many other studies, scientists have learned that HT acts on a number of mechanisms to defeat tumors. Above 43 °C HT induces apoptosis and necrosis, directly killing cells [16]. Unfortunately, these temperatures are difficult to reach and isolate from surrounding healthy tissue. Due to complex internal vasculature, tumors often have hypoxic regions. Moderate HT (temperatures between 40.5 and 43 °C) increases tumor perfusion, which increases oxygenation. These conditions lead to chemo- and radiosensitization, respectively; therefore, HT indirectly enhances the cytotoxicity of CT and RT [14], [16], [27], [28], [31], [93]. While HT does benefit CT and RT, it can also hinder their efficacy. Exposure to HT activates heat shock proteins

(HSPs) and induces thermotolerance for 60-100 hours depending on the dose. As a result, daily HT has no benefit [16], [93]. Figure 2.3 summarizes these findings.

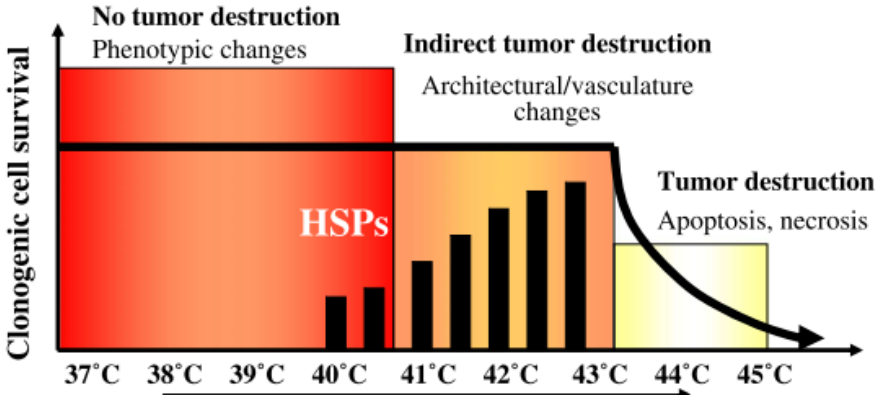

Figure 2.3 Cytotoxic Effects of Hyperthermia [16]

CHAPTER III

OPTIMIZATION REVIEW AND IMPLEMENTATION

Optimization is the search for perfection in the solution of a problem. Unfortunately very few problems with perfect solutions exist in engineering, and tradeoffs must be analyzed to find the *best* solution given a set of constraints. While this *best* solution might be found by manually changing parameters and observing the response (a brute-force trial-and-error approach), a well-defined optimization routine can autonomously perform an intelligent search of the available solutions and present the best candidate upon completion. Since analytical representations of most antennas are difficult to derive with many antennas lacking any formal solution, modeling and simulation are required to estimate a structure's performance before fabrication. With little guidance available for some antennas, determining physical dimensions becomes a matter of trial-and-error, or a problem ideally suited to optimization.

3.1 Review of Optimization

Before discussing specific optimization techniques and applications, it is important to understand the general optimization procedure and terminology. An *objective function* defines the goal of any optimization. The objective function is problem dependent and usually involves the minimization or maximization of some *fitness* function. The fitness function value indicates how closely correlated the current

solution is to the desired solution. One or more parameters compose each problem with each combination of parameters defining a point in the *solution space* – the collection of all possible solutions. An example of a general maximization problem is written as

$$\text{Objective:} \quad \max\big(f(x_i)\big) \qquad i = 1,2,3,\dots,N \tag{3.1}$$

$$\text{Subject to:} \quad a_i < x_i < b_i \quad i = 1,2,3,\dots,N \tag{3.2}$$

where the fitness function, $f(x_i)$, is an arbitrary function of N variables, x_i, bounded by constants a_i and b_i. For a well-known function with a small value of N, this problem is easily solved using basic algebra; even objective functions with many variables can be efficiently solved using a problem-specific heuristic for a well-known function. The expression for the bandwidth, return loss, or any other measure of an antenna is rarely simple and almost never well-known though. Therefore, meta-heuristic optimization methods combined with full-wave simulations are employed to find the best solution available in the restricted search space. While typically orders of magnitude less efficient than problem-specific heuristics, meta-heuristics offer the flexibility and adaptability necessary to solve a wide range of general problems without enumerating all parametric combinations.

While many classes of optimization techniques exist, the most common methods applied to electromagnetics belong to the family of evolutionary algorithms (EAs) and swarm algorithms. These meta-heuristics derive their behavior from natural processes where *good* solutions propagate through the problem and *bad* solutions are abandoned as soon as their fitness is found lacking – survival of the fittest. The mechanisms employed in the determination of the fittest solution vary widely. The remainder of this chapter

discusses the two most prominent methods used in electromagnetics – genetic algorithms and particle swarm optimization.

3.1.1 Genetic Algorithms

Inspired by evolution, nature's optimization routine, genetic algorithms (GA) are perhaps the most literal interpretation of EA. Formally introduced by John Holland at the University of Michigan in the early 1970s, GA imitates the process of biological evolution with steps including reproduction, crossover, and mutation [94]. For over ten years, the electromagnetics community has applied GA to a number of complex problems including patch antenna topology design, broadband absorber design, antenna array beam forming, and side lobe level reduction [95]-[97].

In the simplest case, three procedures comprise a GA: population generation, fitness evaluation, and reproduction. While this may seem simple, each step requires significant computation, particularly reproduction which typically contains a minimum of three complex processes: selection, crossover, and mutation. Since GA borrows its behavior from biology, it also adopts the terminology. The *population* is a group of trial solutions with each possible solution known as a *chromosome*, which is a concatenation of optimization parameters or *genes*. Rather than operating on real-valued parameters, GA's typically map genes to binary-coded strings. By coding the chromosome **x** as suggested in [96] as

$$\begin{aligned} \mathrm{p} &= \{g_j \mid j = 1,2,3,\ldots,N_{gl}\} \\ &= \overbrace{g_1 g_1 \cdots g_{N_1}}^{x_1} \overbrace{g_{N_1+1} g_{N_1+2} \cdots g_{N_2}}^{x_2} \cdots \overbrace{g_{N_{N_x-1}+1} g_{N_{N_x-1}+2} \cdots g_{N_{N_x}}}^{x_{N_x}} \end{aligned} \tag{3.3}$$

where $N_{gl} \equiv N_{N_x}$ is the genetic length, x_l are independent genes, and $g_j \in \{0,1\}$, each gene may be decoded by

$$x_l = x_l^{\min} + 2^{-N_{l-1}} \frac{x_l^{\max} - x_l^{\min}}{2^{N_l - N_{l-1}} - 1} \sum_{j-N_{l-1}+1}^{N_l} g_j 2^{j-1} \tag{3.4}$$

which assumes coding by least significant bit first. The initial population may either be randomly generated or intentionally seeded if good approximations are known prior to beginning the search. Once the initial population is generated and its fitness evaluated, *reproduction* begins. A *selection* procedure chooses a pair of chromosomes as *parents* for the new *generation* and inserts them into the new population. Next a *crossover* operator blends the genetic information of the parents with a predefined probability. Finally, *mutation* randomly changes the genes of some *children*. Breeding continues until the new population reaches the same size as the previous generation and replaces it. Iterations continue until the results satisfy the termination criteria. For GA this may be a fixed number of iterations, population convergence, or a "good enough" condition.

The selection algorithm chooses mating chromosomes to form the next generation and is the only step in GA directly influenced by the fitness function. Rather than employing a greedy strategy and only selecting the fittest parents, GA generally uses one of three techniques that ensure relatively unfit individuals have some chance to contribute to the gene pool: population decimation, proportionate selection, or tournament selection [97].

Of the three methods listed, only population decimation falls into the deterministic category. The selection routine ranks each candidate according to its fitness

and removes any members of the population below the desired threshold. Random pairs then combine as parents to fill the new generation. While the simplicity of this strategy makes it attractive, it has a near-fatal flaw. By only considering the members for removal based on overall fitness, the procedure also eliminates any unique traits that individual might have possessed from the gene pool; only a random mutation can recover this lost information later in the optimization. This removal usually occurs too early in the optimization to determine the value of independent traits, so this selection algorithm proves unsuitable for global exploration.

To avoid the deficiencies of the deterministic population decimation, most GAs implement stochastic selection procedures to keep all genetic variations in the pool. Proportionate selection, often referred to and visualized as roulette wheel selection, chooses breeders based on their probability, with each individual's probability defined as its fitness divided by the population's total fitness. The routine maps each chromosome to an appropriate portion of the number space between zero and 1, and randomly fills the next generation. While highly fit individuals still propagate through the problem most often, less fit chromosomes may still participate in the process. This finite probability allows the gene pool to retain all of the traits generated throughout the optimization for greater diversity. Since this method lacks the greed of population decimation, it may require more generations to converge, but it explores more of the solution space.

As a compromise between population decimation and proportionate selection, tournament selection randomly segregates a sub-population of N chromosomes to do battle. The individual who wins the competition by having the best fitness earns a place in the new generation. All candidates then return to the population to for a chance at

reselection. This technique should converge faster than proportionate selection since the probability of choosing the least fit member is zero for all $N > 1$. The most commonly implemented procedure, binary tournament selection ($N = 2$), gives a greater probability of selecting less fit individuals than variants with higher values of N. Of the three procedures described, tournament selection most nearly mimics nature.

GA defines the primary mechanism of solution space exploration in several variations of the crossover operator including one-point and two-point. Both of these operators achieve the same goal with varying degrees of efficiency: mix the parents' genes to create new traits. To test the quality of unmodified chromosomes through multiple generations, crossover only occurs according to a user-defined probability with an experimentally determined optimal value of 0.6 – 0.8 [97]. As the simplest method, one-point crossover selects a random position within the parents and forms one child by combining the first portion of the first parent with the second portion of the second parent. The remaining sections then join to form a second child. Unfortunately, alleles at the ends of the parents can never remain together in the single-point method. To overcome this disadvantage, two-point crossover fixes two positions in the parent chromosomes, and exchanges the central information to create two children.

Since selection generally favors the fittest individuals and crossover only operates on chunks of these chromosomes, GA largely ignores slight variations in the genetic code that lead to improbably good objective values. To alleviate this issue, the mutation operator randomly selects a single allele from a child immediately following crossover and replaces it with its complement. In a typical binary-coded GA, complementing an allele simply means changing the value of a "0" to "1" or "1" to "0." Applying mutation

to the entirety of the population during all iterations would negate the convergent nature of searching, so the procedure optimally occurs only on 1% to 10% of the chromosomes [97].

3.1.2 Particle Swarm Optimization

By observing the natural phenomenon known as swarm intelligence, James Kennedy and Russell C. Eberhart derived a novel optimization technique, which they introduced as particle swarm optimization (PSO) in 1995 [98]. While sometimes classified as an EA, basic PSO takes advantage of an evolved hive mind more than the direct Darwinian evolution as GA does. Exhibited by colonies of bees, schools of fish, flocks of birds, and even gamblers at a horse race [99], swarm intelligence allows groups of individuals to move and react as a single organism. As a demonstration of this principle, biologists Thomas Seeley and Susannah Buhrman of Cornell University arranged nesting boxes of variable quality to emulate tree cavities, the ideal honey bee dwelling, on an island void of suitable natural homes. They then released a colony of about 4,000 bees and carefully observed the hive selection process. While most of the swarm remained behind, several scouts immediately set out in search of potential sties, and upon finding one judged its fitness based on at least six criteria: "cavity volume; entrance size, height, direction, and proximity to the cavity floor; and presence of combs [from previous colonies] in the cavity" [100]. Each scout returned to the waiting colony and performed a waggle-dance to report its findings; more enthusiastic dancing indicated a better site. Following the recommendations of the first group, more bees left to investigate with the most vigorous dancers attracting more attention to the better cavities. Scouts gathered at the entrance to each box, and once they reached quorum

(experimentally determined as approximately fifteen bees) flew back to inform the colony of the selection. In four of five iterations of this experiment with different colonies, the swarm chose what the scientists believed to be the best nest even with what the authors termed *bounded rationality*, meaning that all honey bees lacked complete knowledge of every possibility [101]. As a meta-heuristic, PSO applies this swarming approach to discover high-quality solutions to any number of human problems without possessing *a priori* or even achieving *a posteriori* knowledge of the entire solution space.

Just as Seeley observed very few steps in honey bee house-hunting, Kennedy and Eberhart describe PSO with three overarching socio-cognitive imperatives: evaluate, compare, imitate [102]-[103]. Like GA, PSO operates on entire populations (*swarms*) of individuals (*particles*) during each iteration with each particle representing a potential solution. The current vogue also refers to individuals as *agents*, but the original authors of PSO philosophically disagree with the term because it implies autonomy and specialization, which swarm members lack as they only follow well-defined rules [103]. Unlike GA with its binary-coded chromosomes, PSO defines particles with real numbers that represent coordinates in the problem's *N*-dimensional solution space. In accordance with the spirit and simplicity of the three principles, PSO requires only a few basic procedures – swarm generation; fitness evaluation and comparison; and particle movement. Rather than breeding to generate new swarms, particles with randomly- or intentionally-seeded initial coordinates *fly* through the solution space, *evaluating* fitness as a function of position. The power of PSO lies in the ability of particles to communicate information about the portions of the solution space that have been explored. Therefore, each individual remembers the location, *pbest*, where it personally

discovered the best fitness and *compares* it with its neighbors. Typical PSO implementations define two types of neighborhoods: *gbest* or *lbest* [103]. A *gbest* (*g* for global) interpretation considers the entire population as a neighborhood. An *lbest* (*l* for local) definition describes a neighborhood composed of an individual and its *k* nearest neighbors. In this case the swarm is typically arranged as a ring structure with the first and last elements connected. Using this information, each particle, *n*, moves through the solution space guided by the following velocity and position equations:

$$\vec{v}_n(t + \Delta t) = \vec{v}_n(t) + \varphi_1\left(\vec{p}_n - \vec{x}_n(t)\right) + \varphi_2\left(\vec{p}_g - \vec{x}_n(t)\right) \tag{3.5}$$

$$\vec{x}_n(t + \Delta t) = \vec{x}_n(t) + \Delta t \cdot \vec{v}_n(t + \Delta t) \tag{3.6}$$

The vectors $\vec{p}_n$ and $\vec{p}_g$ represent the personal and global (or local) best locations, while both φ variables represent uniformly distributed random numbers with predefined upper limits. These variables mimic the unknown influence of self-confidence – φ_1 applied to the personal best – over swarm-confidence – φ_2 applied to the neighborhood best – by randomly weighting them equally or favoring one. Practical versions of the algorithm nearly always assign a value of one to Δt. By considering a global or local best when determining its path, each particle *imitates* its neighbors, fulfilling the last of the three principles.

Due to the stochastic nature of particles' acceleration, oscillations in the velocity may explode and approach infinity over time [103]. To damp this behavior, most practical implementations restrict the velocity to some v_{max} in each dimension, *d*. While PSO thrives in the infinite solution space, such a search undermines the reasonable goal of a speedy optimization. The introduction of boundary conditions confines particles to

the solution space (or at least encourages them to return quickly) to limit wasted computations.

3.1.3 Comparison of Optimization Techniques

While many works in the literature attempt to elevate PSO or GA to a position of supremacy, only one consistent conclusion emerges: each general purpose meta-heuristic performs better under certain specific conditions than the other. This follows from the No Free Lunch Theorem as discussed in [103] and [104]. The theorem states that if averaged over all problems and objectives, all algorithms perform equally. This theorem might appear to call for the deprecation of all methods save one, but the key phrase, "averaged over all problems," actually demands the opposite. It simply reinforces the idea that selecting a proper combination of problem and technique greatly affects the efficiency of the solution process. To further explore this behavior and demonstrate the capabilities of PSO in solving problems related to this thesis, the following section identifies and reviews several treatments from the literature that use both PSO and GA to solve electromagnetics problems.

Multimodal problems offer interesting insights into optimization routines in their lack of a unique solution. By definition multimodality requires a function to have multiple optimal solutions, which appear as peaks when visualizing the fitness. In [105] the authors develop a random multimodal problem generator to compare multiple binary-coded algorithms while controlling problem dimensionality (bit-string length) and number of peaks. The researchers evaluate the performance of four meta-heuristics – GA with selection and mutation (GA-M); GA with selection and crossover (GA-C); standard GA with selection, crossover, and mutation; and PSO – with dimensionalities, N, of 20

and 100 and modalities, *P*, of 20 and 100, repeating each experiment 20 times over 20,000 iterations. After 20 iterations and each multiple of 1,000 up to 20,000, the mean best fitness is recorded, providing insight to the behavior of the methods over time. Under all conditions GA-M outperforms the other techniques during early iterations, quickly approaching a global optimum, but failing to converge in all cases except $N = 20$, $P = 20$. GA and GA-C both lag a bit before progressing toward an optimum. GA-C manages to find a maximum in all cases by the 20,000 evaluation, a feat the standard GA matches except when $N = 100$, $P = 100$. PSO trumps its competitors by locating an optimum first and being the first to outpace GA-M except when $N = 20$, $P = 20$ where it finishes second. Though these results may not hold for all PSO and GA implementations, they do demonstrate the NFL theorem as well as at least par performance between the algorithms.

In [106] the authors compare PSO and GA in two functional benchmarks and six aerospace design problems, using known solutions to calculate the effectiveness and efficiency of the mean of both over 10 iterations of each experiment. The Rosenbrock function whose objective is described in (3.7) has a global minimum at $\mathbf{x} = \mathbf{1}$ in the domain $x_i \in [-10, 10]$.

$$\text{Minimize} \quad f(\mathbf{x}) = \sum_1^{n-1}(100(x_{i+1} - x_i^2)^2 + (x_i - 1)^2) \tag{3.7}$$

Similarly, the global minimum of the two-dimensional Eggcrate function, defined as

$$\text{Minimize} \quad f(\mathbf{x}) = x_1^2 + x_2^2 + 25(\sin^2(x_1) + \sin^2(x_2)) \tag{3.8}$$

lies at [0, 0] within the bounds $[-2\pi, 2\pi]$. The aerospace problems include the design of a Golinski's speed reducer (a seven-dimensional continuous-valued problem); 5, 6, 7, and 8

element telescope arrays; and a communication satellite with 27 discrete design variables. The effectiveness test measures whether the meta-heuristics achieve a quality of greater than 99% of the known solution while the efficiency test compares the computational effort of PSO to GA. For all of the problems except the speed reducer and satellite design, PSO reaches greater than 99% quality with fewer evaluations than GA. Although it only achieves a mean quality of 91% on the Rosenbrock function, GA performs exceptionally well on the remaining problems in terms of quality. In the cases where PSO does not reach the goal, its solutions have mean fitnesses of 98.8% and 96%, respectively; the authors postulate that the inherently continuous nature of PSO limits its performance in the discrete-valued satellite design. Considering standard deviations, both methods generate solutions of nearly identical quality; however, PSO arrives at these results much faster, requiring less than 5,000 evaluations in all cases. While GA comes within 50% of this for both two-dimensional problems, it runs at least twice and as much as six times as many evaluations on the remaining trials. The authors conclude that PSO proves most computationally thrifty "for unconstrained nonlinear problems with continuous design variables" with lower savings "for constrained and mixed integer nonlinear problems" [106].

Based on the previous results, PSO proves its suitability in a variety of situations. However, this success depends heavily on the problem under test as all of the authors state. Since this thesis primarily focuses on antenna design, we will now explore literature directly comparing PSO and GA for various antenna parameter optimizations, including radiation pattern features and frequency response. In [59] the authors investigate a binary PSO (BPSO) in designing a low sidelobe level (SLL) symmetric

thinned array of isotropic radiators. The array creates a $100\lambda_o$ aperture with elements uniformly spaced by one half-wavelength in a single row for a total of 200 elements. A 100-bit binary string represents one half of the array with a value of "1" indicating the *i*-th element is on and a value of "0" off. Using a swarm of 50 particles, the meta-heuristic searches through 200 iterations, arriving at the optimal 77% filled aperture after only 130 moves. Relative to a full aperture, this configuration reduces the peak SLL from -13.3 dB to -22.4 dB with a mean fitness of approximately -21.5 dB. Using 50 chromosomes with 0.7 crossover and 0.05 mutation probabilities, a standard GA finds minimum and mean peak SLL's of -22.1 dB and -21 dB, respectively, after 200 generations. These results hold steady for 20 trials of both methods. Again we see both meta-heuristics approaching nearly identical solutions, but we observe PSO converging more rapidly than GA.

Moving beyond the relatively simple binary experiment in [59], [60] employs EA's to improve the voltage standing wave ration (VSWR), front-to-back gain ratio, and size of conventional three-element stochastic Yagi-Uda arrays. Each wire element (reflector, driven element, and director) is meandered on a two-dimensional grid whose size and spacing is manipulated by the meta-heuristic along with the distances between the independent grids. The paper considers two configurations: coplanar and parallel grids. The authors apply a 60-member PSO with random noise mutation and a basic 100-chromosome GA to both arrays; the random noise mutation seeks to improve global exploration by slightly moving a particle after a predefined number of iterations. As a reference standard, the authors present a conventional Yagi-Uda array operating at 250 MHz with 31.6% bandwidth, 8.96 dBi of forward gain, and an 8.96 front-to-back ratio.

Although the fitness function does not address size directly, parameter constraints force a primary goal of volume reduction. As anticipated in miniaturization problems, none of the optimized solutions produce higher forward gain than the full-sized standard. Nevertheless, coplanar results for both heuristics demonstrate similarly marked improvements in front-to-back ratio and size with small sacrifices in bandwidth and gain. Relative to the conventional array, the PSO solution loses 2.66 dBi of gain and 0.36% bandwidth compared to GA's 2.15 dBi and 0.88%. However, the PSO design manages to maintain a front-to-back ratio of 14.3 while reducing overall length and width by 33.76% and 44.13%, respectively; GA achieves a ratio of 21.31, but only minimizes length by 12.86% and width by 46.10%. The parallel grid designs yield gains of 7.47 and 7.14 dBi, ratios of 7.48 and 8.64, bandwidths of 1.38% and 1.20%, length reductions of 70.92% and 69.10%, and width reductions of 45.67% and 43.99% for PSO and GA, respectively. These relatively insignificant differences again demonstrate the well-matched nature of the algorithms, but also show that PSO can sometimes best GA in physical miniaturization while GA can sometimes retain better performance.

Based on these findings, PSO appears to be a good candidate for complex antenna design as these devices often have many physical dimensions and require many hours to simulate each particle position. In addition to varying the standard parameters to alter swarm behavior, authors have also introduced more complex procedures. Meta PSO (MPSO) divides the whole swarm into smaller groups that have no physical interaction [61]. To use the newly available information, the authors also add a local swarm best to the personal global bests, effectively combining *gbest* and *lbest* neighborhoods. Modified MPSO (M^2PSO) tries to overcome local optima by inter-swarm repulsion.

Stabilized M^2PSO returns some local exploitation by making the swarm containing the global best immune to others' repulsion. On the benchmark and microstrip cascade bandpass filter problems presented in [61], standard PSO and MPSO both stagnate after approximately 300 iterations. While M^2PSO and SM^2PSO average results at least an order-or-magnitude smaller than the others, they require approximately 20 times as many iterations to do so. However with a goal of extreme antenna miniaturization, such extraordinary measures may be necessary to overcome the many local optima.

3.2 Implementation

Implementing PSO requires many decisions from an author. Along with the obvious questions of fitness and termination criteria raised by the basic procedure outlined in Figure 3.1, the selection of parameter values plays a defining role in the stability and capability of this heuristic. This section describes the implementation of PSO used in the next two chapters, first answering the obvious questions and then exploring the effects of each parameter.

In general optimization problems may minimize or maximize the fitness function. Little advantage exists for either, since the following relation holds true.

$$\max(f) = \min(-f) \tag{3.9}$$

In this dissertation all optimizers are selected as minimizers because most of the good fitness values for the presented problems are the minimum.

An optimization may terminate under many conditions: reaching a threshold, failing to reach a threshold in a given amount of time, or failing to make progress. The PSO implementations in this dissertation allow for all three. During each iteration the

optimizer evaluates the fitness of the entire swarm before reaching the termination block. Given the heavy computational cost of antenna simulations near objects other than open air, optimization terminates immediately if a solution within tolerance of the threshold is found. The swarm is then evaluated for stagnation and considered trapped if at least 90% of the particles have converged to some value but the threshold has not been reached. If the swarm stagnates, the process terminates. If neither of these events occurs, optimization terminates after a fixed number of iterations.

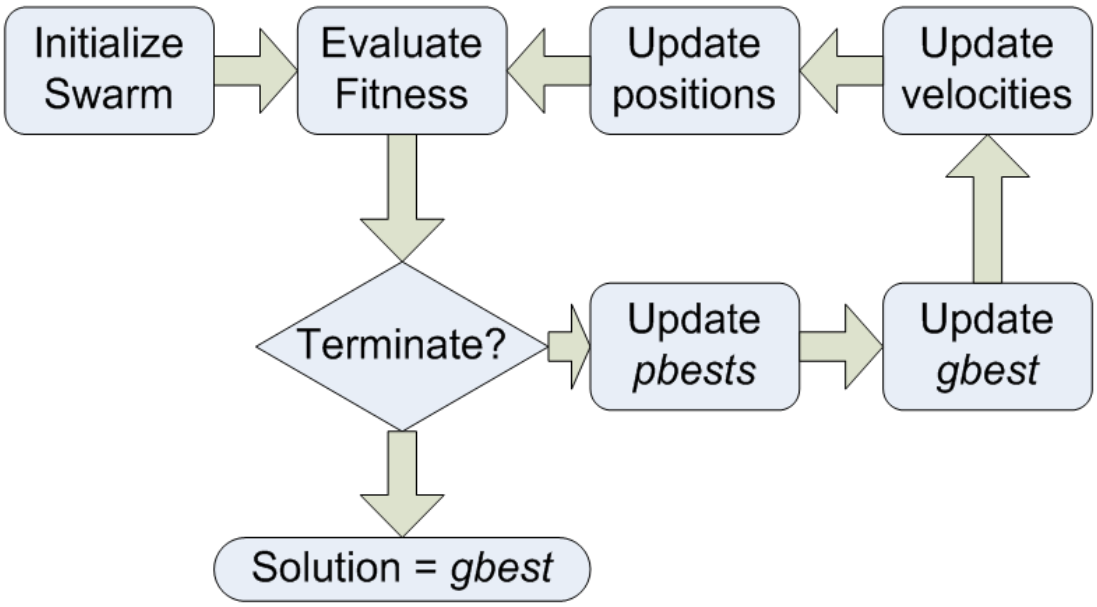

Figure 3.1 PSO Flowchart

The remainder of this chapter explores the influence of each parameter with suggested values from the literature and benchmark results on four well-defined functions. The Ackley function defined as

$$f(\vec{x}) = 20 + e - 20e^{-0.2\sqrt{\frac{1}{n}\sum_1^n x_i^2}} - e^{\frac{1}{n}\sum_1^n cos(2\pi x_i)} \tag{3.10}$$

has a global minimum of zero at **x** = **0** over the interval $x_i \in [-30, 30]$. In the domain $x_i \in [-300, 300]$ the Griewank function has a global minimum of zero at **x** = **100** and is defined as

$$f(\vec{x}) = \sum_1^n \frac{(x_i-100)^2}{4000} - \prod_1^n \cos\frac{x_i-100}{\sqrt{i}} + 1. \tag{3.11}$$

The Rastrigin function has a minimum of zero in the interval $x_i \in [-5.12, 5.12]$ at **x** = **0** and is defined as

$$f(\vec{x}) = 10n + \sum_1^n (x_i^2 - 10\cos(2\pi x_i)). \tag{3.12}$$

Finally, the Rosenbrock function in (3.7) is also considered. Figure 3.2 provides a visual representation of the two-dimensional forms of the problems. Unless otherwise stated the results for each benchmark are organized as described in Table 3.1. The initial PSO parameters are selected from recommendations in the literature.

Table 3.1 Benchmark Result Key

No. Successful Runs
(Mean No. Iterations for Successful Runs ; Mean No. Iterations for All Runs)
Mean gbest of Successful Runs
Mean gbest of Unsuccessful Runs

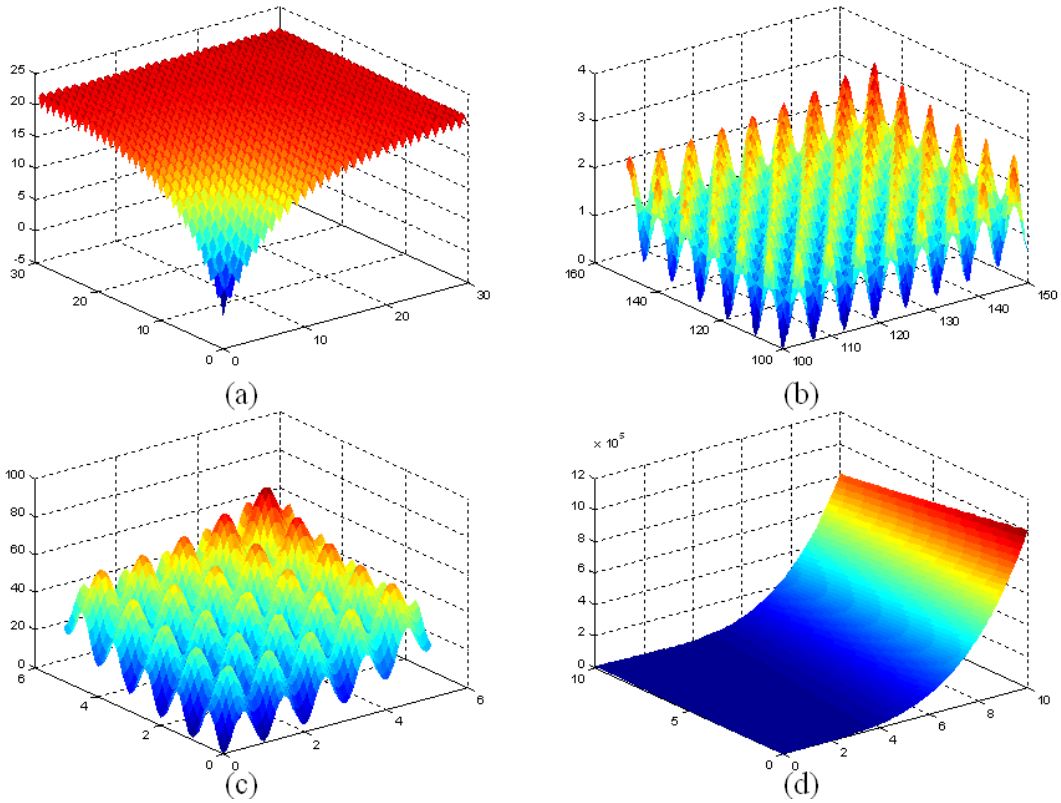

Figure 3.2 Two-Dimensional Test Functions

(a) Ackley
(b) Griewank
(c) Rastrigin
(d) Rosenbrock

3.2.1 Number of Particles

The number of particles primarily affects the amount of the solution space during per iteration. By using a large number of particles, more positions are visited during each iteration, but the longer duration of the iteration results in slower movement. Some recommendations in the literature suggest a dynamic number of particles on the order of 2–10 times the number of dimensions while others prefer a static 20–30 [57], [59], [60], [107].

Table 3.2 defines the static parameters for 100 runs of a standard PSO on each test function at 2, 5, and 10 dimensions. For each dimension, the number of particles is set to 1, 2, 4, or 10 times the number of dimensions as appropriate. The results in Tables 3.3, 3.4, and 3.5 indicate that effective optimization requires a minimum of twice as many particles as dimensions.

Table 3.2 Static PSO Parameters for Particle Testing

Particles	**k**	**V_{max}**	**c_1**	**c_2**	**ω**
*	Global	0.5	1.47	1.47	[0.9, 0.4]
ω_{method}	**$Iterations_{Max}$**	**Threshold**	**Tolerance**	**Pop. Init.**	**Boundary Condition**
Linear	10,000	0	10^{-8}	Random	Invisible

Table 3.3 Comparison of Number of Particles Relative to Dimensions, D = 2

	2x	4x	10x
Ackley	100	100	100
	(1193 ; 1193)	(1069 ; 1069)	(954 ; 954)
	7.1145E-09	6.81725E-09	6.79509E-09
	-	-	-
Griewank	44	71	89
	(1296 ; 1403)	(1376 ; 1529)	(1225 ; 1392)
	5.92817E-09	4.95384E-09	5.4244E-09
	0.117219	0.0220354	0.00739604
Rastrigin	98	100	100
	(823 ; 826)	(672 ; 672)	(565 ; 565)
	5.3092E-09	4.76464E-09	4.72795E-09
	0.994959	-	-
Rosenbrock	72	99	99
	(1433 ; 1355)	(1204 ; 1193)	(972 ; 962)
	6.0913E-09	6.32874E-09	6.07069E-09
	33.1945	5.41876	12.5585

Table 3.4 Comparison of Number of Particles Relative to Dimensions, D = 5

	1x	2x	4x	10x
Ackley	86	100	100	100
	(1715 ; 1723)	(1581 ; 1581)	(1490 ; 1490)	(1391 ; 1391)
	8.57694E-09	8.60193E-09	8.63406E-09	8.59805E-09
	3.29399E-08	-	-	-
Griewank	0	2	6	25
	(0 ; 2745)	(2783 ; 3405)	(3370 ; 4721)	(3456 ; 6160)
	-	9.86711E-09	8.1182E-09	8.38656E-09
	0.0505284	0.0296105	0.0184217	0.0718029
Rastrigin	27	65	95	100
	(1727 ; 1769)	(1668 ; 1817)	(1497 ; 1525)	(1227 ; 1227)
	8.115E-09	7.19505E-09	7.2711E-09	7.52243E-09
	1.64918	1.19395	0.994959	-
Rosenbrock	0	0	0	28
	(0 ; 3344)	(0 ; 5895)	(0 ; 9134)	(7112 ; 9183)
	-	-	-	9.90142E-09
	1.16137	0.188684	0.0414092	3.11659E-06

Table 3.5 Comparison of Number of Particles Relative to Dimensions, D = 10

	1x	2x	4x	10x
Ackley	91	100	100	100
	(2130 ; 2134)	(1979 ; 1979)	(1882 ; 1882)	(1768 ; 1768)
	9.34713E-09	9.26182E-09	9.15903E-09	9.10709E-09
	2.05422E-08	-	-	-
Griewank	0	0	0	0
	(0 ; 2954)	(0 ; 3314)	(0 ; 4853)	(0 ; 607)
	-	-	-	-
	0.09496	0.0713079	0.39186	5.8069
Rastrigin	1	2	22	62
	(2331 ; 2607)	(2318 ; 3006)	(2807 ; 4306)	(2442 ; 4216)
	9.94101E-09	9.21553E-09	8.90777E-09	8.08073E-09
	4.32154	2.74121	1.95165	2.6735
Rosenbrock	0	0	0	1
	(0 ; 7283)	(0 ; 9715)	(0 ; 9990)	(6433 ; 9964)
	-	-	-	9.99668E-09
	1.58177	0.837561	0.462614	0.142916

3.2.2 Neighborhood Size

The size of a particle's neighborhood controls how quickly information about a new best position passes through the swarm. In the case of gbest, all particles are omnisciently aware of the best position of all of the other particles, while lbest limits communication to just a few neighbors. The reduced level of communication slows the spread of information, and in theory can prevent particles from being pulled to newly-discovered local optima and being trapped prematurely. The overwhelming majority of PSO in the literature employs a global neighborhood, particularly in the electromagnetics

community, but some problems have shown themselves better suited to smaller neighborhoods [57], [59], [60], [107], [108].

A PSO with the parameters given in Table 3.6 is used to test neighborhoods occupying approximately 10%, 25%, 50%, 75%, and 100% of the swarm at 2, 5, 10, and 30 dimensions for 30 runs. The results (Tables 3.7, 3.8, 3.9, and 3.10) reveal no statistically significant difference for any of the neighborhoods.

Table 3.6 Static PSO Parameters for Neighborhood Testing

Particles	**k**	**V_{max}**	**c_1**	**c_2**	**ω**
30	*	0.5	1.47	1.47	[0.9, 0.4]
ω_{method}	**$Iterations_{Max}$**	**Threshold**	**Tolerance**	**Pop. Init.**	**Boundary Condition**
Linear	10,000	0	10^{-8}	Random	Invisible

Table 3.7 Comparison of Neighborhood Size, D = 2

	k=2	k=6	k=14	k=21	k=29
Ackley	30	30	30	30	30
	(889 ; 889)	(908 ; 908)	(893 ; 893)	(912 ; 912)	(937 ; 937)
	7.17E-09	6.67E-09	7.23E-09	6.96E-09	7.28E-09
	-	-	-	-	-
Griewank	29	30	29	30	30
	(984 ; 1060)	(1163 ; 1163)	(1133 ; 1309)	(1084 ; 1084)	(1012 ; 1012)
	5.27E-09	5.81E-09	5.32E-09	4.97E-09	5.84E-09
	0.00739604	-	0.00739604	-	-
Rastrigin	30	30	30	30	30
	(519 ; 519)	(525 ; 525)	(539 ; 539)	(506 ; 506)	(500 ; 500)
	5.17E-09	5.26E-09	6.17E-09	4.72E-09	5.08E-09
	-	-	-	-	-
Rosenbrock	30	30	29	30	29
	(897 ; 897)	(922 ; 922)	(904 ; 877)	(906 ; 906)	(905 ; 875)
	6.23E-09	5.75E-09	6.03E-09	6.17E-09	5.04E-09
	-	-	4.70097	-	8.21762

Table 3.8 Comparison of Neighborhood Size, D = 5

	k=2	k=6	k=14	k=21	k=29
Ackley	30	30	30	30	30
	(1445 ; 1445)	(1441 ; 1441)	(1436 ; 1436)	(1426 ; 1426)	(1461 ; 1461)
	8.39E-09	8.58E-09	8.86E-09	8.35E-09	8.71E-09
	-	-	-	-	-
Griewank	8	2	8	1	5
	(3269 ; 5380)	(2597 ; 4339)	(3686 ; 4631)	(2997 ; 5198)	(4310 ; 5912)
	7.90E-09	9.26E-09	6.77E-09	9.72E-09	9.05E-09
	0.0152263	0.01478	0.0146676	0.177998	0.0169474
Rastrigin	30	30	30	29	29
	(1369 ; 1369)	(1420 ; 1420)	(1334 ; 1334)	(1354 ; 1437)	(1385 ; 1420)
	7.61E-09	7.89E-09	7.81E-09	7.99E-09	7.62E-09
	-	-	-	0.994959	0.994959
Rosenbrock	0	2	0	0	1
	(0 ; 9817)	(7779 ; 9764)	(0 ; 9912)	(0 ; 9935)	(6347 ; 9804)
	-	9.96E-09	-	-	9.96E-09
	1.00E-05	2.39E-06	6.47E-05	0.000153408	0.136138

Table 3.9 Comparison of Neighborhood Size, D = 10

	k=2	k=6	k=14	k=21	k=29
Ackley	30	30	30	30	30
	(1921 ; 1921)	(1928 ; 1928)	(1924 ; 1924)	(1918 ; 1918)	(1925 ; 1925)
	9.02E-09	9.23E-09	9.23E-09	9.13E-09	9.05E-09
	-	-	-	-	-
Griewank	0	0	0	0	0
	(0 ; 4729)	(0 ; 3961)	(0 ; 4625)	(0 ; 4261)	(0 ; 4162)
	-	-	-	-	-
	0.0679559	0.271849	0.060995	0.0595322	0.0607519
Rastrigin	1	1	4	6	5
	(3288 ; 3514)	(2415 ; 4196)	(2159 ; 4064)	(2469 ; 3468)	(2229 ; 3139)
	7.80E-09	8.82E-09	7.61E-09	8.57E-09	9.05E-09
	2.19577	2.12715	2.02819	2.28011	2.06951
Rosenbrock	0	0	0	0	0
	(0 ; 10000)	(0 ; 10000)	(0 ; 10000)	(0 ; 10000)	(0 ; 9985)
	-	-	-	-	-
	0.98052	0.357666	0.369715	0.390025	0.373964

Table 3.10 Comparison of Neighborhood Size, D = 30

	k=2	k=6	k=14	k=21	k=29
Ackley	0	1	0	0	0
	(0 ; 3109)	(2897 ; 3035)	(0 ; 3022)	(0 ; 3057)	(0 ; 3015)
	-	9.87E-09	-	-	-
	0.0310435	0.136432	0.166371	3.01E-08	0.094739
Griewank	13	9	9	7	7
	(2627 ; 2604)	(2560 ; 2603)	(2569 ; 2640)	(2530 ; 2520)	(2551 ; 2615)
	9.51E-09	9.44E-09	9.44E-09	9.48E-09	9.12E-09
	1.60867	0.0369201	0.0390886	1.97197	0.0262809
Rastrigin	0	0	0	0	0
	(0 ; 3260)	(0 ; 3395)	(0 ; 3164)	(0 ; 3065)	(0 ; 3208)
	-	-	-	-	-
	35.5863	36.5481	37.3109	35.4205	33.7291
Rosenbrock	0	0	0	0	0
	(0 ; 9952)	(0 ; 10000)	(0 ; 10000)	(0 ; 9980)	(0 ; 9782)
	-	-	-	-	-
	14.1947	14.2466	17.328	18.0772	27.4628

3.2.3 Confidence Factors

As previously discussed, the confidence factors determine how strongly a particle will trust its own best relative to the neighbors' best. Although the confidence factors are represented by single characters, φ_1 and φ_2, in (3.5), each value is defined as

$$\varphi_i = \text{rand}() \cdot c_i \tag{3.13}$$

where rand() is a call to a random number generator and c_i is a positive real number. Many papers suggest setting both c_1 and c_2 to 2.0, but others have had better success with unequal weights or smaller confidence factors [57], [59], [60], [107], [108].

A PSO with the parameters given in Table 3.11 is used to compare popular confidence factors from the literature at 2, 5, 10, and 30 dimensions for 30 runs. The results (Tables 3.12, 3.13, 3.14, and 3.15) reveal no very little in dimensions 2, 5, or 10; however, at 30 dimensions the mean fitness improves for the Ackley and Rastrigin functions as the sum of the confidence factors approaches 4. The behavior of the other functions is opposite as the mean fitness increases as the sum of the confidence factors increases. Recommendations of approximately 1.5-2.0 seem reasonable.

Table 3.11 Static PSO Parameters for Confidence Factor Testing

Particles	**k**	**V_{max}**	**c_1**	**c_2**	**ω**
30	9	0.5	*	*	[0.9, 0.4]
ω_{method}	**$Iterations_{Max}$**	**Threshold**	**Tolerance**	**Pop. Init.**	**Boundary Condition**
Linear	10,000	0	10^{-8}	Random	Invisible

Table 3.12 Comparison of Confidence Factors, D = 2

	Ackley	Griewank	Rastrigin	Rosenbrock
c_1 = 1.00 c_2 = 1.00	30	29	30	30
	(493 ; 493)	(637 ; 656)	(256 ; 256)	(402 ; 402)
	7.63E-09	5.19E-09	5.29E-09	5.87E-09
	-	0.00739604	-	-
c_1 = 1.25 c_2 = 1.25	30	29	30	30
	(653 ; 653)	(707 ; 749)	(348 ; 348)	(613 ; 613)
	6.66E-09	5.18E-09	4.47E-09	4.80E-09
	-	0.00739604	-	-
c_1 = 1.50 c_2 = 1.50	30	29	30	30
	(936 ; 936)	(1221 ; 1269)	(527 ; 527)	(919 ; 919)
	6.96E-09	6.14E-09	5.43E-09	5.44E-09
	-	0.00739604	-	-
c_1 = 1.75 c_2 = 1.75	30	30	30	30
	(1440 ; 1440)	(1634 ; 1634)	(907 ; 907)	(1486 ; 1486)
	6.50E-09	5.11E-09	5.40E-09	5.95E-09
	-	-	-	-
c_1 = 2.00 c2=2.00	30	28	30	30
	(2271 ; 2271)	(2297 ; 2478)	(1630 ; 1630)	(2399 ; 2399)
	6.68E-09	6.18E-09	5.70E-09	6.51E-09
	-	0.801953	-	-
c_1 = 2.05 c2=2.05	30	29	30	29
	(2511 ; 2511)	(2463 ; 2714)	(1857 ; 1857)	(2571 ; 2486)
	7.04E-09	4.52E-09	6.20E-09	5.10E-09
	-	0.00739604	-	10.0912
c_1 = 2.80 c_2 = 1.30	30	29	30	30
	(3129 ; 3129)	(3092 ; 2992)	(2365 ; 2365)	(3142 ; 3142)
	7.34E-09	4.56E-09	4.70E-09	5.09E-09
	-	0.177307	-	-
c_1 = 2.04 c_2 = 0.95	30	30	30	30
	(1122 ; 1122)	(1349 ; 1349)	(665 ; 665)	(1229 ; 1229)
	6.54E-09	5.12E-09	5.63E-09	6.38E-09
	-	-	-	-

Table 3.12 (Continued)

c_1 = 1.30 c_2 = 2.80	30	26	30	30
	(3121 ; 3121)	(3056 ; 2869)	(2411 ; 2411)	(3138 ; 3138)
	7.17E-09	5.63E-09	5.06E-09	6.73E-09
	-	0.704173	-	-
c_1 = 0.95 c_2 = 2.04	30	29	30	30
	(1181 ; 1181)	(1320 ; 1485)	(716 ; 716)	(1126 ; 1126)
	7.08E-09	5.38E-09	5.95E-09	5.34E-09
	-	0.00739604	-	-

Table 3.13 Comparison of Confidence Factors, D = 5

	Ackley	Griewank	Rastrigin	Rosenbrock
c_1 = 1.00 c_2 = 1.00	30	1	21	5
	(666 ; 666)	(716 ; 3723)	(669 ; 777)	(3446 ; 4878)
	8.82E-09	7.38E-09	7.63E-09	9.98E-09
	-	0.0205578	1.54771	0.15725
c_1 = 1.25 c_2 = 1.25	30	3	25	2
	(989 ; 989)	(1325 ; 4623)	(1006 ; 1132)	(4790 ; 7762)
	8.43E-09	8.34E-09	7.26E-09	9.99E-09
	-	0.0172423	0.994959	0.140392
c_1 = 1.50 c_2 = 1.50	30	8	30	1
	(1511 ; 1511)	(3003 ; 4979)	(1427 ; 1427)	(7358 ; 9880)
	8.45E-09	7.52E-09	7.38E-09	9.94E-09
	-	0.0156744	-	7.31816E-06
c_1 = 1.75 c_2 = 1.75	30	3	30	0
	(2268 ; 2268)	(4639 ; 7757)	(2108 ; 2108)	(0 ; 10000)
	8.87E-09	9.17E-09	7.16E-09	-
	-	0.0139588	-	0.000109369
c_1 = 2.00 c_2 = 2.00	30	3	30	0
	(3537 ; 3537)	(5601 ; 8308)	(3203 ; 3203)	(0 ; 10000)
	8.31E-09	7.17E-09	7.95E-09	-
	-	0.514792	-	0.00329328

Table 3.13 (Continued)

c_1 = 2.05 c_2 = 2.05	30	5	30	0
	(3837 ; 3837)	(7962 ; 9062)	(3542 ; 3542)	(0 ; 10000)
	8.79E-09	7.29E-09	7.94E-09	-
	-	0.0934392	-	0.00494325
c_1 = 2.80 c_2 = 1.30	30	2	30	0
	(4446 ; 4446)	(7606 ; 7423)	(4143 ; 4143)	(0 ; 10000)
	9.03E-09	8.74E-09	7.97E-09	-
	-	0.460677	-	0.0738881
c_1 = 2.04 c_2 = 0.95	30	10	30	0
	(1714 ; 1714)	(3964 ; 6530)	(1677 ; 1677)	(0 ; 9658)
	8.61E-09	8.26E-09	7.72E-09	-
	-	0.0120717	-	0.0049962
c_1 = 1.30 c_2 = 2.80	30	1	30	0
	(4540 ; 4540)	(5422 ; 6279)	(4154 ; 4154)	(0 ; 10000)
	8.81E-09	9.71E-09	7.46E-09	-
	-	0.82501	-	0.0027625
c_1 = 0.95 c_2 = 2.04	30	1	30	30
	(1817 ; 1817)	(3269 ; 4081)	(1619 ; 1619)	(6045 ; 6045)
	8.67E-09	8.75E-09	6.76E-09	9.92E-09
	-	0.150657	-	-

Table 3.14 Comparison of Confidence Factors, D = 10

	Ackley	Griewank	Rastrigin	Rosenbrock
c_1 = 1.00 c_2 = 1.00	30	0	0	0
	(841 ; 841)	(0 ; 2101)	(0 ; 1389)	(0 ; 8701)
	9.31E-09	-	-	-
	-	0.0845304	4.14566	0.538457
c_1 = 1.25 c_2 = 1.25	30	0	2	0
	(1322 ; 1322)	(0 ; 3515)	(1609 ; 2528)	(0 ; 9919)
	9.41E-09	-	8.93E-09	-
	-	0.0633034	2.77167	0.19406

Table 3.14 (Continued)

c_1 = 1.50 c_2 = 1.50	30	0	2	0
	(2017 ; 2017)	(0 ; 4621)	(2383 ; 3849)	(0 ; 10000)
	9.12E-09	-	7.51E-09	-
	-	0.0569101	2.09652	0.291238
c_1 = 1.75 c_2 = 1.75	30	0	5	0
	(3010 ; 3010)	(0 ; 5896)	(3738 ; 4844)	(0 ; 10000)
	9.06E-09	-	8.39E-09	-
	-	0.437791	1.71133	0.66802
c_1 = 2.00 c_2 = 2.00	30	0	9	0
	(4568 ; 4568)	(0 ; 6706)	(5233 ; 6970)	(0 ; 10000)
	9.24E-09	-	8.36E-09	-
	-	1.70755	1.84778	0.999363
c_1 = 2.05 c_2 = 2.05	30	0	10	0
	(5011 ; 5011)	(0 ; 6361)	(5740 ; 7947)	(0 ; 10000)
	9.27E-09	-	8.29E-09	-
	-	2.97348	1.44269	1.38567
c_1 = 2.80 c_2 = 1.30	30	0	10	0
	(5667 ; 5667)	(0 ; 790)	(6473 ; 8624)	(0 ; 10000)
	9.39E-09	-	8.81E-09	-
	-	5.87112	1.2437	2.33216
c_1 = 2.04 c_2 = 0.95	30	1	5	0
	(2145 ; 2145)	(2632 ; 7276)	(2824 ; 4824)	(0 ; 9906)
	9.40E-09	7.36E-09	9.00E-09	-
	-	0.344898	1.55214	1.42862
c_1 = 1.30 c_2 = 2.80	30	0	12	0
	(5853 ; 5853)	(0 ; 4860)	(6406 ; 8267)	(0 ; 10000)
	9.12E-09	-	8.84E-09	-
	-	4.11512	1.54771	0.828921
c_1 = 0.95 c_2 = 2.04	30	0	1	6
	(2387 ; 2387)	(0 ; 3259)	(2343 ; 3499)	(8337 ; 9631)
	8.83E-09	-	9.62E-09	9.97E-09
	-	1.9476	2.43593	0.334084

Table 3.15 Comparison of Confidence Factors, D = 30

	Ackley	Griewank	Rastrigin	Rosenbrock
c_1 = 1.00 c_2 = 1.00	0	1	0	0
	(0 ; 1120)	(1113 ; 1079)	(0 ; 1280)	(0 ; 8079)
	-	9.89E-09	-	-
	1.5201	0.0340989	52.7327	18.7332
c_1 = 1.25 c_2 = 1.25	0	8	0	0
	(0 ; 2069)	(1732 ; 1781)	(0 ; 2200)	(0 ; 9528)
	-	9.27E-09	-	-
	0.372844	0.0324635	41.0254	15.6171
c_1 = 1.50 c_2 = 1.50	0	8	0	0
	(0 ; 3218)	(2708 ; 2814)	(0 ; 3487)	(0 ; 10000)
	-	9.21E-09	-	-
	2.50662E-08	0.017451	37.5099	15.9434
c_1 = 1.75 c_2 = 1.75	5	4	0	0
	(4660 ; 4666)	(4038 ; 3394)	(0 ; 5646)	(0 ; 10000)
	9.48E-09	9.49E-09	-	-
	1.50215E-08	11.6175	26.3332	18.2049
c_1 = 2.00 c_2 = 2.00	28	6	0	0
	(7060 ; 7064)	(6363 ; 2289)	(0 ; 9112)	(0 ; 10000)
	9.68E-09	8.80E-09	-	-
	1.57406E-08	49.1439	22.0881	25.5176
c_1 = 2.05 c_2 = 2.05	30	3	0	0
	(7783 ; 7783)	(7002 ; 3022)	(0 ; 9604)	(0 ; 10000)
	9.70E-09	9.34E-09	-	-
	-	39.3698	22.9172	41.2177
c_1 = 2.80 c_2 = 1.30	30	0	0	0
	(8016 ; 8016)	(0 ; 755)	(0 ; 9956)	(0 ; 10000)
	9.72E-09	-	-	-
	-	58.0455	22.9173	42.1724
c_1 = 2.04 c_2 = 0.95	11	6	0	0
	(3036 ; 3054)	(2650 ; 2710)	(0 ; 4734)	(0 ; 9336)
	9.53E-09	9.66E-09	-	-
	0.0705485	4.07968	29.1191	26.5938

Table 3.15 (Continued)

c_1 = 1.30 c_2 = 2.80	30	5	0	0
	(9218 ; 9218)	(8226 ; 5244)	(0 ; 10000)	(0 ; 10000)
	9.69E-09	9.82E-09	-	-
	-	34.1938	18.7052	47.6438
c_1 = 0.95 c_2 = 2.04	0	5	0	0
	(0 ; 3906)	(3309 ; 3127)	(0 ; 3687)	(0 ; 9933)
	-	9.37E-09	-	-
	7.85352E-08	4.86791	34.3924	2.06761

3.2.4 Velocity Limitation

Unrestrained velocity may lead to swarm instability over time, and even if the swarm remains stable large velocities tend to drive the particles from the solution space. Therefore, a maximum velocity that is often linked to the dynamic range of the solution space is introduced to clamp the velocity. The parameter, v_{max}, is typically set to equal to or equal to half of the dynamic range in each dimension [57], [107], [109], [110].

A PSO with the parameters given in Table 3.16 is used to evaluate v_{max} relative to the dynamic range in each dimension at 2, 5, 10, and 30 dimensions for 30 runs. According to the results (Tables 3.17, 3.18, 3.19, and 3.20), setting v_{max} equal to one-quarter to one-half of the range produces the most consistently good results.

Table 3.16 Static PSO Parameters for v_{max} Testing

Particles	**k**	**V_{max}**	**c_1**	**c_2**	**ω**
30	9	*	1.47	1.47	[0.9, 0.4]
ω_{method}	**$Iterations_{Max}$**	**Threshold**	**Tolerance**	**Pop. Init.**	**Boundary Condition**
Linear	10,000	0	10^{-8}	Random	Invisible

Table 3.17 Comparison of v_{max}, D = 2

	0.10x	0.25x	0.50x	1.00x
Ackley	30	30	30	30
	(853 ; 853)	(906 ; 906)	(903 ; 903)	(929 ; 929)
	6.98E-09	7.06E-09	6.55E-09	5.86E-09
	-	-	-	-
Griewank	28	29	29	21
	(815 ; 961)	(883 ; 1034)	(1221 ; 1270)	(1048 ; 760)
	3.96E-09	5.04E-09	5.92E-09	4.10E-09
	0.00739604	0.00739604	0.00739604	0.753761
Rastrigin	30	30	30	20
	(407 ; 407)	(454 ; 454)	(527 ; 527)	(735 ; 533)
	5.44E-09	4.93E-09	5.80E-09	5.18E-09
	-	-	-	3.03807
Rosenbrock	30	30	30	24
	(770 ; 770)	(811 ; 811)	(881 ; 881)	(1082 ; 877)
	4.77E-09	6.09E-09	5.79E-09	4.94E-09
	-	-	-	5.83204

Table 3.18 Comparison of v_{max}, D = 5

	0.10x	0.25x	0.50x	1.00x
Ackley	30	30	30	27
	(1381 ; 1381)	(1426 ; 1426)	(1441 ; 1441)	(1481 ; 1342)
	8.47E-09	8.70E-09	7.95E-09	8.53E-09
	-	-	-	8.56493
Griewank	4	3	3	1
	(2314 ; 5702)	(2561 ; 5665)	(3387 ; 5555)	(4732 ; 989)
	7.68E-09	7.05E-09	8.75E-09	9.94E-09
	0.0134553	0.0170587	0.0124082	1.58507
Rastrigin	25	30	30	8
	(1141 ; 1224)	(1219 ; 1219)	(1367 ; 1367)	(1551 ; 468)
	7.38E-09	7.48E-09	7.54E-09	7.38E-09
	0.994959	-	-	21.7121
Rosenbrock	0	1	1	1
	(0 ; 9842)	(9980 ; 9718)	(6391 ; 9757)	(8498 ; 6891)
	-	9.99E-09	9.98E-09	9.99E-09
	4.63505E-06	1.97768E-05	2.66829E-05	313.472

Table 3.19 Comparison of v_{max}, D = 10

	0.10x	0.25x	0.50x	1.00x
Ackley	30	30	30	10
	(1853 ; 1853)	(1890 ; 1890)	(1914 ; 1914)	(1950 ; 693)
	9.04E-09	9.25E-09	9.21E-09	9.30E-09
	-	-	-	14.4293
Griewank	0	0	0	0
	(0 ; 4972)	(0 ; 4209)	(0 ; 4278)	(0 ; 31)
	-	-	-	-
	0.0696876	0.0628004	0.0694511	9.80161
Rastrigin	1	4	2	0
	(1721 ; 2579)	(2342 ; 3240)	(2300 ; 3951)	(0 ; 278)
	9.51E-09	7.67E-09	8.41E-09	-
	3.87691	2.41086	1.95438	63.857
Rosenbrock	0	0	0	0
	(0 ; 10000)	(0 ; 10000)	(0 ; 10000)	(0 ; 1389)
	-	-	-	-
	0.544089	0.394241	0.521834	16114

3.2.5 Inertia Weight

In 1998 Shi and Eberhart introduced the concept of an inertia weight, ω, which is applied to the previous velocity term of (3.5) to encourage either global exploration or local exploitation [111]. In most implementations, the inertia weight is linearly decreased from 0.9 to 0.4 across the maximum number of iterations; a few publications have suggested improvement from linearly increasing the inertia weight. The weight may also be constant or varied exponentially rather than linearly [57], [107]–[110].

A PSO with the parameters given in Table 3.20 is used to evaluate ω at 2, 5, and 10 dimensions for 30 runs. According to the results (Tables 3.21, 3.22, and 3.23), inertia weights greater than one should be avoided. The amplification of the velocity tends to

ram particles into the walls of the solutions space and lead to early stagnation. Similarly, beginning with a very small weight or rapid exponential decay tends to clamp the particles early. Only the Rosenbrock function displays any significant benefit from a constant weight. The best performers are the commonly suggested, decreasing 0.9 to 0.4.

Table 3.20 Static PSO Parameters for ω Testing

Particles	**k**	**V_{max}**	**c_1**	**c_2**	**ω**
20	19	0.5	1.47	1.47	*
ω_{method}	**$Iterations_{Max}$**	**Threshold**	**Tolerance**	**Pop. Init.**	**Boundary Condition**
*	10,000	0	10^{-8}	Random	Invisible

Table 3.21 Comparison of ω, D = 2

	Ackley	Griewank	Rastrigin	Rosenbrock
0.9-0.4, Lin	30	26	30	30
	(975 ; 975)	(1588 ; 1746)	(553 ; 553)	(919 ; 919)
	6.73E-09	5.49E-09	5.06E-09	4.61E-09
	-	0.00739604	-	-
0.9-0.4, Exp	30	23	30	29
	(538 ; 538)	(730 ; 885)	(354 ; 354)	(566 ; 548)
	7.87E-09	4.58E-09	5.01E-09	6.62E-09
	-	0.00739604	-	11.6134
0.4-0.9, Lin	30	16	22	28
	(60 ; 60)	(97 ; 303)	(45 ; 53)	(242 ; 245)
	6.20E-09	4.98E-09	4.47E-09	7.58E-09
	-	0.0133828	1.2437	1.85E-08
0.4-0.9, Exp	30	8	22	26
	(60 ; 60)	(169 ; 389)	(46 ; 56)	(203 ; 214)
	6.70E-09	4.78E-09	3.67E-09	5.96E-09
	-	0.0133356	1.11933	0.000815591

Table 3.21 (Continued)

1.4-0.0, Lin	0	0	0	0
	(0 ; 14)	(0 ; 13)	(0 ; 14)	(0 ; 13)
	-	-	-	-
	5.62931	0.958674	5.55677	9.77865
1.4-0.0, Exp	0	0	0	0
	(0 ; 15)	(0 ; 14)	(0 ; 14)	(0 ; 14)
	-	-	-	-
	6.43357	0.907458	6.8379	8.22532
0.01-1.4, Lin	19	4	15	6
	(30 ; 36)	(120 ; 199)	(31 ; 45)	(149 ; 151)
	6.26E-09	5.15E-09	5.53E-09	6.22E-09
	0.237446	0.0493071	0.796018	0.532646
0.01-1.4, Exp	18	3	16	0
	(30 ; 38)	(407 ; 392)	(37 ; 43)	(0 ; 118)
	7.07E-09	4.36E-09	4.19E-09	-
	0.43539	0.0341532	1.13723	0.764549
1.2, Con	0	0	0	0
	(0 ; 22)	(0 ; 19)	(0 ; 23)	(0 ; 22)
	-	-	-	-
	5.13409	0.756171	4.26879	10.1276
1.0, Con	0	0	0	0
	(0 ; 9309)	(0 ; 68)	(0 ; 8542)	(0 ; 1189)
	-	-	-	-
	0.345216	0.294021	0.0796748	0.859356
0.9, Con	30	26	30	30
	(3425 ; 3425)	(2823 ; 3780)	(1073 ; 1073)	(2735 ; 2735)
	7.08E-09	4.76E-09	5.78E-09	6.10E-09
	-	0.00441968	-	-
0.4, Con	30	7	21	27
	(60 ; 60)	(115 ; 356)	(51 ; 58)	(188 ; 203)
	6.61E-09	4.01E-09	5.65E-09	7.23E-09
	-	0.0173659	1.43716	0.00310974
0.7298, Con	30	23	27	30
	(179 ; 179)	(353 ; 460)	(104 ; 115)	(234 ; 234)
	7.13E-09	5.23E-09	5.64E-09	6.25E-09
	-	0.00915653	0.994959	-

Table 3.22 Comparison of ω, D = 5

	Ackley	Griewank	Rastrigin	Rosenbrock
0.9-0.4, Lin	30	2	29	0
	(1477 ; 1477)	(4339 ; 5659)	(1511 ; 1529)	(0 ; 9145)
	8.44E-09	7.18E-09	7.12E-09	-
	-	0.0183879	0.994959	0.0016083
0.9-0.4, Exp	30	1	19	0
	(733 ; 733)	(3793 ; 2697)	(786 ; 859)	(0 ; 4953)
	8.51E-09	1.56E-09	7.58E-09	-
	-	0.0241278	1.08541	0.0126721
0.4-0.9, Lin	28	0	1	0
	(89 ; 89)	(0 ; 661)	(118 ; 89)	(0 ; 407)
	8.07E-09	-	8.30E-09	-
	0.823112	0.1011	6.00406	8.28E+00
0.4-0.9, Exp	23	0	0	0
	(90 ; 85)	(0 ; 388)	(0 ; 108)	(0 ; 382)
	8.26E-09	-	-	-
	1.17587	0.131234	4.21199	3.07159
1.4-0.0, Lin	0	0	0	0
	(0 ; 12)	(0 ; 9)	(0 ; 13)	(0 ; 12)
	-	-	-	-
	13.5896	4.75513	32.9723	4743.1
1.4-0.0, Exp	0	0	0	0
	(0 ; 12)	(0 ; 10)	(0 ; 13)	(0 ; 13)
	-	-	-	-
	13.492	4.87077	28.9913	6033.15
0.01-1.4, Lin	0	0	0	0
	(0 ; 78)	(0 ; 141)	(0 ; 114)	(0 ; 96)
	-	-	-	-
	5.81673	0.629936	6.06471	297.042
0.01-1.4, Exp	0	0	0	0
	(0 ; 76)	(0 ; 143)	(0 ; 123)	(0 ; 93)
	-	-	-	-
	6.08059	0.695325	4.99625	196.099
1.2, Con	0	0	0	0
	(0 ; 24)	(0 ; 13)	(0 ; 23)	(0 ; 21)
	-	-	-	-
	11.7279	4.05549	29.5645	3091.39

Table 3.22 (Continued)

1.0, Con	0	0	0	0
	(0 ; 9816)	(0 ; 30)	(0 ; 7073)	(0 ; 6399)
	-	-	-	-
	5.85851	2.42154	10.476	213.095
0.9, Con	0	0	0	0
	(0 ; 10000)	(0 ; 10000)	(0 ; 10000)	(0 ; 10000)
	-	-	-	-
	0.00395506	0.0984957	0.00265188	0.90113
0.4, Con	23	0	0	0
	(88 ; 95)	(0 ; 346)	(0 ; 110)	(0 ; 276)
	8.04E-09	-	-	-
	0.235201	0.127366	3.51552	7.45004
0.7298, Con	30	0	6	27
	(264 ; 264)	(0 ; 2210)	(329 ; 373)	(6866 ; 7179)
	8.15E-09	-	7.19E-09	9.94E-09
	-	0.042777	2.07283	3.93084

Table 3.23 Comparison of ω, D = 10

	Ackley	Griewank	Rastrigin	Rosenbrock
0.9-0.4, Lin	30	0	2	0
	(1968 ; 1968)	(0 ; 3974)	(2982 ; 3182)	(0 ; 9751)
	9.14E-09	-	9.66E-09	-
	-	0.0608501	2.84274	0.908099
0.9-0.4, Exp	30	1	1	0
	(934 ; 934)	(1072 ; 1542)	(1267 ; 1190)	(0 ; 9481)
	9.25E-09	2.98E-09	8.38E-09	-
	-	0.0843242	4.04845	1.69972
0.4-0.9, Lin	0	0	0	0
	(0 ; 444)	(0 ; 398)	(0 ; 573)	(0 ; 1040)
	-	-	-	-
	3.29052	0.349713	20.3845	1.47E+02
0.4-0.9, Exp	0	0	0	0
	(0 ; 306)	(0 ; 329)	(0 ; 366)	(0 ; 584)
	-	-	-	-
	3.2021	0.347206	18.6778	144.805

Table 3.23 (Continued)

1.4-0.0, Lin	0	0	0	0
	(0 ; 13)	(0 ; 10)	(0 ; 17)	(0 ; 13)
	-	-	-	-
	17.3571	17.3709	94.2767	82844.8
1.4-0.0, Exp	0	0	0	0
	(0 ; 13)	(0 ; 10)	(0 ; 15)	(0 ; 14)
	-	-	-	-
	17.1264	18.9773	86.2756	92453
0.01-1.4, Lin	0	0	0	0
	(0 ; 84)	(0 ; 82)	(0 ; 109)	(0 ; 115)
	-	-	-	-
	11.2028	6.30069	28.4326	7206.98
0.01-1.4, Exp	0	0	0	0
	(0 ; 86)	(0 ; 80)	(0 ; 110)	(0 ; 113)
	-	-	-	-
	12.0872	6.33673	28.8909	8727.36
1.2, Con	0	0	0	0
	(0 ; 34)	(0 ; 15)	(0 ; 39)	(0 ; 38)
	-	-	-	-
	16.8654	17.7711	85.4511	74593.8
1.0, Con	0	0	0	0
	(0 ; 9795)	(0 ; 43)	(0 ; 8118)	(0 ; 6463)
	-	-	-	-
	12.8296	10.2301	53.4649	9896.2
0.9, Con	0	0	0	0
	(0 ; 10000)	(0 ; 10000)	(0 ; 10000)	(0 ; 10000)
	-	-	-	-
	1.8044	0.661701	14.6653	48.1802
0.4, Con	0	0	0	0
	(0 ; 260)	(0 ; 300)	(0 ; 346)	(0 ; 498)
	-	-	-	-
	3.4793	0.432263	18.0662	85.6532
0.7298, Con	24	0	0	0
	(400 ; 383)	(0 ; 541)	(0 ; 424)	(0 ; 10000)
	9.16E-09	-	-	-
	1.29001	0.0964437	8.55664	0.665619

3.2.6 Population Initialization

In a typical PSO, the initial swarm positions are randomly seeded because the fitness landscape is likely unknown, and random starting positions allow the algorithm to proceed without bias. However, some areas of the solution space may be overlooked if all of the particles happen to be seeded near one another. Linearly distributing the particles throughout the space ensures that each region receives some attention in the first iteration. Additionally, some authors have suggested the application of orthogonal arrays (OA) to define the initial positions [112]. An OA contains a finite set of numbers that are organized to ensure that all combinations of the numbers appear an identical number of times for every combination of t columns in the table. The parameter N identifies the number of rows (equivalent to particles) in the matrix; k defines the number of columns which relate to the number of dimensions in the problem; and s is the number of number of levels, or the finite set of consecutive numbers, that appear in the table. An OA may be named as OA(N, k, s, t).

A PSO with the parameters given in Table 3.24 is used to evaluate the initialization method at 2, 5, 10, and 30 dimensions for 30 runs. For the first three dimensions, OA(36, 13, 3, 2) is selected; at 30 dimensions OA(81, 40, 3, 2) is used. According to the results (Tables 3.24, 3.25, 3.26, and 3.27), no method predictably or consistently outperforms the others.

Table 3.24 Static PSO Parameters for Population Intialization Testing

Particles	**k**	**V_{max}**	**c_1**	**c_2**	**ω**
30	9	0.5	1.47	1.47	[0.9, 0.4]
ω_{method}	**$Iterations_{Max}$**	**Threshold**	**Tolerance**	**Pop. Init.**	**Boundary Condition**
Linear	10,000	0	10^{-8}	*	Invisible

Table 3.25 Comparison of Population Initialization Methods, D = 2

	Ackley	Griewank	Rastrigin	Rosenbrock
Random	30	28	30	30
	(907 ; 907)	(1097 ; 1273)	(504 ; 504)	(926 ; 926)
	6.89E-09	5.96E-09	5.61E-09	5.70E-09
	-	0.00739604	-	-
Linear	30	29	30	30
	(708 ; 708)	(1125 ; 1216)	(462 ; 462)	(873 ; 873)
	4.91E-09	5.78E-09	4.85E-09	5.90E-09
	-	0.00739604	-	-
OA	30	21	30	30
	(1 ; 1)	(1758 ; 1965)	(1 ; 1)	(1274 ; 1274)
	-8.88E-16	5.78E-09	0	5.29E-09
	-	0.00739604	-	-

Table 3.26 Comparison of Population Initialization Methods, D = 5

	Ackley	Griewank	Rastrigin	Rosenbrock
Random	30	4	30	0
	(1438 ; 1438)	(2899 ; 5327)	(1373 ; 1373)	(0 ; 9826)
	8.25E-09	7.43E-09	6.87E-09	-
	-	0.0157276	-	1.17219E-05
Linear	30	2	29	21
	(1457 ; 1457)	(2789 ; 5392)	(1386 ; 1435)	(6408 ; 7437)
	8.62E-09	9.24E-09	7.50E-09	9.98E-09
	-	0.0146042	0.994959	9.57184E-08
OA	30	2	30	14
	(1 ; 1)	(3891 ; 6672)	(1 ; 1)	(8166 ; 9144)
	-8.88E-16	8.58E-09	0	9.97E-09
	-	0.0150443	-	7.06366E-07

Table 3.27 Comparison of Population Initialization Methods, D = 10

	Ackley	Griewank	Rastrigin	Rosenbrock
Random	30	0	3	0
	(1931 ; 1931)	(0 ; 4307)	(2516 ; 3298)	(0 ; 10000)
	9.22E-09	-	8.79E-09	-
	-	0.0625544	2.46897	0.539518
Linear	30	0	1	0
	(1998 ; 1998)	(0 ; 4340)	(2064 ; 7357)	(0 ; 10000)
	8.77E-09	-	9.67E-09	-
	-	0.0771466	3.43089	3.8075E-06
OA	30	0	30	0
	(1 ; 1)	(0 ; 6091)	(1 ; 1)	(0 ; 10000)
	-8.88E-16	-	0	-
	-	0.0599264	-	0.291215

Table 3.28 Comparison of Population Initialization Methods, D = 30

	Ackley	Griewank	Rastrigin	Rosenbrock
Random	0	8	0	0
	(0 ; 3077)	(2589 ; 2635)	(0 ; 3298)	(0 ; 10000)
	-	9.37E-09	-	-
	0.0885632	0.022675	33.5301	27.8483
Linear	0	9	0	0
	(0 ; 4550)	(2522 ; 2598)	(0 ; 10000)	(0 ; 9910)
	-	9.67E-09	-	-
	2.41198	0.0284232	25.4378	3.83345E-06
OA	30	12	0	0
	(2992 ; 2992)	(2627 ; 2912)	(0 ; 3279)	(0 ; 5000)
	9.54E-06	9.19E-06	-	-
	-	0.03113	25.8026	11.0715

3.2.7 Boundary Conditions

Boundary conditions (BCs) define the behavior of particles when they exceed the limits of the solution space. A few broad categories of boundary conditions exists: hard, soft, and periodic. Hard boundary conditions (HBCs) immediately return a particle to the barrier it broke. Soft boundary conditions (SBCs)—or invisible walls—allow a particle to remain outside the solution space, but encourage it to return by assigning a poor fitness value to any invalid positions. Periodic boundary conditions (PBCs) calculate the distance from the nearest boundary that a particle has traveled and reinsert the particle into the solution space at an equal distance from the opposite boundary [113]. BCs may also modify a particle's velocity in conjunction with relocating or scolding it. The absorbing boundary condition (ABC) zeroes a particle's velocity. The reflecting boundary condition (RBC) only changes the direction of the velocity. The damping boundary condition (DBC) reduces the particles velocity by a random percentage and

changes its direction. Various combinations of these techniques are used in the literature, but the majority of electromagnetics optimizations rely on invisible boundary conditions without velocity modification [57], [113]. This may be because the introduction of dependent constraints, such as those required by complex antenna geometries, makes determining the nearest acceptable boundary an optimization problem in itself.

BCs are explored with a PSO defined by the parameters in Table 3.29. Unless explicitly stated, HBCs are assumed. Over the course of all of the runs summarized in Tables 3.30, 3.31, and 3.32, none of the BCs outperform the others consistently.

Table 3.29 Static PSO Parameters for Boundary Condition Testing

Particles	**k**	**V_{max}**	**c_1**	**c_2**	**Ω**
30	9	0.35	1.4962	1.4962	[0.9, 0.6]
ω_{method}	**$Iterations_{Max}$**	**Threshold**	**Tolerance**	**Pop. Init.**	**Boundary Condition**
Linear	10,000	0	10^{-8}	Linear	*

Table 3.30 Comparison of Boundary Conditions, D = 2

	Ackley	Griewank	Rastrigin	Rosenbrock
Absorbing	30	30	30	30
	(1177 ; 1177)	(1374 ; 1374)	(599 ; 599)	(1105 ; 1105)
	6.84E-09	5.88E-09	5.25E-09	5.66E-09
	-	-	-	-
Damping	30	30	30	30
	(1108 ; 1108)	(1187 ; 1187)	(619 ; 619)	(1060 ; 1060)
	7.05E-09	5.51E-09	4.60E-09	5.50E-09
	-	-	-	-

Table 3.30 (Continued)

Reflecting	30	30	30	30
	(1134 ; 1134)	(1324 ; 1324)	(576 ; 576)	(1051 ; 1051)
	7.67E-09	5.58E-09	5.01E-09	5.86E-09
	-	-	-	-
Invisible	30	29	30	30
	(1107 ; 1107)	(1325 ; 1530)	(595 ; 595)	(1047 ; 1047)
	7.76E-09	4.57E-09	4.00E-09	5.82E-09
	-	0.00739604	-	-
Invisible Absorbing	30	30	30	30
	(1117 ; 1117)	(1376 ; 1376)	(605 ; 605)	(1092 ; 1092)
	7.53E-09	5.72E-09	5.67E-09	6.78E-09
	-	-	-	-
Invisible Damping	30	30	30	30
	(1194 ; 1194)	(1426 ; 1426)	(634 ; 634)	(1099 ; 1099)
	7.66E-09	6.12E-09	4.87E-09	5.75E-09
	-	-	-	-
Invisible Reflecting	30	30	30	30
	(1148 ; 1148)	(1332 ; 1332)	(594 ; 594)	(1042 ; 1042)
	7.04E-09	4.32E-09	5.45E-09	5.13E-09
	-	-	-	-
Periodic Absorbing	30	30	30	30
	(1122 ; 1122)	(1271 ; 1271)	(589 ; 589)	(1152 ; 1152)
	6.79E-09	5.10E-09	6.05E-09	5.69E-09
	-	-	-	-
Periodic Damping	30	30	30	30
	(1150 ; 1150)	(1361 ; 1361)	(613 ; 613)	(1087 ; 1087)
	6.83E-09	5.14E-09	4.65E-09	4.76E-09
	-	-	-	-
Periodic Reflecting	30	29	30	30
	(1171 ; 1171)	(1475 ; 1593)	(603 ; 603)	(1111 ; 1111)
	6.46E-09	5.19E-09	5.25E-09	5.74E-09
	-	0.00739604	-	-

Table 3.31 Comparison of Boundary Conditions, D = 5

	Ackley	Griewank	Rastrigin	Rosenbrock
Absorbing	30	10	30	29
	(2020 ; 2020)	(5009 ; 6678)	(1759 ; 1759)	(7769 ; 7844)
	8.66E-09	6.39E-09	7.40E-09	9.96E-09
	-	0.0144111	-	1.5241E-08
Damping	30	7	30	30
	(2005 ; 2005)	(4290 ; 7034)	(1778 ; 1778)	(7576 ; 7576)
	8.60E-09	6.92E-09	7.75E-09	9.95E-09
	-	0.0155271	-	-
Reflecting	30	8	30	29
	(2007 ; 2007)	(4676 ; 6797)	(1811 ; 1811)	(8102 ; 8166)
	8.67E-09	6.68E-09	7.71E-09	9.96E-09
	-	0.0133233	-	2.00414E-08
Invisible	30	5	29	30
	(2029 ; 2029)	(3214 ; 6863)	(1762 ; 1818)	(7786 ; 7786)
	8.85E-09	7.12E-09	7.04E-09	9.97E-09
	-	0.0141892	0.994959	-
Invisible Absorbing	30	10	30	30
	(2010 ; 2010)	(4441 ; 6743)	(1866 ; 1866)	(7647 ; 7647)
	8.74E-09	6.97E-09	7.40E-09	9.95E-09
	-	0.0156407	-	-
Invisible Damping	30	4	30	30
	(2018 ; 2018)	(5058 ; 7428)	(1893 ; 1893)	(7818 ; 7818)
	8.35E-09	9.41E-09	7.43E-09	9.97E-09
	-	0.0459231	-	-
Invisible Reflecting	30	6	30	30
	(2026 ; 2026)	(4698 ; 6601)	(1878 ; 1878)	(7363 ; 7363)
	9.26E-09	6.85E-09	7.41E-09	9.96E-09
	-	0.0185753	-	-
Periodic Absorbing	30	8	29	29
	(2008 ; 2008)	(4237 ; 6543)	(1792 ; 1855)	(7669 ; 7747)
	8.77E-09	8.50E-09	7.79E-09	9.97E-09
	-	0.0158995	0.994959	7.61E-08

Table 3.31 (Continued)

Periodic Damping	30	3	30	29
	(1992 ; 1992)	(3708 ; 6544)	(1799 ; 1799)	(7888 ; 7958)
	8.75E-09	8.97E-09	8.21E-09	9.96E-09
	-	0.0156926	-	3.4187E-08
Periodic Reflecting	30	7	30	29
	(2005 ; 2005)	(4097 ; 7201)	(1749 ; 1749)	(7775 ; 7849)
	8.78E-09	8.11E-09	7.26E-09	9.94E-09
	-	0.0142447	-	8.35463E-08

Table 3.32 Comparison of Boundary Conditions, D = 10

	Ackley	Griewank	Rastrigin	Rosenbrock
Absorbing	30	0	2	2
	(2816 ; 2816)	(0 ; 6570)	(3304 ; 7872)	(8905 ; 9927)
	9.33E-09	-	9.70E-09	9.91E-09
	-	0.0663198	2.16759	5.25801E-07
Damping	30	0	3	4
	(2835 ; 2835)	(0 ; 6123)	(4377 ; 7939)	(9448 ; 9926)
	9.10E-09	-	7.89E-09	1.00E-08
	-	0.058066	2.28472	7.11002E-07
Reflecting	30	0	3	3
	(2830 ; 2830)	(0 ; 6377)	(3370 ; 8093)	(8950 ; 9895)
	9.23E-09	-	8.38E-09	9.95E-09
	-	0.0705044	2.28472	4.16724E-07
Invisible	30	0	3	4
	(2826 ; 2826)	(0 ; 6812)	(5661 ; 8384)	(8804 ; 9840)
	8.83E-09	-	9.38E-09	1.00E-08
	-	0.0646889	2.32157	5.15878E-07
Invisible Absorbing	26	0	2	3
	(2827 ; 2486)	(0 ; 118)	(3768 ; 8569)	(9376 ; 9938)
	9.09E-09	-	9.48E-09	9.97E-09
	3.80074	1.09878	2.52293	3.44118E-07

Table 3.32 (Continued)

Invisible Damping	28	0	1	2
	(2836 ; 2676)	(0 ; 1049)	(5224 ; 8461)	(9467 ; 9964)
	9.43E-09	-	8.67E-09	9.98E-09
	3.80074	0.957772	2.47024	3.38768E-07
Invisible Reflecting	30	0	3	4
	(2845 ; 2845)	(0 ; 6148)	(5469 ; 8300)	(8666 ; 9822)
	9.35E-09	-	8.48E-09	9.97E-09
	-	0.061496	2.02677	5.25217E-07
Periodic Absorbing	30	0	3	3
	(2856 ; 2856)	(0 ; 6615)	(5131 ; 8359)	(8559 ; 9856)
	9.29E-09	-	9.38E-09	9.98E-09
	-	0.0668196	2.24787	3.2403E-07
Periodic Damping	30	0	2	1
	(2849 ; 2849)	(0 ; 5829)	(4551 ; 8326)	(9116 ; 9971)
	9.29E-09	-	7.83E-09	9.96E-09
	-	0.0605967	2.02545	4.86036E-07
Periodic Reflecting	30	0	1	2
	(2824 ; 2824)	(0 ; 7096)	(3651 ; 8588)	(9084 ; 9939)
	9.20E-09	-	8.40E-09	9.99E-09
	-	0.0679677	2.33301	8.98274E-07

3.2.8 Meta PSO

Introduced in [61], Meta PSO is effectively a combination of the lbest and gbest PSO models. However, rather than calling local groups neighborhoods, the authors term them swarms within the swarm. The authors redefine velocity update equation (3.5) as

$$\vec{v}_{j,i}(t+\Delta t) = \omega \cdot \vec{v}_{j,i}(t) + \varphi_1\left(\vec{p}_{j,i} - \vec{x}_{j,i}(t)\right) + \varphi_2\left(\vec{p}_g - \vec{x}_{j,i}(t)\right) \ldots + \varphi_3\left(\vec{p}_j - \vec{x}_{j,i}(t)\right) \quad . \qquad (3.14)$$

Like the previous confidence factors, the local swarm confidence is defined by a scalar and a random number. To encourage exploration and avoid stagnation, the authors add an inter-swarm repulsion term and call this Modified MPSO (M^2PSO). The velocity is then updated as

$$\vec{v}_{j,i}(t+\Delta t) = \cdots - \sum_{s \neq j} \text{rand}() \cdot \xi \frac{\overrightarrow{B_s}(t) - \overrightarrow{x_{j,i}}(t)}{\left|\overrightarrow{B_s}(t) - \overrightarrow{x_{j,i}}(t)\right|^{\gamma}} . \quad (3.15)$$

The distance factor, γ, determines the distance over which the repulsive weight, ξ, can act. The barycenter, **B**, of each swarm is calculated as

$$\vec{B}_j(t) = \frac{1}{N_p}\sum_{i=1}^{N_p} \vec{x}_{j,i}(t). \quad (3.16)$$

Perhaps realizing that M^2PSO encourages too much exploration, the authors allow the swarm containing gbest to be shielded from repulsion in Stabilized M^2PSO (SM^2PSO).

To explore these new parameters, an SM^2PSO defined by the parameters in Table 3.33 is applied at 2, 5, and 10 dimensions for 30 runs. For these runs, the neighborhood size is reduced to 5 to increase the number of local swarms from 3 to 6. Unless otherwise indicated, the suggested values of the new parameters (c_3 = 2, ξ = 2/3, and γ = 2) are used.

Table 3.33 Static Standard PSO Parameters for SM^2PSO Testing

Particles	**k**	**V_{max}**	**c_1**	**c_2**	**ω**
30	5	0.35	1.47	1.47	[0.9, 0.4]
ω_{method}	**$Iterations_{Max}$**	**Threshold**	**Tolerance**	**Pop. Init.**	**Boundary Condition**
Linear	10,000	0	10^{-8}	Random	Invisible

3.2.8.1 Local Swarm Confidence

The results from Tables 3.34, 3.35, and 3.36 demonstrate that the local swarm confidence only affects the performance of the optimizer on the Rastrigin function. In that situation, the suggested value far outperforms the others.

Table 3.34 Comparison of c_3, D = 2

	0.5	1.0	1.5	2.0
Ackley	30	30	30	30
	(1056 ; 1056)	(1343 ; 1343)	(2109 ; 2109)	(3619 ; 3619)
	7.03E-09	6.66E-09	6.79E-09	6.85E-09
	-	-	-	-
Griewank	30	30	30	30
	(1302 ; 1302)	(1423 ; 1423)	(2069 ; 2069)	(3328 ; 3328)
	4.96E-09	5.79E-09	6.39E-09	5.90E-09
	-	-	-	-
Rastrigin	27	29	30	30
	(1029 ; 931)	(1113 ; 1077)	(1725 ; 1725)	(2858 ; 2858)
	5.42E-09	5.60E-09	6.34E-09	5.36E-09
	2.27197	5.32634	-	-
Rosenbrock	28	29	29	29
	(1505 ; 1406)	(1721 ; 1665)	(2473 ; 2391)	(4157 ; 4021)
	5.84E-09	5.95E-09	6.64E-09	5.95E-09
	17.0834	4.38494	12.7596	5.06121

Table 3.35 Comparison of c_3, D = 5

	0.5	1.0	1.5	2.0
Ackley	30	30	30	30
	(1681 ; 1681)	(2165 ; 2165)	(3115 ; 3115)	(5262 ; 5262)
	8.74E-09	8.95E-09	8.46E-09	8.92E-09
	-	-	-	-
Griewank	0	1	1	1
	(0 ; 10000)	(2672 ; 9756)	(4051 ; 9802)	(5759 ; 9859)
	-	9.58E-09	4.59E-09	5.15E-09
	0.0353136	0.029392	0.0268431	0.0355125
Rastrigin	8	14	16	28
	(1980 ; 7197)	(2100 ; 6313)	(3008 ; 6271)	(5094 ; 5088)
	8.09E-09	7.25E-09	7.84E-09	7.87E-09
	3.96364	1.18151	1.27923	19.3903
Rosenbrock	0	0	0	0
	(0 ; 10000)	(0 ; 10000)	(0 ; 10000)	(0 ; 10000)
	-	-	-	-
	0.37862	0.183075	0.0373582	0.0957791

Table 3.36 Comparison of c_3, D = 10

	0.5	1.0	1.5	2.0
Ackley	25	30	30	30
	(2431 ; 3693)	(3015 ; 3015)	(4270 ; 4270)	(7567 ; 7567)
	9.42E-09	9.11E-09	9.43E-09	9.45E-09
	1.32678	-	-	-
Griewank	0	0	0	0
	(0 ; 10000)	(0 ; 10000)	(0 ; 10000)	(0 ; 10000)
	-	-	-	-
	0.119012	0.0934138	0.100532	0.127152
Rastrigin	0	0	0	2
	(0 ; 10000)	(0 ; 9672)	(0 ; 9668)	(7235 ; 9816)
	-	-	-	8.04E-09
	7.2632	8.12661	7.48062	2.98488
Rosenbrock	0	0	0	0
	(0 ; 10000)	(0 ; 10000)	(0 ; 10000)	(0 ; 10000)
	-	-	-	-
	5.08625	2.794	3.50441	8.64694

3.2.8.2 Repulsive Weight

According to Tables 3.37, 3.38 and 3.39, altering the repulsive weight in isolation has no statistically significant impact on the behavior of SM^{2}PSO.

Table 3.37 Comparison of ξ, D = 2

	0.10	0.40	0.70	1.00
Ackley	30	30	30	30
	(3558 ; 3558)	(3562 ; 3562)	(3583 ; 3583)	(3546 ; 3546)
	7.21E-09	7.83E-09	7.34E-09	6.36E-09
	-	-	-	-
Griewank	30	30	30	30
	(3384 ; 3384)	(3356 ; 3356)	(3629 ; 3629)	(3527 ; 3527)
	5.43E-09	4.79E-09	6.13E-09	5.73E-09
	-	-	-	-
Rastrigin	30	30	30	29
	(2658 ; 2658)	(2913 ; 2913)	(3003 ; 3003)	(3141 ; 3039)
	5.05E-09	5.83E-09	5.87E-09	6.01E-09
	-	-	-	3.84716
Rosenbrock	29	30	30	30
	(3999 ; 3866)	(3963 ; 3963)	(4093 ; 4093)	(4212 ; 4212)
	6.54E-09	5.64E-09	6.33E-09	6.62E-09
	7.11816	-	-	-

Table 3.38 Comparison of ξ, D = 5

	0.10	0.40	0.70	1.00
Ackley	30	30	30	30
	(5304 ; 5304)	(5294 ; 5294)	(5287 ; 5287)	(5279 ; 5279)
	8.85E-09	8.18E-09	8.94E-09	7.94E-09
	-	-	-	-
Griewank	2	0	0	0
	(7866 ; 9858)	(0 ; 10000)	(0 ; 10000)	(0 ; 10000)
	6.44918E-09	-	-	-
	0.0283463	0.0302499	0.034727	0.0309895
Rastrigin	26	28	27	25
	(4858 ; 5543)	(5002 ; 5335)	(5155 ; 5640)	(5249 ; 5046)
	7.18E-09	7.73E-09	8.14E-09	7.13E-09
	1.2437	0.994959	0.994959	15.9906
Rosenbrock	0	0	0	0
	(0 ; 10000)	(0 ; 10000)	(0 ; 10000)	(0 ; 10000)
	-	-	-	-
	0.074825	0.239591	0.136908	0.1528

Table 3.39 Comparison of ξ, D = 10

	0.10	0.40	0.70	1.00
Ackley	30	30	30	30
	(7528 ; 7528)	(7473 ; 7473)	(7567 ; 7567)	(7555 ; 7555)
	9.15E-09	9.26E-09	9.43E-09	9.10E-09
	-	-	-	-
Griewank	0	0	0	0
	(0 ; 10000)	(0 ; 10000)	(0 ; 10000)	(0 ; 10000)
	-	-	-	-
	0.125197	0.113771	0.108084	0.0843775
Rastrigin	1	1	0	0
	(6671 ; 9889)	(8644 ; 9955)	(0 ; 10000)	(0 ; 8737)
	9.4064E-09	9.78981E-09	-	-
	2.9851	2.88197	2.62006	11.6842
Rosenbrock	0	0	0	0
	(0 ; 10000)	(0 ; 10000)	(0 ; 10000)	(0 ; 10000)
	-	-	-	-
	3.42891	3.29591	3.81357	3.62984

3.2.8.3 Distance Factor

Again the Rastrigin function is the only one affected by changing this parameter. According to Tables 3.40, 3.41, and 3.42, increasing the distance factor to more than the recommended 2.0 decreases the chance of success on the Rastrigin function by approximately half.

Table 3.40 Comparison of γ, D = 2

	1.00	2.00	3.00	4.00
Ackley	30	30	30	30
	(3540 ; 3540)	(3516 ; 3516)	(3536 ; 3536)	(3678 ; 3678)
	6.64E-09	6.69E-09	7.10E-09	6.65E-09
	-	-	-	-
Griewank	30	30	30	29
	(3539 ; 3539)	(3298 ; 3298)	(3667 ; 3667)	(3797 ; 3672)
	5.20E-09	5.80E-09	5.30E-09	5.06E-09
	-	-	-	2.12026
Rastrigin	30	30	19	9
	(2622 ; 2622)	(2857 ; 2857)	(4052 ; 2586)	(7352 ; 2593)
	5.18E-09	6.15E-09	5.60E-09	4.32E-09
	-	-	6.75799	5.95434
Rosenbrock	30	30	26	21
	(3850 ; 3850)	(3674 ; 3674)	(4987 ; 4328)	(6613 ; 5980)
	5.79E-09	5.86E-09	6.02E-09	6.30E-09
	-	-	4.8047	1.50819

Table 3.41 Comparison of γ, D = 5

	1.00	2.00	3.00	4.00
Ackley	30	30	30	30
	(5354 ; 5354)	(5339 ; 5339)	(5305 ; 5305)	(5348 ; 5348)
	8.46E-09	8.61E-09	8.56E-09	8.57E-09
	-	-	-	-
Griewank	0	0	0	0
	(0 ; 10000)	(0 ; 10000)	(0 ; 10000)	(0 ; 10000)
	-	-	-	-
	0.030219	0.0304632	0.0334216	0.0389216
Rastrigin	28	26	14	3
	(4876 ; 5217)	(4898 ; 5246)	(6140 ; 5888)	(7578 ; 3117)
	7.59E-09	7.97E-09	6.69E-09	7.32E-09
	0.994959	10.0376	10.598	26.5719
Rosenbrock	0	0	0	0
	(0 ; 10000)	(0 ; 10000)	(0 ; 9369)	(0 ; 9015)
	-	-	-	-
	0.103521	0.0876706	22.1733	34.9598

Table 3.42 Comparison of γ, D = 10

	1.00	2.00	3.00	4.00
Ackley	30	30	30	30
	(7449 ; 7449)	(7602 ; 7602)	(7551 ; 7551)	(7519 ; 7519)
	9.15E-09	9.31E-09	9.31E-09	9.07E-09
	-	-	-	-
Griewank	0	0	0	0
	(0 ; 10000)	(0 ; 9336)	(0 ; 10000)	(0 ; 10000)
	-	-	-	-
	0.134971	0.608866	0.118739	0.094139
Rastrigin	1	2	1	0
	(7764 ; 9925)	(8455 ; 9897)	(8246 ; 8317)	(0 ; 4083)
	9.61952E-09	7.83286E-09	9.95728E-09	-
	2.91626	2.70061	17.9779	53.6415
Rosenbrock	0	0	0	0
	(0 ; 10000)	(0 ; 10000)	(0 ; 9948)	(0 ; 9669)
	-	-	-	-
	2.80571	3.3328	2.61896	436.407

3.2.9 Comparison of Heuristic Variations

Taking the previous results (or lack of significant differences in results) under consideration standard PSO, MPSO, M^{2}PSO, and SM^{2}PSO are compared here for 30 runs at 2, 5, 10, and 30 dimensions. The standard parameters are defined in Table 3.43, and the additional MPSO parameters are c_3 = 2, ξ = 0.4, and γ = 1.5. The mean number of evaluations is also added to the results as shown in Table 3.44.

The results (Tables 3.46, 3.47, 3.48, and 3.49) generally behave as those found in the literature. The most striking result is the failure of M^{2}PSO to find the global minimum even once. By abandoning local exploitation for global exploration, this variant never settles long enough to find good solutions near the current position. MPSO and SM^{2}PSO tend to arrive at the same results as PSO, but require at least twice as many

iterations. The mean fitness plots for all 2 and 30 dimensional runs of the Rosenbrock function in Figures 3.3 and 3.4 illustrate the swarm behavior over time. MPSO and SM^{2}PSO do not begin to show significant improvement until approximately 8,000 iterations with 30 dimensions. The higher energy in the modified swarms does seem to prevent local trapping since all three MPSOs usually terminate at the maximum number of iterations if the optimum is not found. For computationally inexpensive fitness functions, MPSO and SM^{2}PSO seem to be excellent candidates, but for the antenna problems presented in this paper, running 10,000 iterations would require in the vicinity of 100 days. Therefore, a standard PSO seems the better candidate here.

Table 3.43 Static Standard PSO Parameters for Heuristic Variation Testing

Particles	**K**	**V_{max}**	**c_1**	**c_2**	**ω**
30	9	0.35	1.4962	1.4962	[0.9, 0.5]
ω_{method}	**$Iterations_{Max}$**	**Threshold**	**Tolerance**	**Pop. Init.**	**Boundary Condition**
Linear	10,000	0	10^{-8}	Linear	Invisible

Table 3.44 Benchmark Result Key

No. Successful Runs
(Mean No. Iterations for Successful Runs ; Mean No. Iterations for All Runs)
Mean gbest of Successful Runs
Mean gbest of Unsuccessful Runs
(Mean No. Evaluations for Successful Runs ; Mean No. Evalutions for All Runs)

Table 3.45 Comparison of Heuristics, D = 2

	Ackley	Griewank	Rastrigin	Rosenbrock
PSO	30	30	30	30
	(1007 ; 1007)	(1161 ; 1161)	(544 ; 544)	(981 ; 981)
	7.63E-09	4.76E-09	5.37E-09	5.63E-09
	-	-	-	-
	[30218 ; 30218]	[34726 ; 34726]	[16315 ; 16315]	[29412 ; 29412]
MPSO	30	30	30	30
	(3972 ; 3972)	(3830 ; 3830)	(2929 ; 2929)	(4043 ; 4043)
	7.22E-09	5.72E-09	6.34E-09	5.44E-09
	-	-	-	-
	[119146 ; 119146]	[114831 ; 114831]	[87863 ; 87863]	[121138 ; 121138]
M^2PSO	0	0	0	0
	(0 ; 10000)	(0 ; 10000)	(0 ; 10000)	(0 ; 10000)
	-	-	-	-
	0.0142131	9.54E-06	0.00217619	0.000153799
	[0 ; 299992]	[0 ; 299995]	[0 ; 299951]	[0 ; 299978]
SM^2PSO	30	30	30	30
	(4231 ; 4231)	(3776 ; 3776)	(3108 ; 3108)	(4302 ; 4302)
	7.10E-09	4.93E-09	5.72E-09	5.65E-09
	-	-	-	-
	[126908 ; 126908]	[113217 ; 113217]	[93218 ; 93218]	[128927 ; 128927]

Table 3.46 Comparison of Heuristics, D = 5

	Ackley	Griewank	Rastrigin	Rosenbrock
PSO	30	3	30	23
	(1703 ; 1703)	(3539 ; 6228)	(1511 ; 1511)	(6727 ; 7491)
	8.55E-09	8.67E-09	7.75E-09	9.96E-09
	-	0.0155083	-	2.11376E-08
	[51022 ; 51022]	[105822 ; 183783]	[45339 ; 45339]	[201369 ; 224277]
MPSO	30	0	30	0
	(6306 ; 6306)	(0 ; 10000)	(5605 ; 5605)	(0 ; 10000)
	8.82E-09	-	7.78E-09	-
	-	0.0261473	-	0.00231468
	[188306 ; 188306]	[0 ; 296924]	[168093 ; 168093]	[0 ; 295195]
M^2PSO	0	0	0	0
	(0 ; 10000)	(0 ; 10000)	(0 ; 10000)	(0 ; 10000)
	-	-	-	-
	0.890971	4.35E-02	3.4208	0.513748
	[0 ; 300000]	[0 ; 300000]	[0 ; 300000]	[0 ; 300000]
SM^2PSO	30	5	30	0
	(6497 ; 6497)	(8008 ; 9668)	(5759 ; 5759)	(0 ; 10000)
	8.72E-09	7.33E-09	7.88E-09	-
	-	0.0256227	-	0.000818859
	[194018 ; 194018]	[238353 ; 287213]	[172646 ; 172646]	[0 ; 295271]

Table 3.47 Comparison of Heuristics, D = 10

	Ackley	Griewank	Rastrigin	Rosenbrock
PSO	30	0	2	0
	(2362 ; 2362)	(0 ; 5601)	(3373 ; 7504)	(0 ; 10000)
	9.24E-09	-	9.36E-09	-
	-	0.073049	2.45186	2.10653E-06
	[70200 ; 70200]	[0 ; 165935]	[100681 ; 221231]	[0 ; 298434]
MPSO	30	0	15	0
	(9117 ; 9117)	(0 ; 10000)	(9035 ; 9517)	(0 ; 10000)
	9.05E-09	-	8.67E-09	-
	-	0.152055	1.21637	0.00279292
	[268458 ; 268458]	[0 ; 294041]	[268688 ; 283030]	[0 ; 293544]
M^2PSO	0	0	0	0
	(0 ; 10000)	(0 ; 10000)	(0 ; 10000)	(0 ; 10000)
	-	-	-	-
	3.26447	3.32E-01	26.1365	1.15593
	[0 ; 300000]	[0 ; 300000]	[0 ; 300000]	[0 ; 300000]
SM^2PSO	29	0	7	0
	(9366 ; 9387)	(0 ; 10000)	(8836 ; 9728)	(0 ; 10000)
	9.34E-09	-	8.16E-09	-
	4.52771E-08	0.119928	1.99091	0.0023779
	[275810 ; 276410]	[0 ; 293952]	[262680 ; 288468]	[0 ; 293400]

Table 3.48 Comparison of Heuristics, D = 30

	Ackley	Griewank	Rastrigin	Rosenbrock
PSO	1	11	0	29
	(3897 ; 4916)	(2775 ; 2977)	(0 ; 10000)	(6769 ; 6876)
	9.20E-06	9.42E-06	-	9.98E-06
	2.28951	0.0262267	25.1393	1.49947E-05
	[115285 ; 145728]	[82232 ; 88363]	[0 ; 293752]	[201510 ; 204756]
MPSO	0	0	0	0
	(0 ; 10000)	(0 ; 10000)	(0 ; 10000)	(0 ; 10000)
	-	-	-	-
	3.52968	0.939203	56.1779	2.23137
	[0 ; 290553]	[0 ; 291651]	[0 ; 290866]	[0 ; 290765]
M^2PSO	0	0	0	0
	(0 ; 10000)	(0 ; 10000)	(0 ; 10000)	(0 ; 10000)
	-	-	-	-
	3.79775	1.03E+00	101.161	3.72467
	[0 ; 300000]	[0 ; 300000]	[0 ; 300000]	[0 ; 300000]
SM^2PSO	0	0	0	0
	(0 ; 10000)	(0 ; 10000)	(0 ; 10000)	(0 ; 10000)
	-	-	-	-
	3.57189	0.947421	59.9444	2.29237
	[0 ; 290535]	[0 ; 291704]	[0 ; 290805]	[0 ; 290732]

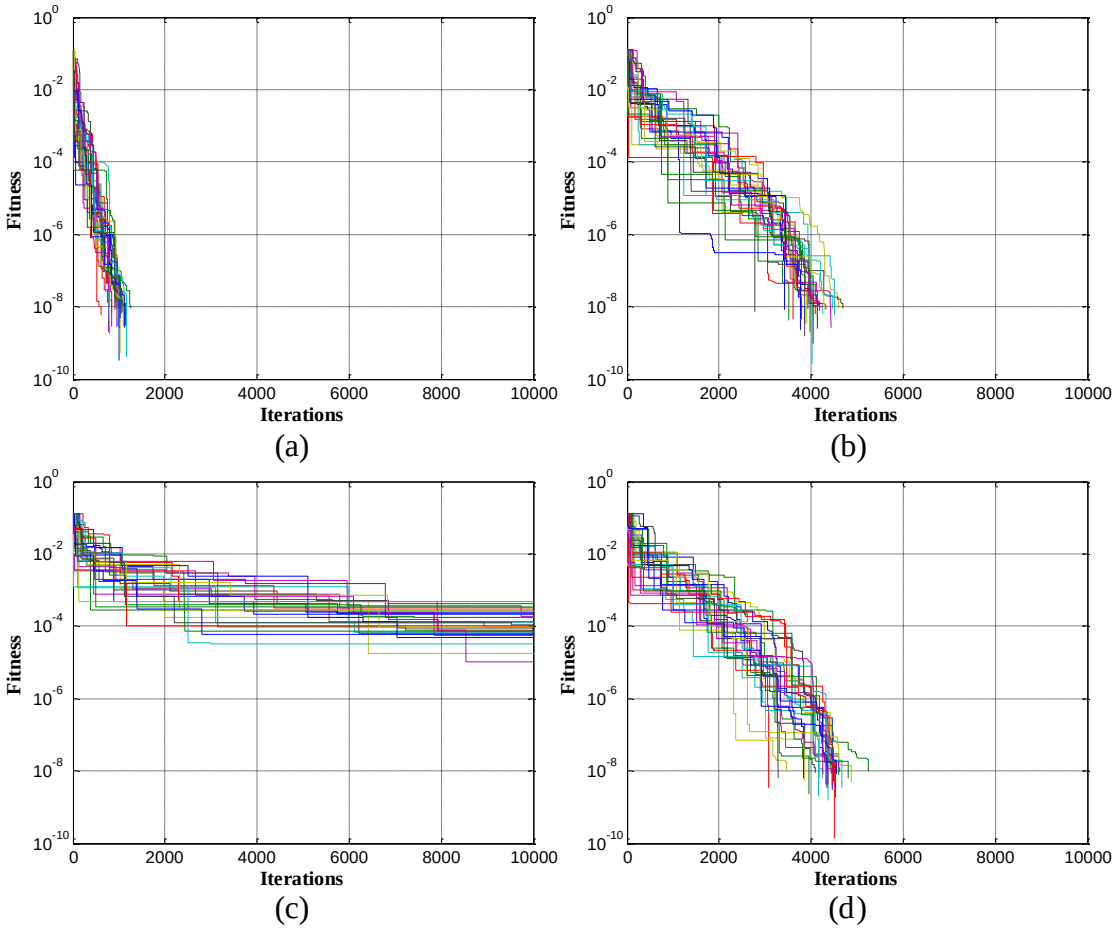

Figure 3.3 Comparison of PSO Variants Applied to the 2D Rosenbrock Function

(a) PSO
(b) MPSO
(c) M^2PSO
(d) SM^2PSO

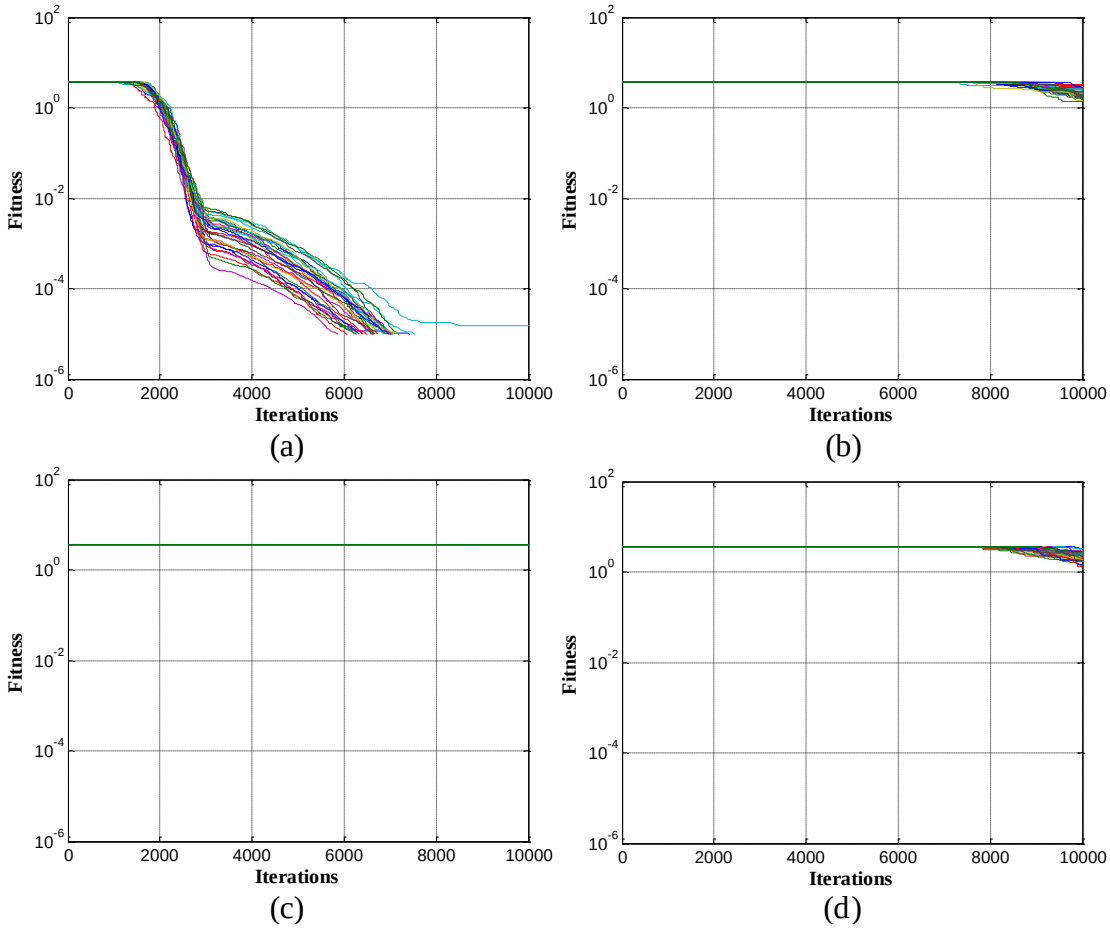

Figure 3.4 Comparison of PSO Variants Applied to the 30D Rosenbrock Function

(a) PSO
(b) MPSO
(c) M^2PSO
(d) SM^2PSO

CHAPTER IV

OPTIMIZATION OF IMPLANTABLE ANTENNAS

Released in 2005 the Zarlink ZL70101 transceiver introduces an interesting design target for IMDs. To minimize energy consumption, the chip pairs a highly efficient wakeup receiver operating at the 2.45 GHz industrial, scientific, and medical (ISM) band with a MICS transceiver that only powers up on demand [77]. To achieve the longest life, implants employing this chip must have antennas for both the MICS and ISM bands. The complex geometry required to operate at the requisite bands in the tiny volume available lends itself to design by optimization since the solution cannot be directly calculated analytically.

4.1 Model and Optimization Definition

As the antenna is intended for use inside the human body, it is important to understand the electrical characteristics of the operating environment. As discussed in section 2.1, the dielectric properties of tissue exhibit frequency-dependent behavior. The targeted applications for this optimization are sub-dermal, so skin is the only tissue of consequence. Figure 4.1 gives the permittivity and conductivity of skin [6]-[8].

A serpentine PIFA geometry is selected for optimization due to its adaptability in dual-frequency use. Based on recommendations of high permittivity in [4], we choose Rogers RO3210 (ε_r = 10.2, tan δ = 0.003) as the as the sub- and superstrate. A block of

skin (30.5 mm x 30.5 mm x 8.5 mm) surrounds the antenna. Figure 4.2 illustrates the model configuration.

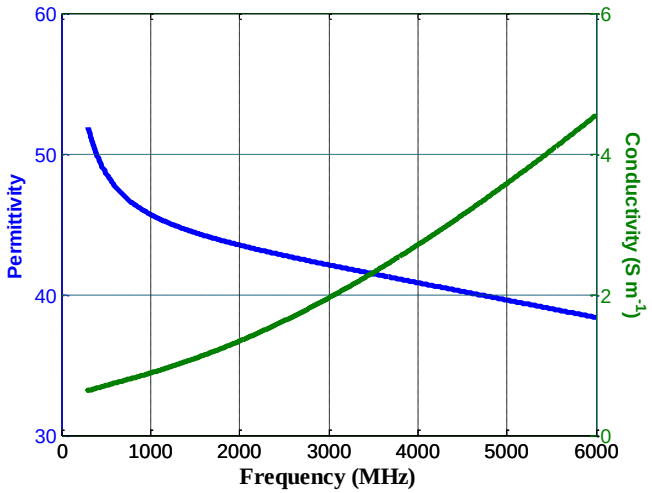

Figure 4.1 Dielectric Properties of Human Skin

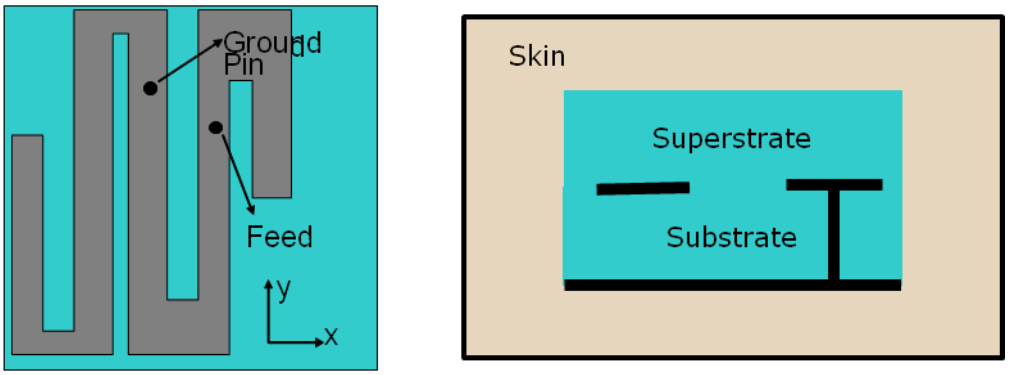

Figure 4.2 Implantable Serpentine PIFA Model

(a) Top View
(b) Profile

Beginning with a rough approximation of the necessary dimensions, the geometry is parameterized as shown in Figure 4.3. A standard gbest PSO with the parameters

given in Table 4.1 controls the behavior of the particle swarm and passes each candidate geometry to Ansys's High Frequency Structure Simulator (HFSS) for fitness evaluation. The optimization procedure maintains constant sub- and superstrate and patch perimeters: L_{sub} = W_{sub} = 22.5 mm; thickness = 1.25 mm; L_p = 22 mm; and W_p = 17.75 mm. Three parameters – center position, P_s; width, W_s; and length, L_s – define each of the four slots. L_c determines the length of the right strip. The remaining parameters – F_y, P_x, and P_y – locate the feeding and shorting pins. These parameters constitute a 16-D solution with possible values listed in Table I subject to the following constraints:

$$L_{si} < L_p, i = 1,2,3 \tag{4.1}$$

$$P_{s1} - \frac{W_{s1}}{2} > -10.75 \tag{4.2}$$

$$P_{s4} + \frac{W_{s4}}{2} > 7 \tag{4.3}$$

$$P_{si} + \frac{W_{si}}{2} < P_{s(i+1)} - \frac{W_{s(i+1)}}{2}, i = 1,2,3 \tag{4.4}$$

$$L_c < L_{s4} \tag{4.5}$$

Because the goal of the optimization is improving antenna performance around the center frequencies of the MICS and ISM bands (402 MHz and 2.4 GHz), we define the fitness function as

$$fitness = \max(S_{11@402\text{MHz}}, S_{11@2.4\text{GHz}}) \tag{4.6}$$

and the objective is, therefore, to minimize the fitness function. If the return loss in both bands falls below -10 dB, then the antenna should satisfy its purpose. Rather than waiting for convergence or a fixed number of iterations, the procedure halts if the

objective value drops below -20 dB. Using a threshold twice as low as the desired result should encourage better than bare-minimum solutions.

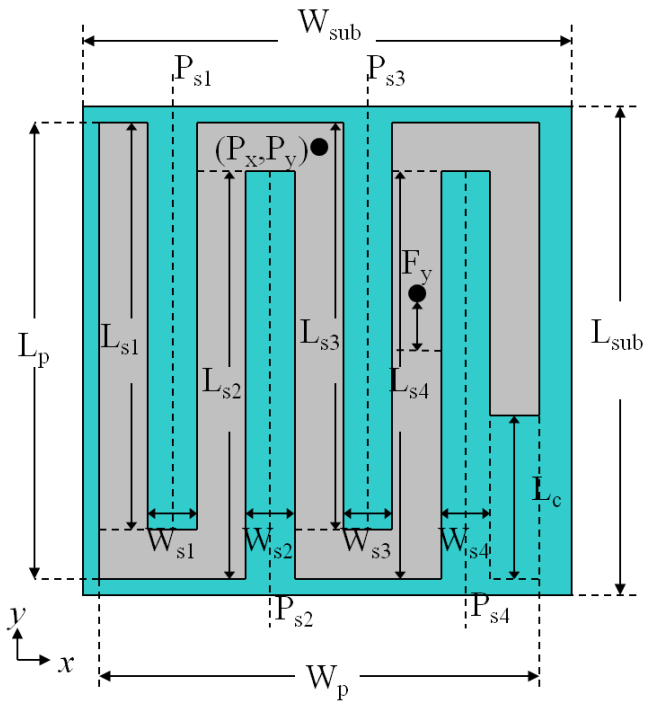

Figure 4.3 Parameterization of the Serpentine Geometry

Table 4.1 PSO Parameters for Implantable Antenna Optimization

Particles	**k**	**V_{max}**	**c_1**	**c_2**	**ω**
10	9	0.1	2.0	2.0	[0.9, 0.4]
ω_{method}	**$Iterations_{Max}$**	**Threshold**	**Tolerance**	**Pop. Init.**	**Boundary Condition**
Linear	500	-20	10^{-5}	Random	Invisible

4.2 Results and Refinement

After 133 iterations, the optimization returns the geometry defined by Table 4.2 with a fitness value of -21.1976. Analysis of the swarm behavior during the run shows that while the mean fitness fluctuated widely, the minimum at each iteration always fell near gbest as shown in Figure 4.4. Given that any fitness less than -10 dB would have technically solved the problem, the optimizer found many candidate solutions. The full frequency response of the optimized antenna is given in Figure 4.5. The radiation and gain patterns in Figures 4.6 and 4.7 reveal the low levels expected from such a small aperture. The maximum gain is approximately -25 dBi for MICS and -8 dBi for ISM.

Table 4.2 Serpentine Optimization Parameters

Symbol	Range (mm)	Optimized (mm)
P_{s1}	[-8 , -6]	-7.0
W_{s1}	[0.5 , 3]	2.7
L_{s1}	[19 , 21]	19.1
P_{s2}	[-4 , -3]	-3.9
W_{s2}	[0.3 , 3]	0.5
L_{s2}	[19 , 21]	20.1
P_{s3}	[0 , 1]	0.5
W_{s3}	[0.5 , 3]	2.0
L_{s3}	[17 , 18.5]	18.0
P_{s4}	[3.0 , 4.5]	3.5
W_{s4}	[0.5 , 3]	0.6
L_{s4}	[16.5 , 18.5]	17.5
L_c	[6 , 11]	9.6
F_y	[- 2, 2]	0.1
P_x	[0.1 , 1.5]	0.2
P_y	[0.1 , 5]	0.2

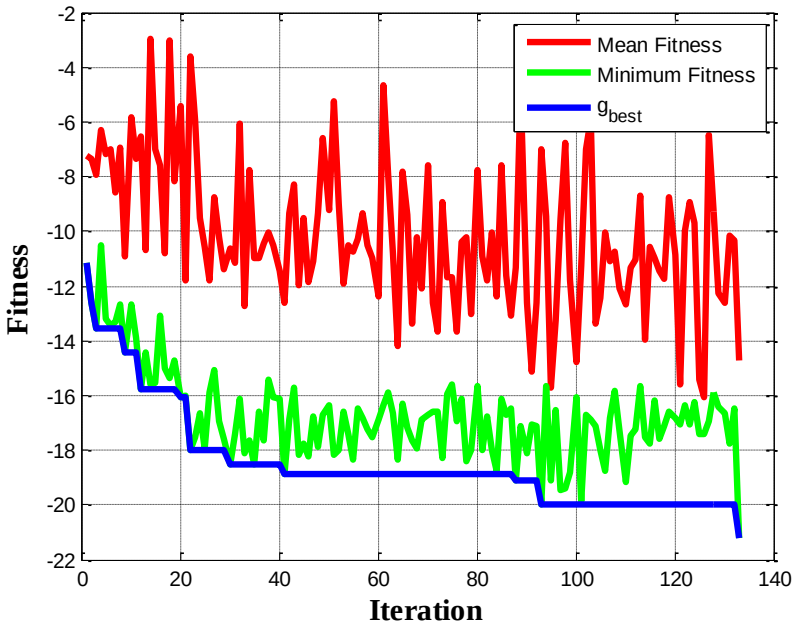

Figure 4.4 Comparison of Fitness Values During Implantable Antenna Optimization

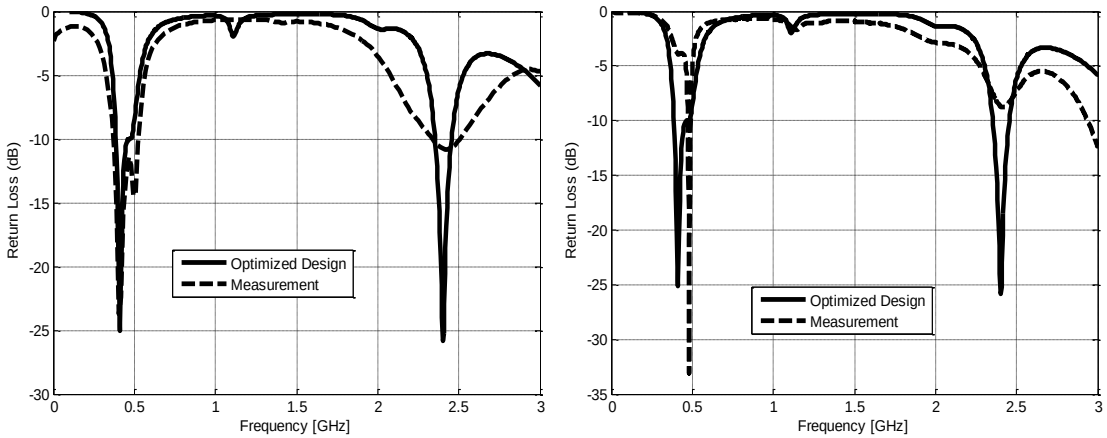

Figure 4.5 Comparison of Simulated and Measured Serpentine Antenna Return Loss

(a) MICS
(b) ISM

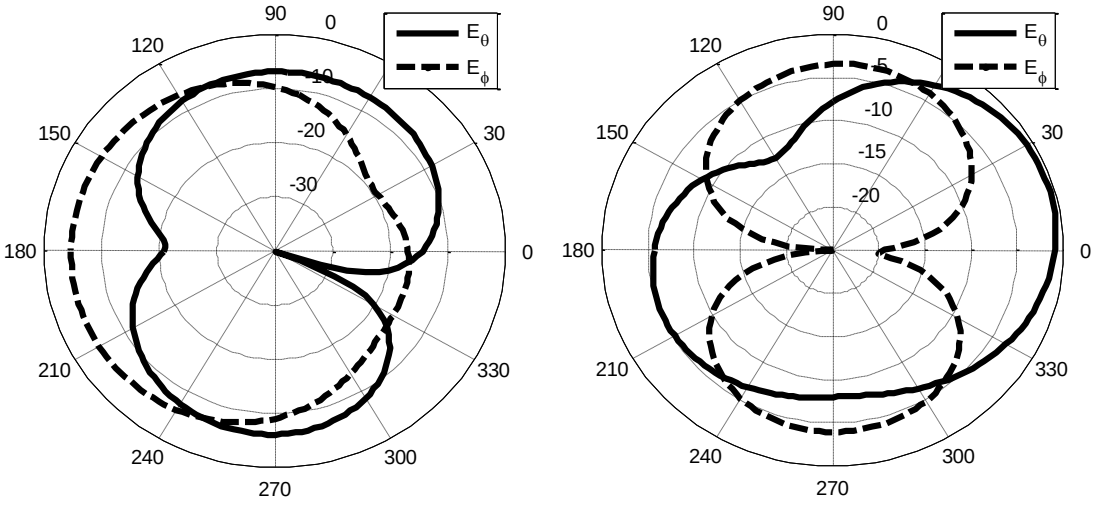

(a) (b)

Figure 4.6 Simulated Radiation Patterns of the Optimized Antenna

(a) 402 MHz
(b) 2.4 GHz

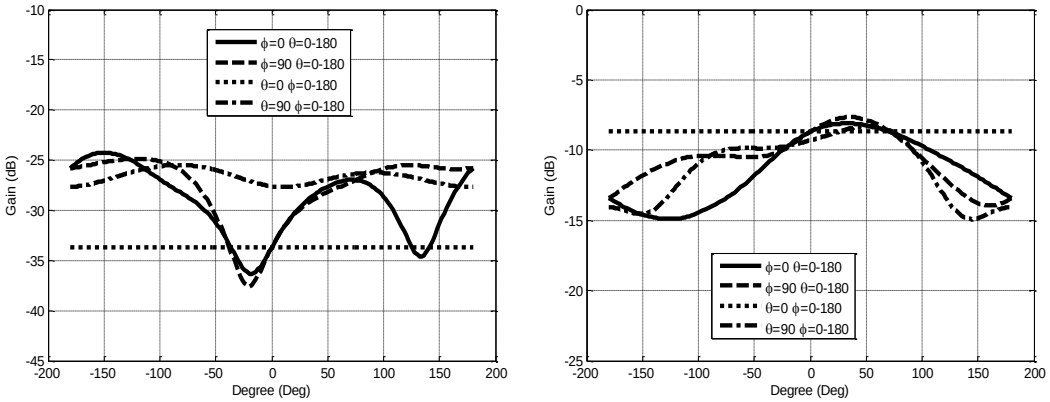

(a) (b)

Figure 4.7 Simulated Gain Patterns of the Optimized Antenna

(a) 402 MHz
(b) 2.4 GHz

With no humans lining up for experimental antenna implants, gels were developed to mimic skin's dielectric properties in order to validate the fabricated antenna's performance. Using the HP8753D configuration shown in Figure 4.8, the

fabricated antenna (Figure 4.9) produces the measured results of Figure 4.5. Results demonstrate -10 dB bandwidths of 35% and 7% for MICS and ISM operation, respectively. As of this writing the journal paper [9] describing this work has more than 120 citations.

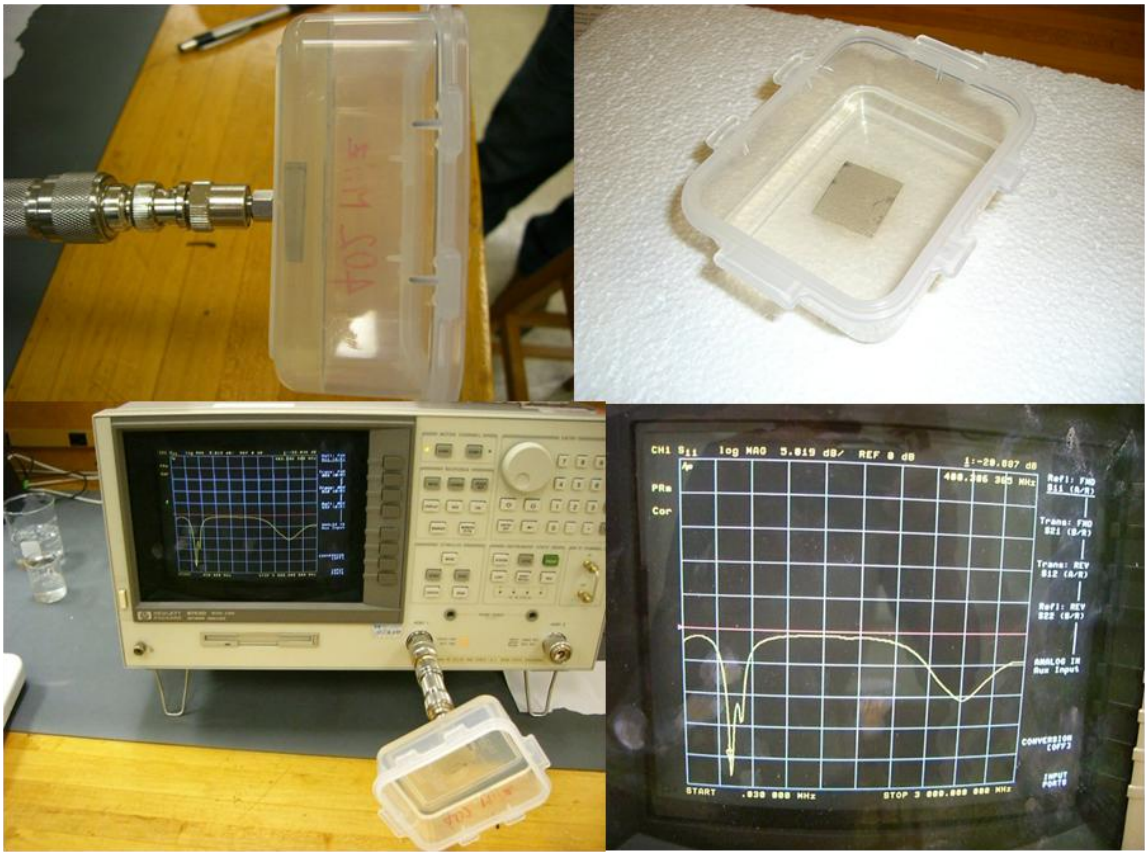

Figure 4.8 Antenna Measurement Setup

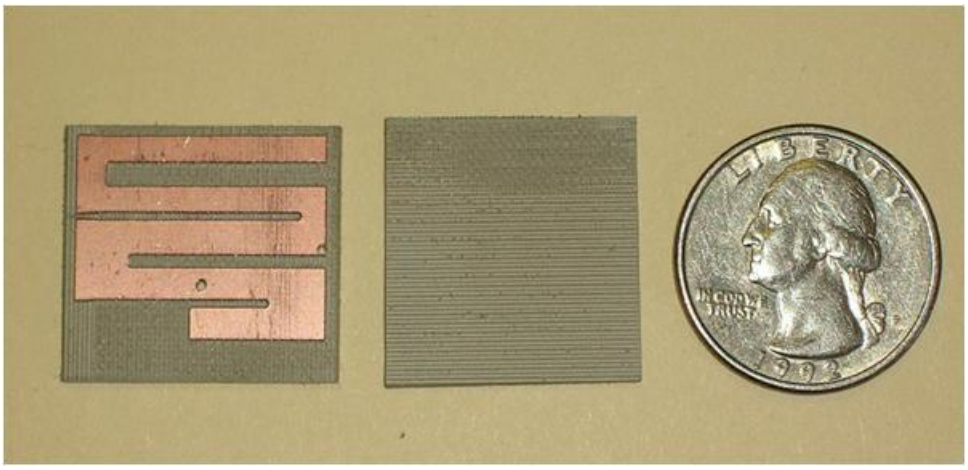

Figure 4.9 Fabricated Serpentine PIFA Layers

Since human testing is heavily regulated and very expensive, animal testing offers a reasonable (though still regulated and expensive) alternative. In [10] the MSU electromagnetics research group measures the complex permittivity of excised nude rat skin from 500 MHz to 20 GHz with the assistance of the MSU College of Veterinary Sciences. From this data, new mimicking gels are developed to test the performance of the antenna from [9]. [11] shows the refinement of the ISM gel to more accurately reflect the skin's properties. Permittivity and conductivity differ from measurements by 0.5% and 3.4%, respectively, and the S_{11} results match more closely. Finally from 2010, [78] presents the results of *in vivo* testing of the antenna. Although functional, the antenna measurements and simulations display many discrepancies. Contributing factors may include air pockets between the skin and antenna and the lack of interstitial fluid in simulations.

In the quest for a miniaturized version of this antenna, the previous optimization is performed again, but the length and width of the patch of the patch are added

dimensions [79]. Because the objective is to minimize surface area and return loss of the antenna, a term describing the normalized area is added to the objective function.

$$\min\left(\frac{A - A_{\min}}{A_{\max} - A_{\min}} + \frac{\max(S_{11@402\text{MHz}}, S_{11@2.4\text{GHz}})}{10}\right) \tag{4.7}$$

Optimization produces a result (Figure 4.10 and Table 4.3) that occupies only 57% of the surface area of its predecessor. While simulations show its efficacy (Figure 4.10), this antenna has not been fabricated because the second slot is too small at 0.14 mm for the available milling tools. The scale representation shown in Figure 4.3 offers some perspective.

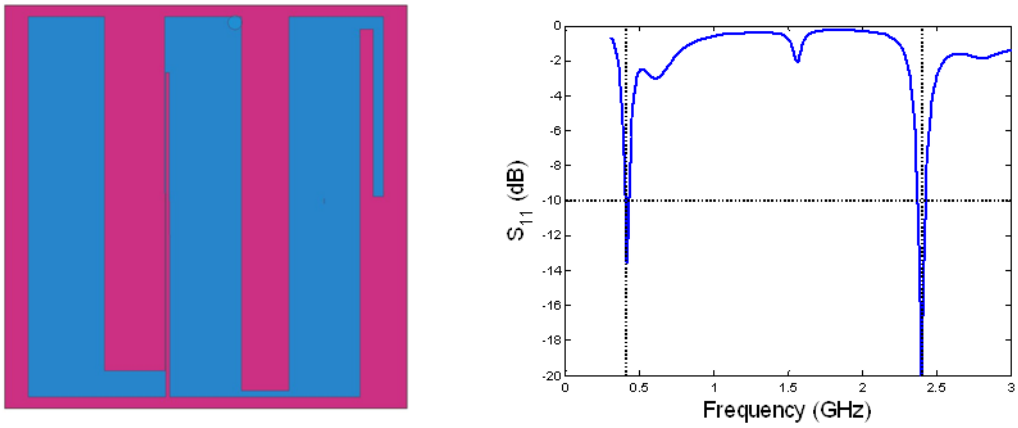

(a) (b)

Figure 4.10 Miniaturized Serpentine PIFA Geometry and Frequency Response

(a) Scale View
(b) Simulated Return Loss

Table 4.3 Miniaturized Serpentine Optimization Parameters

Symbol	Range (mm)	Optimized (mm)
P_{s1}	[-8.5, -6]	-6.24
W_{s1}	[0.1, 3]	2.58
L_{s1}	[10, 21]	15.09
P_{s2}	[-5, -2]	-4.84
W_{s2}	[0.1, 1.5]	0.14
L_{s2}	[10, 21]	14.77
P_{s3}	[-1, 2]	-0.96
W_{s3}	[1, 3]	1.95
L_{s3}	[10, 21]	16.11
P_{s4}	[2.5, 4.5]	3.61
W_{s4}	[0.1, 1.5]	0.55
L_{s4}	[10, 21]	15.61
L_c	[8, 10.5]	8.39
F_y	[-0.5, 0.5]	0.24
P_x	[0.1 , 0.5]	0.27
P_y	[0.1 , 0.5]	0.22
W_p	[15, 22]	16.54
L_p	[15, 17.75]	15.05

Since the FCC added the MICS spectrum to the available ISM bands for medical applications, more than 70 papers have been published regarding implantable antennas, but only about 10 consider dual-band operation. Among those, there are only four research groups and four antenna geometries concerned. The MSU serpentine is discussed above. In [80] and [81], researchers present a short-circuited split ring resonator (SRR). Its active elements only require circle of diameter 13.4 mm on an ARLON1000 substrate, but with the feeding layer, the total height is 3.81 mm. The

paper does not specify dimensions for the ground plane but given the 14 mm feed line and a scale drawing, it's estimated to be 20 mm x 20 mm. [82]-[84] describe an implantable capsule of approximate size 000 (10 mm diameter, 32.1 mm length) with a stepped pyramidal PIFA. This concept integrates electronics and batteries with the antenna in a single package. At 10 mm x 10 mm x 2.54 mm, the four-layer stacked PIFA in [85] claims triple-band coverage, but actually behaves like a dual-band antenna. The wide lower band simply covers the named MICS and 433 MHz ISM bands in addition to the 2.4 GHz ISM band.

CHAPTER V

OPTIMIZATION OF ANTENNAS FOR ADJUVANT HYPERTHERMIA IN BREAST CANCER TREATMENT

While hyperthermia has been shown to be effective in treating cancer, application of the therapy is typically cumbersome. Shielded rooms are required. Constant thermometry, often via magnetic resonance imaging, is required. A system that eliminates these requirements could increase the availability of thermotherapy by allowing it to be applied in a less restrictive environment such as a standard chemotherapy center. In the case of breast cancer, for instance, patients could wear a brassiere-like device while sitting in a chair, reading a magazine. In order to eliminate the shielded room, power requirements must be low. To eliminate the thermometry, temperature application must be consistently predictable.

To more easily accomplish this task, it makes sense to use frequency bands that have already been allocated for medical use. The ISM bands allow unlicensed operation with low power levels. In the United States, the available bands are 915 MHz, 2.4 GHz, and 5.8 GHz; in Europe, the 433 MHz band is also available. In systems employing multiple channels and frequency-hopping, transmitted power may be as high as 4 W [114].

Solving this problem involves a series of decisions. First, the frequency of operation should be selected. Second, several antenna elements should be optimized for

the breast applicator system and compared. Third, the selected element should be organized into an array, and the specific absorption rate (SAR) should be optimized for uniformity across the breast. SAR defines the average amount of power absorbed over a sample volume of human tissue, and is calculated as

$$\mathrm{SAR} = \int \frac{\sigma(\mathbf{r})|\mathbf{E}(\mathbf{r})|^2}{\rho(\mathbf{r})} d\mathbf{r} \tag{5.1}$$

Selecting the most appropriate frequency requires tradeoffs between antenna size and penetration depth of the field. To do this, I optimize a series of rectangular patches for each ISM band on a rectangular layered model consisting of a bolus, skin, and adipose breast tissue.

5.1 Model Definition

Evaluating the most appropriate frequency for hyperthermia requires an anatomically accurate (though perhaps simplified) model. For electromagnetic simulations of biological entities, all aspects of the subject are important including the geometry, electrical properties, and physical properties of the tissue.

While there is no reliable consensus as to the most common breast size, U.S. brassiere sizes 34B or 36C are often identified. The number in the size indicates the circumference of the chest in inches, while the letter specifies the cup size of each breast relative to the chest circumference. Unfortunately this is another measurement that is only approximately standardized across manufacturers, but sizes 34B and 36C roughly translate to breast diameters of 114 mm and 131 mm, respectively [115]. For the initial

optimization, size 34B may be most appropriate as the problem should be easier to scale up in size than down.

As shown in Figure 5.1 there are four primary tissue regions involved in the human breast: skin, breast tissue, muscle, and bone [116]. Skin surrounding the breast ranges in thickness from 0.8-3.0 mm [117] with a mean of 1.55 mm ± 0.25 mm [118]. Breast tissue is a bit more complicated in that it contains three distinct, non-homogeneous tissues that are non-uniformly distributed or concentrated across individuals. Adipose tissue (fat) occupies the bulk of the breast in most women with the remainder composed of fibrous tissue (ligaments and other connective components) and glandular tissue (lactation ducts and glands). A fourth subtype not found in Figure 5.1 but present in breast cancer patients is malignant tissue. The breast attaches to the chest wall, which is primarily muscle, vertically occupying the space bounded by the second and sixth ribs. Bones comprise two types of tissue, cortical and cancellous. Cortical bone makes the hard outer shell of bones while the slightly spongier cancellous bone fills the interior. For the purposes of this work, cancellous bone can be assumed to occupy approximately the center half of each rib. By approximating the median size of the ribs as an ellipse of major diameter 12 mm and minor diameter 7 mm, the thickness of the chest wall can be estimated at a minimum of 15 mm. When calculating SAR, the mass density of an object is required; typical values for the requisite tissues are shown in Table 5.1.

Table 5.1 Mass Density of Breast Tissues

Tissue	Skin	Breast, Type 1	Breast, Type 2	Breast, Type 3	Breast, Malignant	Muscle	Bone, Cortical	Bone, Cancellous
Density ($kg \cdot m^{-3}$)	1109	1058	984.5	911	1058	1090	1908	1178

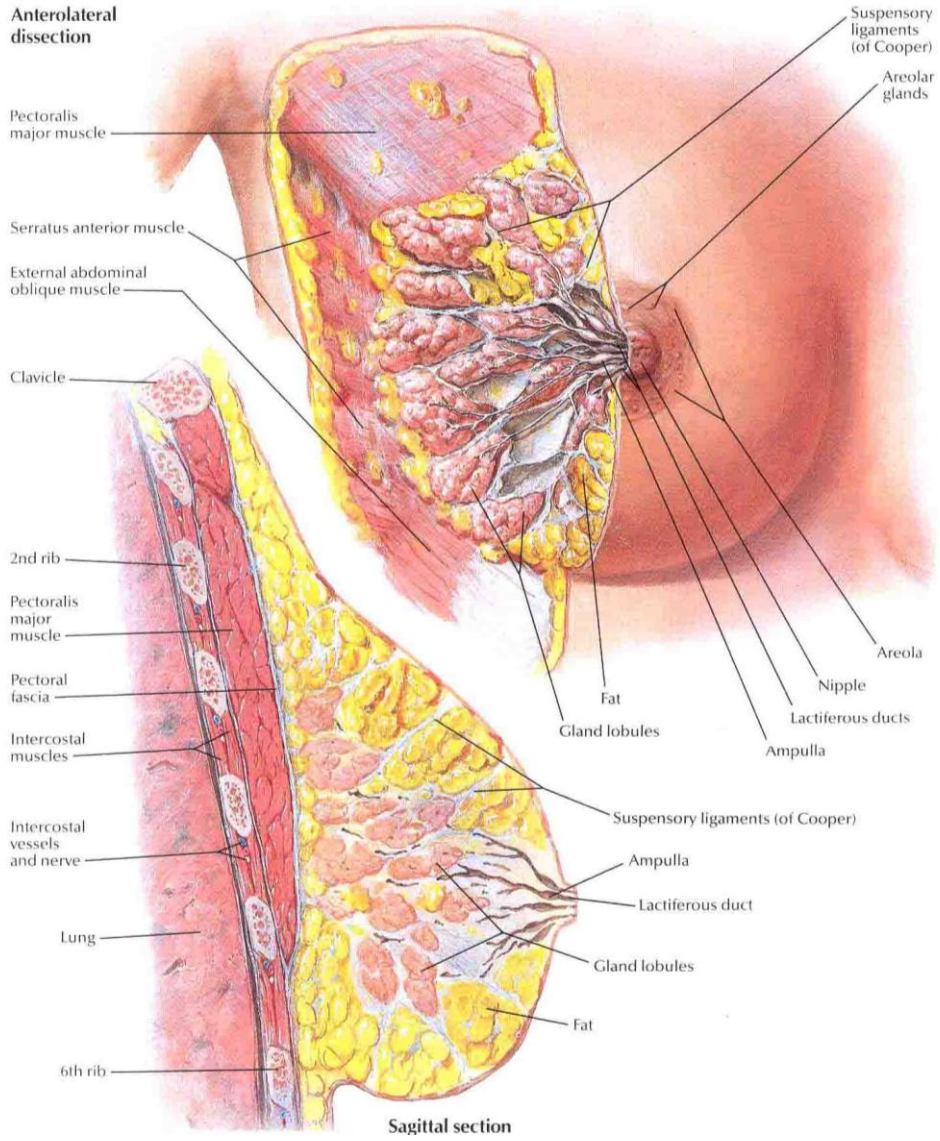

Figure 5.1 Breast Anatomy Illustration by Frank H. Netter, M.D. [116]

The dielectric properties of skin in this situation are identical to those previously shown in Figure 4.1. The permittivity and conductivity of the remaining tissues as described in [6-8] are shown in Figure 5.2. Astute readers may notice the lack of diverse breast tissues. To address this shortfall, a team comprising scientists from the Universities of Wisconsin and Calgary conducted experimental measurements of dielectric properties on normal and cancerous breast tissue samples collected from 289 patients undergoing breast reduction, lumpectomy, mastectomy, or biopsy procedures [119]–[121]. Pathologists categorized each sample by its status and adipose content as malignant (type 4) or normal types 1 (containing 0-30% adipose tissue), 2 (containing 31-84% adipose tissue), and 3 (containing 85-100% adipose tissue). From the measurements, the authors developed Cole-Cole and Debye models of the complex permittivity of each type of tissue. The Debye model is defined by

$$\begin{aligned}\hat{\varepsilon}_d(\omega) &= \varepsilon'_d(\omega) - j\varepsilon''_d(\omega) \\ &= \varepsilon_\infty + \sum_{n=1}^{N} \frac{\Delta\varepsilon_{dn}}{1 + j\omega\tau_{dn}} + \frac{\sigma_s}{j\omega\varepsilon_0}\end{aligned} \tag{5.2}$$

where the subscript *d* indicates Debye and *N* denotes the number of poles. Applying the second order Debye parameters from Table 5.2 [121] yields the frequency-dependent permittivity and conductivity curves shown in Figure 5.3.

In addition to the natural components, a hyperthermia applicator typically includes a fluid bolus, which serves two purposes. The first is to enhance the physical and electromagnetic coupling between the radiating elements and the tissue. The second is to assist in heat distribution and cooling the skin's surface to prevent hot spots and blisters [122]–[123]. While most bolus designs in the literature specify water as the fluid,

[124] investigates the effectiveness of silicone oil. The authors find that a silicone oil bolus provides a smoother and deeper SAR distribution than a water bolus of equivalent thickness. The result is attributed to the increased effective wavelength of the radiating element when exposed to silicone oil which has a relative permittivity of 2.1-2.8 versus approximately 81 for water. Based on the results, the authors suggest a bolus thickness of 2.5-5 mm. Although the permittivity of water varies quite a bit with frequency and temperature, the permittivity of silicone oil is relatively stable. Silicone oil also benefits from lower conductivity, $\sigma = 10^{-13}$ S·m^{-1}, than water, $\sigma = 10^{-4}$ S·m^{-1}, which results in lower power dissipation in the bolus.

Table 5.2 Two-Pole Debye Model Parameters for Breast Tissue [121]

	Type 1	Type 2	Type 3	Type 4
ε_∞	7.82	5.57	3.14	6.75
σ_s (S·m^{-1})	0.71	0.52	0.04	0.79
$\Delta\varepsilon_{d1}$	20.81	19.64	0.58	25.61
$\Delta\varepsilon_{d2}$	20.22	14.23	1.09	23.91
τ_{d1} (ps)	7.39	5.81	8.07	7.22
τ_{d2} (ps)	15.18	16.49	19.25	15.30

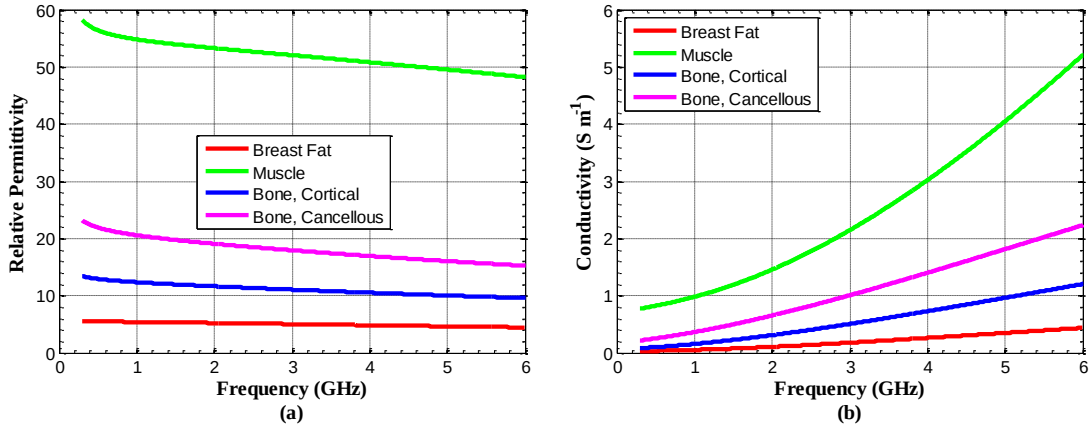

Figure 5.2 Dielectric Properties of Tissues Surrounding the Breast [6]-[8]

(a) Relative Permittivity
(b) Conductivity

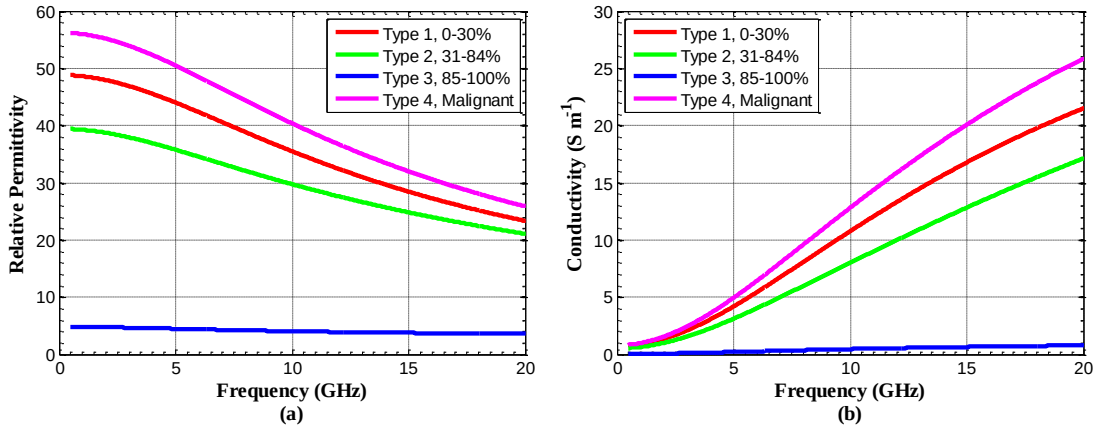

Figure 5.3 Dielectric Properties of Breast Tissues [121]

(a) Relative Permittivity
(b) Conductivity

5.2 Hyperthermia Array Optimization

Using the described tissue properties, three simulation configurations are defined to complete different phases of the optimization. First, a rectangular, layered model is used for single antenna optimization. Second, a simplified, geometrically accurate model with electrically uniform breast tissue as defined by normal type 3 ([119]–[121]) is used

to arrange array elements and optimize SAR distribution. Third, normal tissue types 1 and 2 are added to the previous model to examine the effects of heterogeneous dielectrics.

5.2.1 Element Optimization

5.2.1.1 Optimization Configuration

To evaluate the frequency options, simple rectangular patches are optimized using an OAPSO procedure to resonate at each MICS band (433 MHz, 915 MHz, 2.441 GHz, and 5.8 GHz). As described in Chapter IV, the optimizer passes the candidate geometry to HFSS for fitness evaluation. Each antenna is mounted on a 1.28 mm thick Rogers RO3010 (ε_r = 10.2, tan δ = 0.0035) substrate; by using a dielectric with relatively high permittivity, a small size reduction is realized compared to a lower permittivity substrate. Figure 5.4 captures the basic geometry of the model; however, the exact geometry for each frequency is a bit different. The height of each layer is consistent for all simulations, but the length and width are determined as the maximum of 50 mm or half the wavelength of the frequency of interest in free space plus the length or width of the ground plane. Additionally the ribs are dynamically generated based on the space available with an upper limit of seven; a distance equal to the major-radius of cortical bone separates each rib. For instance at 433 MHz the width (547 mm) far exceeds the space required for seven ribs (120 mm), while the model can only contain 2 ribs at 5.8 GHz. The dimensions of each model are given in Table 5.3.

Each antenna is evaluated as a three-dimensional optimization problem defined by the length, L, and width, W, of the patch and the distance of the feed, $D_{f,}$ from the center

of the patch along the length of the element (Figure 5.4(b)). The return loss for each antenna is minimized by the fitness function

$$fitness = S_{11}(f_c) \tag{5.3}$$

where f_c is the frequency of interest, subject to the constraints

$$D_f \leq {}^{L}/_{2} \tag{5.4}$$

The PSO parameters are given in Table 5.4, and Table 5.5 lists the constrained values.

Table 5.3 Single Element Model Dimensions

Optimization	433 MHz	915 MHz	2441 MHz	5800 MHz
L_{sample} (mm)	547	264	102	50
W_{sample} (mm)				
$L_{substrate}$ (mm)	200	100	40	20
$W_{substrate}$ (mm)				
$h_{substrate}$ (mm)	1.28			
h_{bolus} (mm)	2.50			
h_{skin} (mm)	1.55			
h_{breast} (mm)	100.00			
h_{muscle} (mm)	20.00			
$d_{maj,cortical}$ (mm)	12.00			
$d_{min,cortical}$ (mm)	7.00			
$d_{maj,cancellous}$ (mm)	6.00			
$d_{min,cancellous}$ (mm)	3.50			

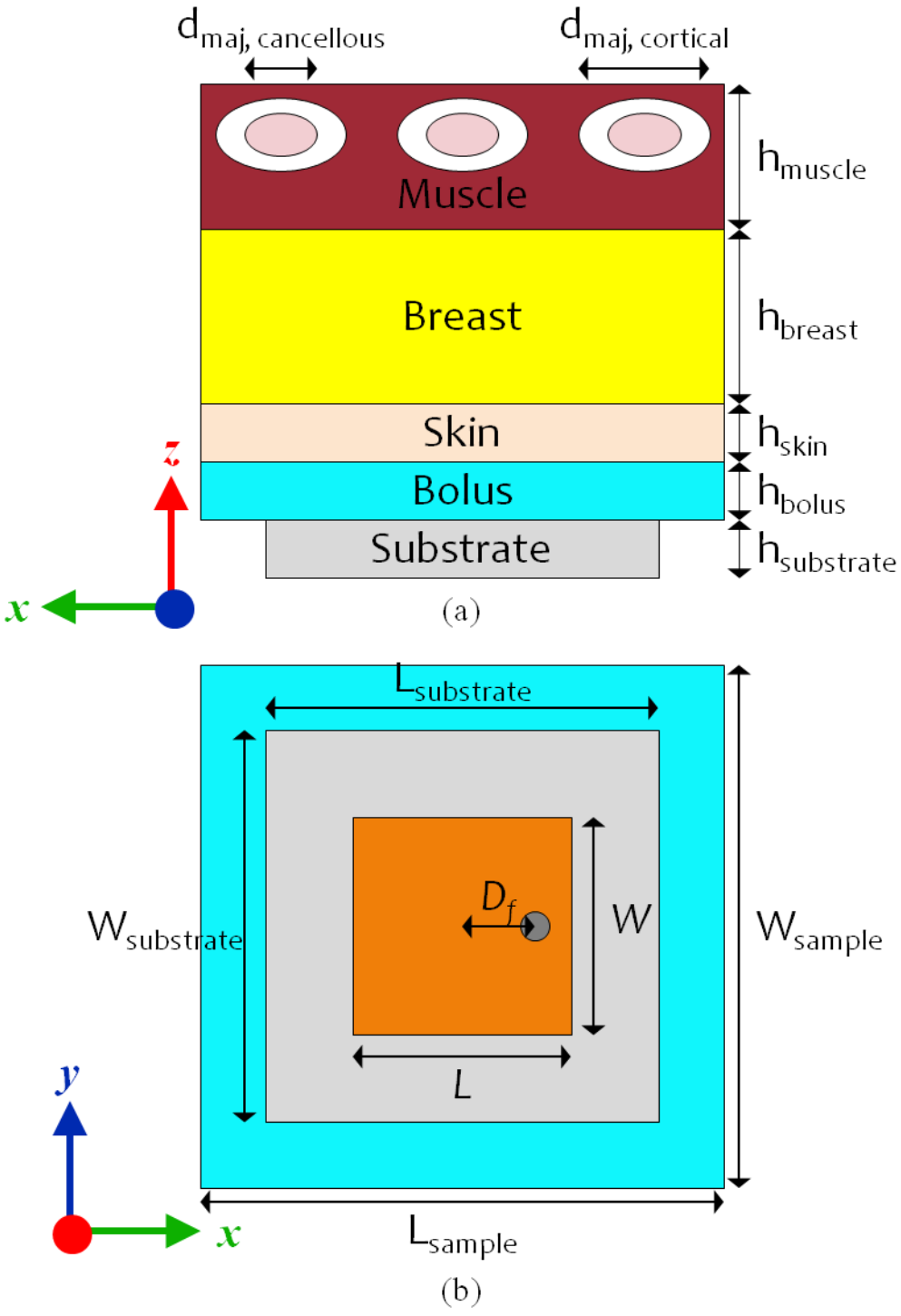

Figure 5.4 Layered Rectangular Geometry for Hyperthermia Element Optimization

(a) Vertical Cross-Section
(b) Horizontal Cross-Section at the Bolus-Substrate Boundary

Table 5.4 OAPSO Parameters for Patch Antenna Optimization

Particles	**k**	**V_{max}**	**c_1**	**c_2**	**ω**
27	9	0.5	1.4962	1.4962	[0.9, 0.5]
ω_{method}	**$Iterations_{Max}$**	**Threshold**	**Tolerance**	**Pop. Init.**	**Boundary Condition**
Linear	200	-15	10^{-2}	OA(27,3,3,2)	Damping

Table 5.5 PSO Position Constraints

Optimization (MHz)	L (mm)	W (mm)	D_f (mm)
433	[80, 160]		[0, 79.5]
915	[35, 75]		[0, 35]
2441	[10, 30]		[0, 14.5]
5800	[4, 15]		[0, 7]

5.2.1.2 Optimization Results

Table 5.6 lists the optimized values for each frequency along with the number of iterations required and the fitness. Figure 5.5 compares the average fitness to the best fitness at each iteration for all frequencies. The return loss for the optimized antennas is given in Figure 5.6. From the vector electric field plots (Figure 5.7), we can see that all of the antennas except the solution for 5.8 GHz exhibit half-wave behavior. This result leads to the expectation that the 433 MHz, 915 MHz, and 2.441 GHz antennas will behave as a typical patch antenna with a large front-to-back ratio, an expectation confirmed in Figure 5.8. The oddly shaped radiation pattern at 5.8 GHz may be attributed to the full-wave mode of the antenna or the ground plane that is very nearly the same size as the patch.

Figures 5.9 and 5.10 compare the SAR distribution in vertical cross-sections of the breast, muscle, and bone; each horizontal black line in the breast tissue region designates a distance of 2 cm from the skin/breast interface. Figures 5.11, 5.12, 5.13, and 5.14 compare the SAR in horizontal cross-sections of the breast tissue at depths of 0 mm, 1 mm, 5 mm, and 10 mm. Analysis of the SAR reveals higher levels near the breast tissue surface for the 2.441 GHz and 5.8 GHz antennas than the lower frequencies as expected. When considering a plane wave propagating in breast tissue, a lossy medium, the attenuation constant is defined as

$$\alpha = \text{real}\left(j\omega\sqrt{\mu\varepsilon}\sqrt{1-\frac{\sigma}{\omega\epsilon}}\right). \tag{5.5}$$

Therefore, electromagnetic waves propagating in lossy media lose power proportional to the square of their frequency. Since the region of interest for this application lies in the antennas' near-fields, the wave fronts will not be planes, but the same concept applies. Figure 5.15 demonstrates the power loss of representative plane waves traveling in normal type 3 breast tissue. At 5 cm the 433 MHz and 915 MHz waves have lost approximately 30% of their power, while the 2.441 GHz and 5.8 GHz waves have lost 50% and 90%, respectively.

From these results, it becomes clear that operating at only 5.8 GHz offers very little benefit in this application aside from its naturally small size; the slightly larger 2.441 GHz element provides much greater penetration. The two lowest bands offer the most uniform penetration, but the elements are too large to form a conformal breast array since both are nearly larger or larger than the diameter of the breast. For a clearer understanding of the size of each antenna relative to the breast diameter, see Figure 5.16.

To further explore the possibility of operating at 433 MHz or 915 MHz, the next section investigates miniaturization efforts.

Table 5.6 Optimized Antenna Dimensions and Optimization Details

Optimization (MHz)	L (mm)	W (mm)	D_f (mm)	Fitness (dB)	Iterations	Unique Evaluations
433	106.29	120.05	41.07	-13.1887	14	354
915	49.98	51.05	24.99	-15.4743	3	76
2441	17.99	14.96	8.995	-15.3831	6	157
5800	15.00	15.00	3.50	-18.2768	1	24

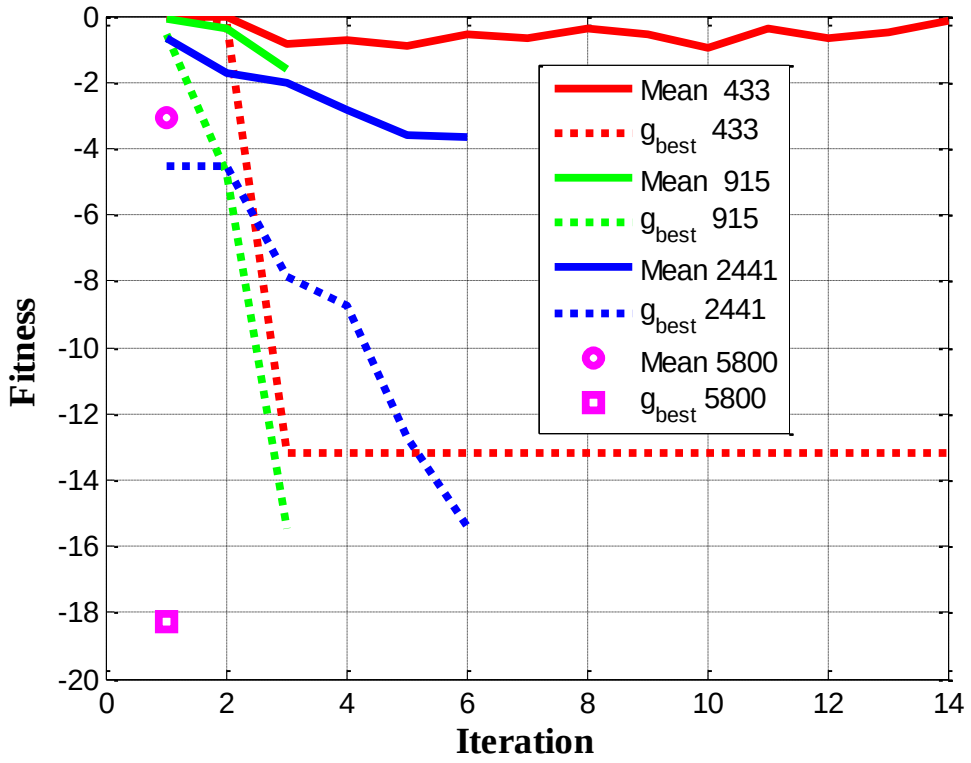

Figure 5.5 Comparison of Mean Fitness to g_{best} for Single Antenna Optimization

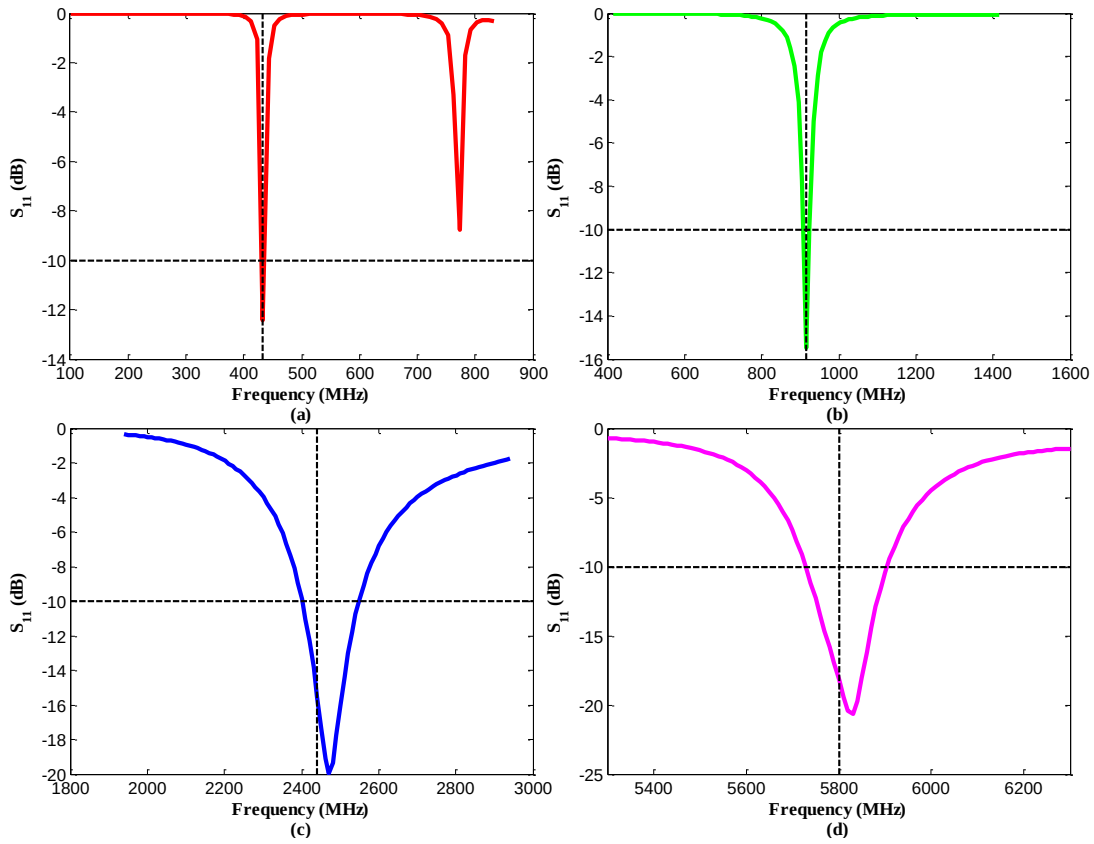

Figure 5.6 Optimized Antenna Return Loss

(a) 433 MHz
(b) 915 MHz
(c) 2.441 GHz
(d) 5.8 GHz

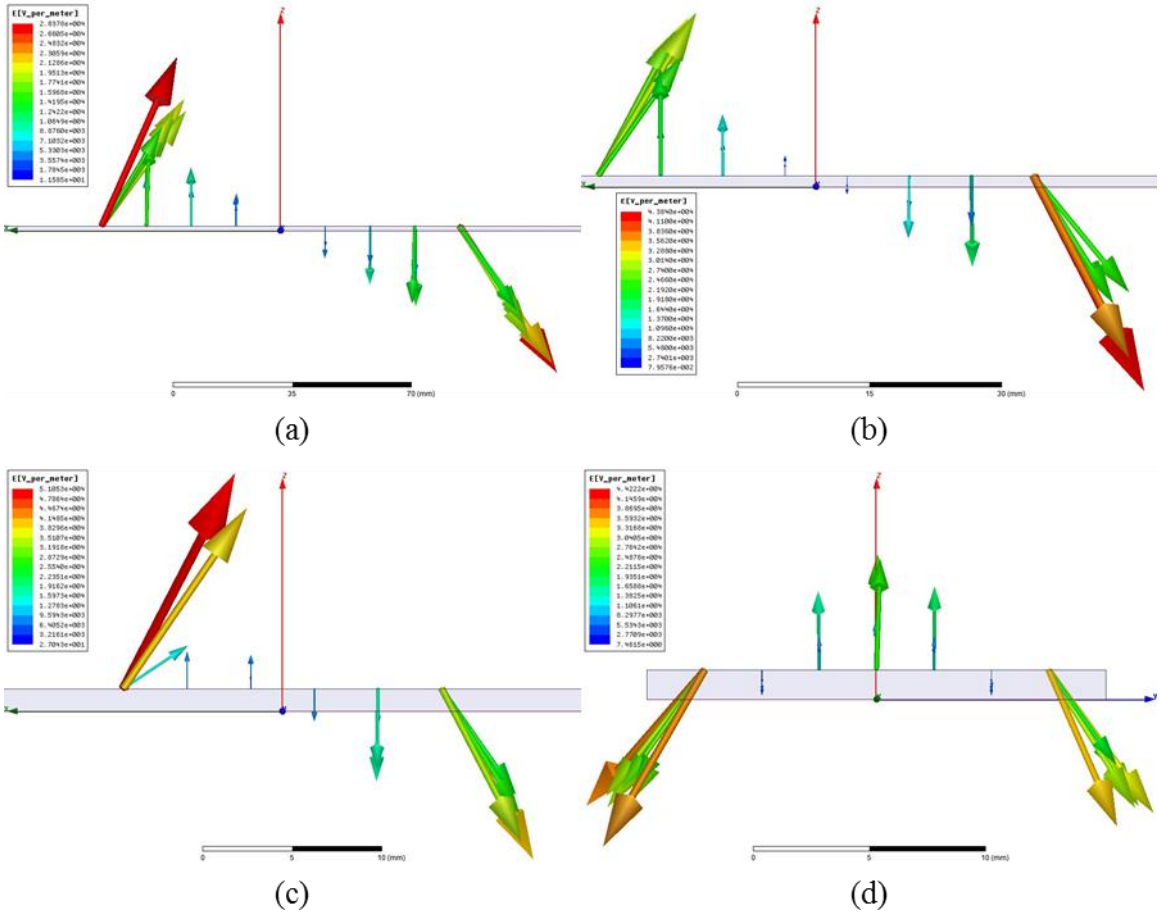

Figure 5.7 Optimized Antenna Vector Electric Field

(a) 433 MHz
(b) 915 MHz
(c) 2.441 GHz
(d) 5.8 GHz

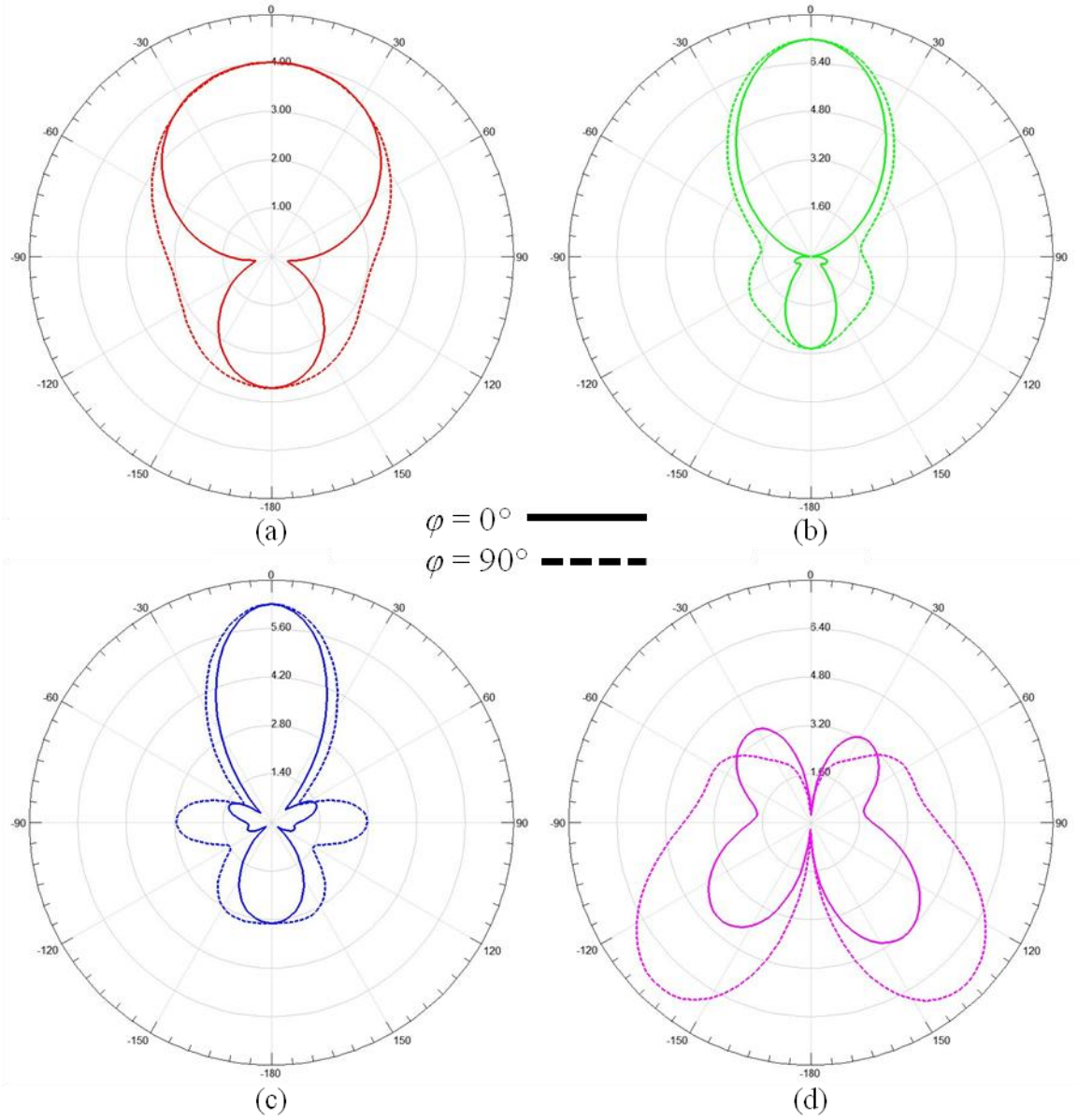

Figure 5.8 Optimized Antenna Array Patterns

(a) 433 MHz
(b) 915 MHz
(c) 2.441 GHz
(d) 5.8 GHz

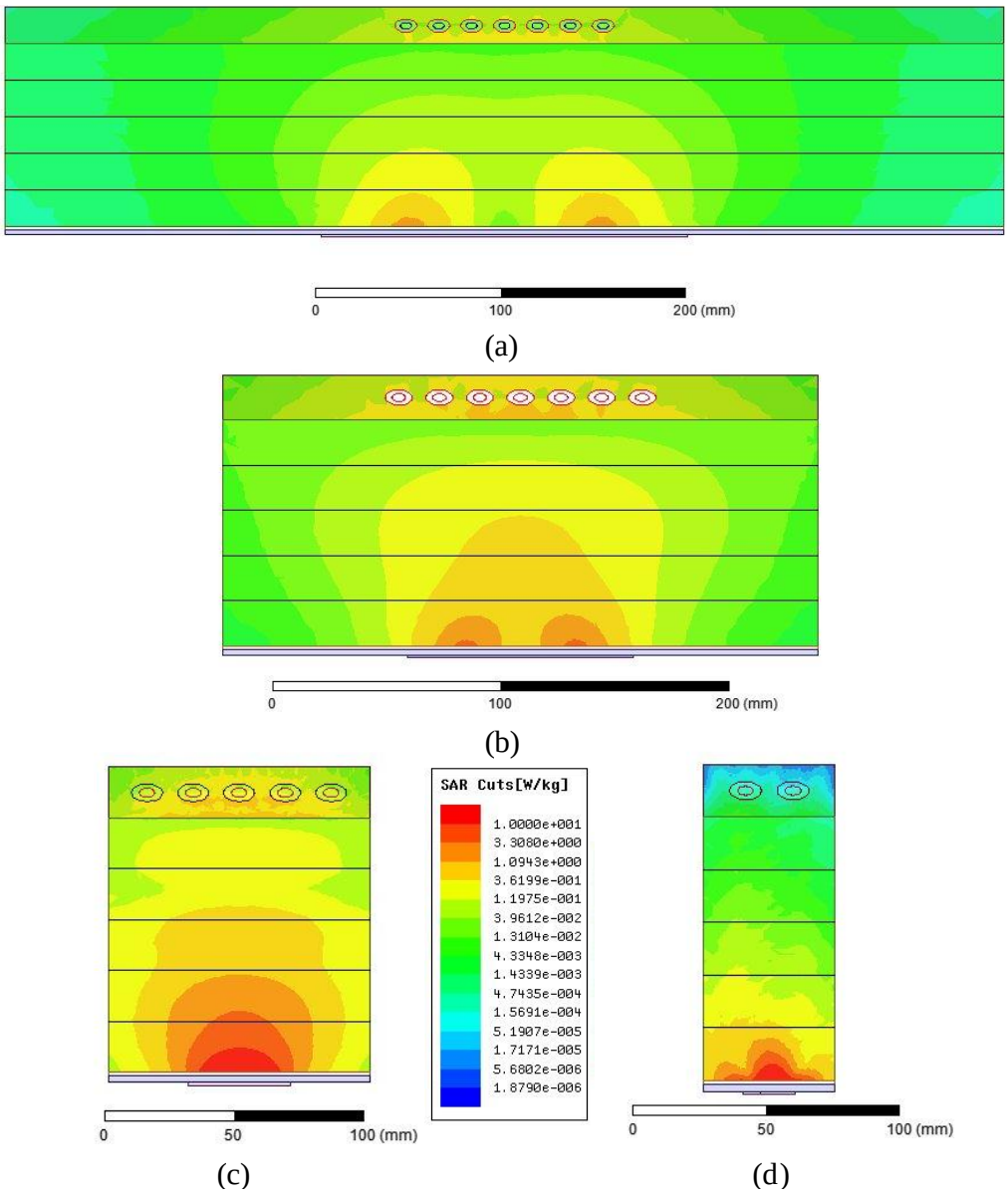

Figure 5.9 Optimized Antenna SAR Distribution in the *xz*-plane

(a) 433 MHz
(b) 915 MHz
(c) 2.441 GHz
(d) 5.8 GHz

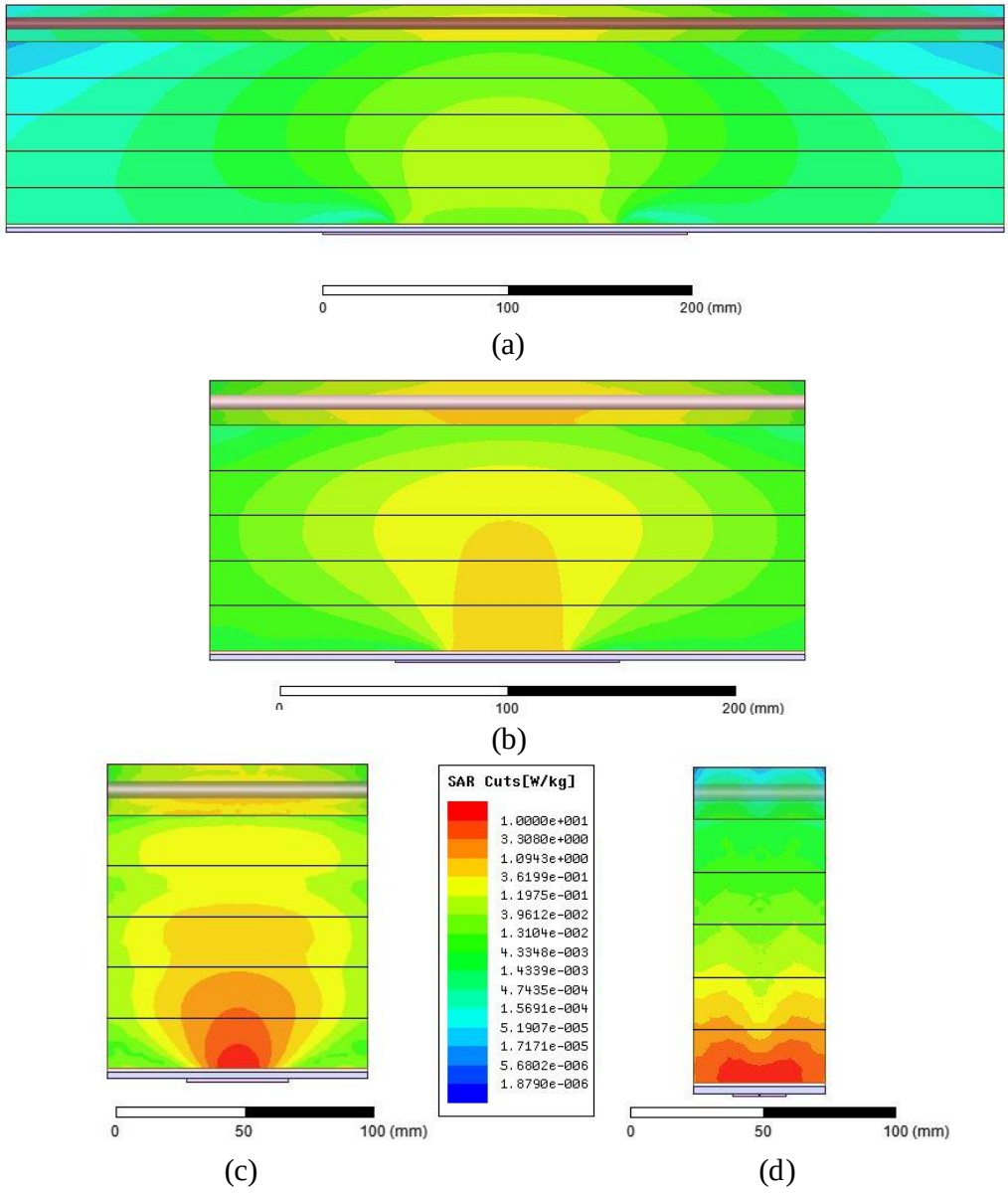

Figure 5.10 Optimized Antenna SAR Distribution in the *yz*-plane

(a) 433 MHz
(b) 915 MHz
(c) 2.441 GHz
(d) 5.8 GHz

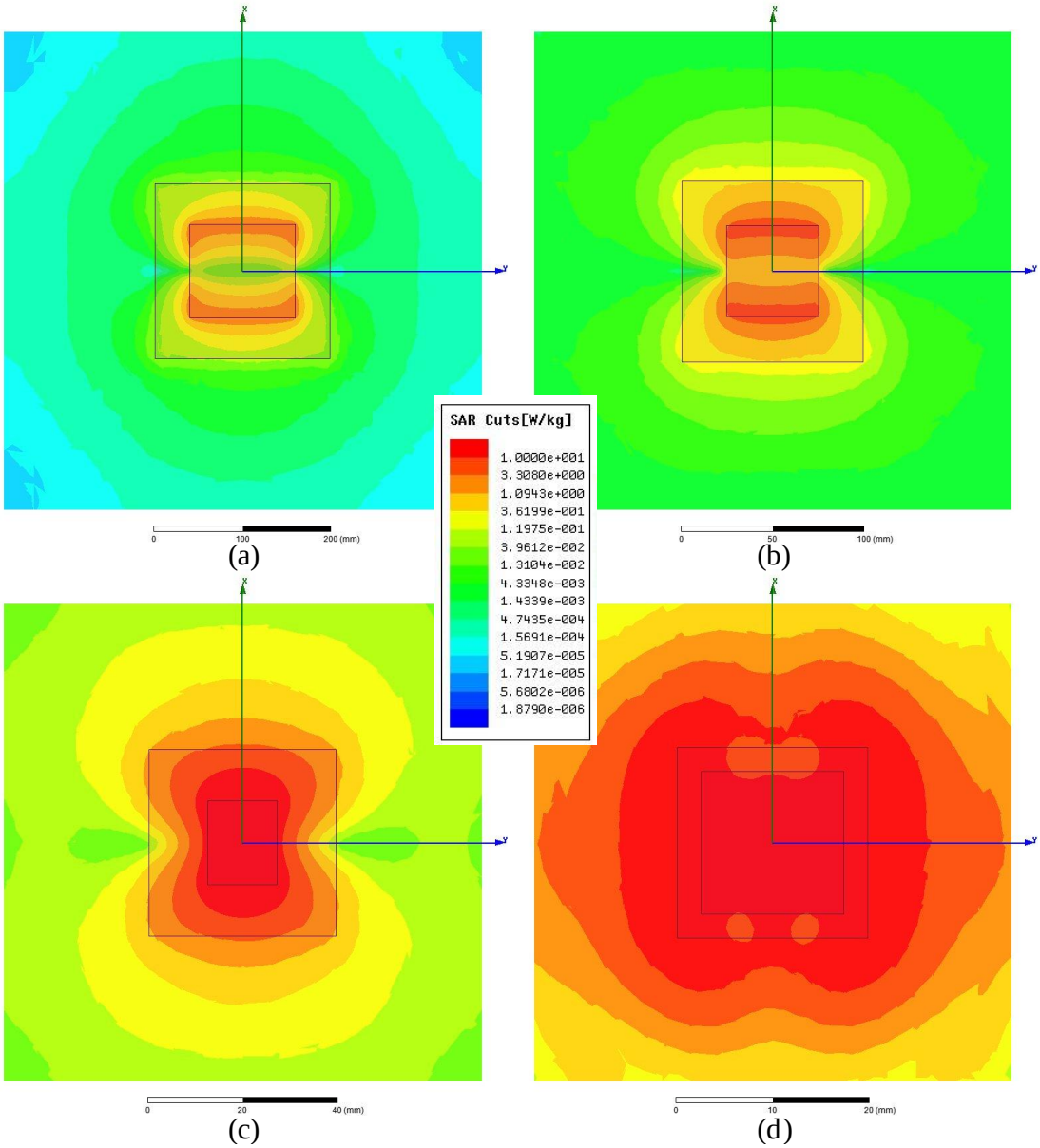

Figure 5.11 Optimized Antenna SAR Distribution in the *xy*-plane at 0 mm

(a) 433 MHz
(b) 915 MHz
(c) 2.441 GHz
(d) 5.8 GHz

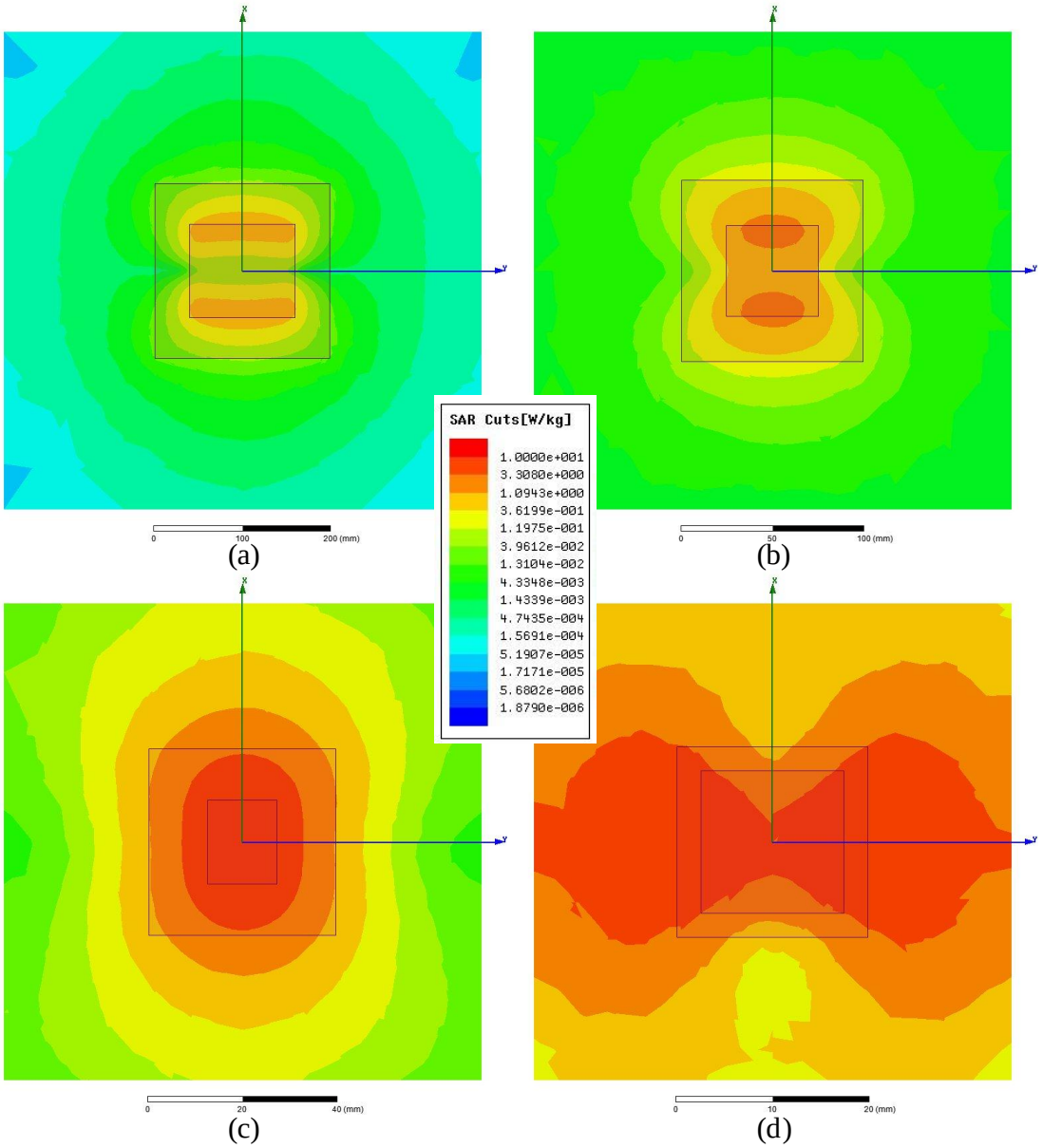

Figure 5.12 Optimized Antenna SAR Distribution in the *xy*-plane at 1 mm

(a) 433 MHz
(b) 915 MHz
(c) 2.441 GHz
(d) 5.8 GHz

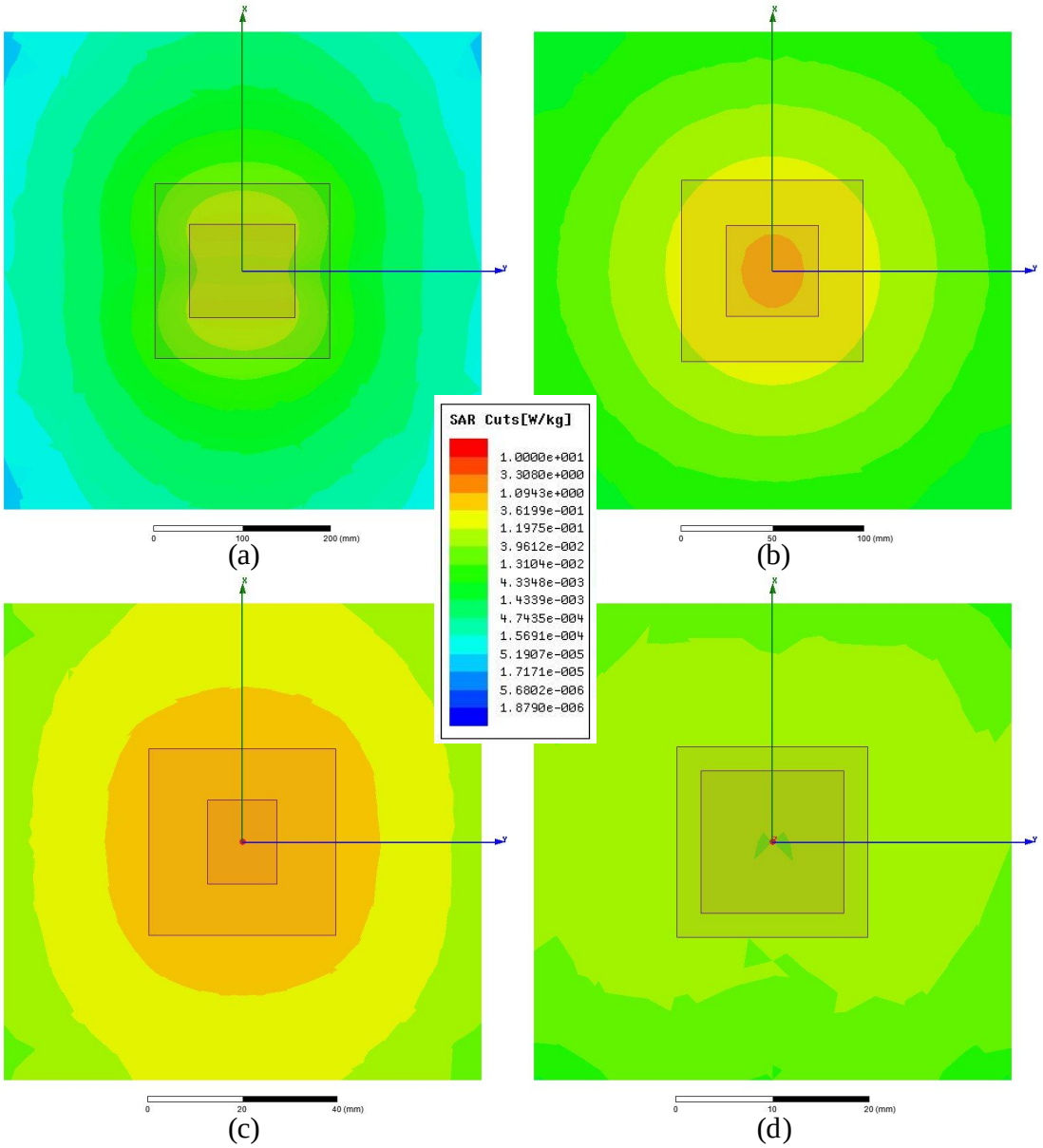

Figure 5.13 Optimized Antenna SAR Distribution in the *xy*-plane at 5 mm

(a) 433 MHz
(b) 915 MHz
(c) 2.441 GHz
(d) 5.8 GHz

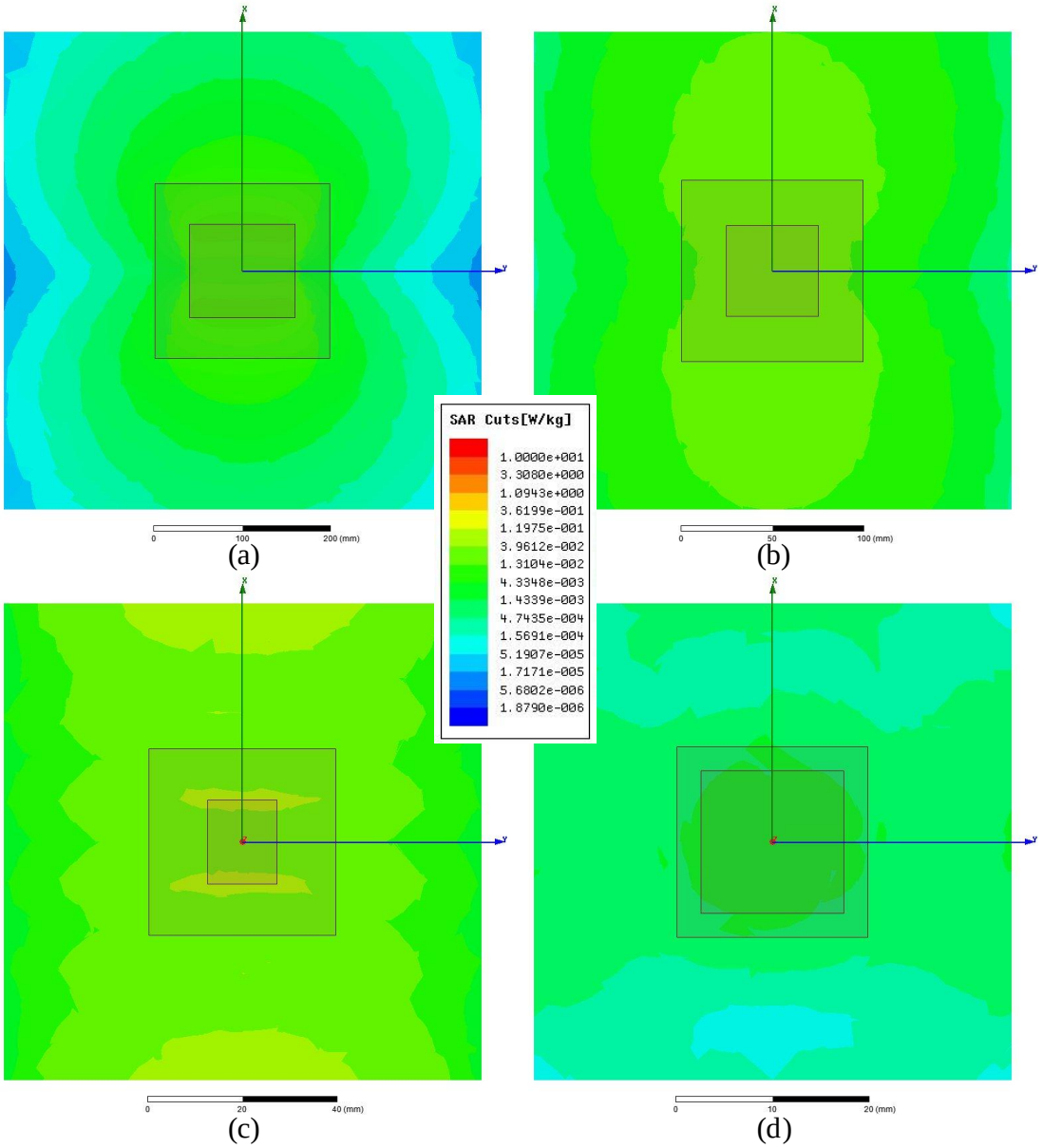

Figure 5.14 Optimized Antenna SAR Distribution in the *xy*-plane at 10 mm

(a) 433 MHz
(b) 915 MHz
(c) 2.441 GHz
(d) 5.8 GHz

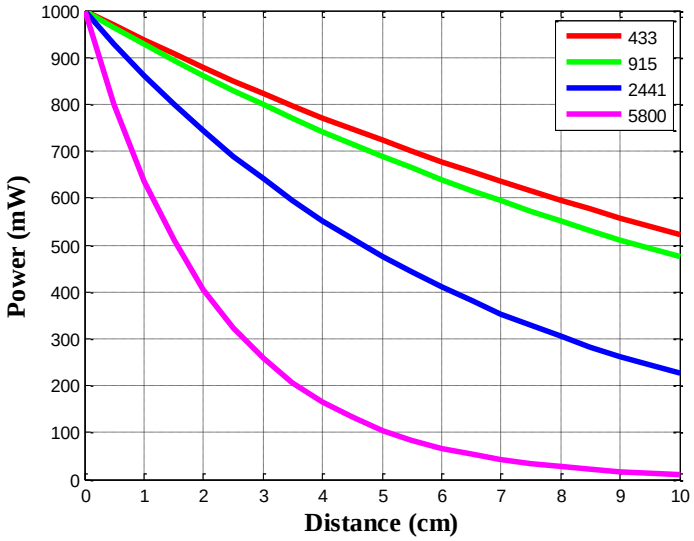

Figure 5.15 Plane Wave Propagation in Normal Type 3 Breast Tissue

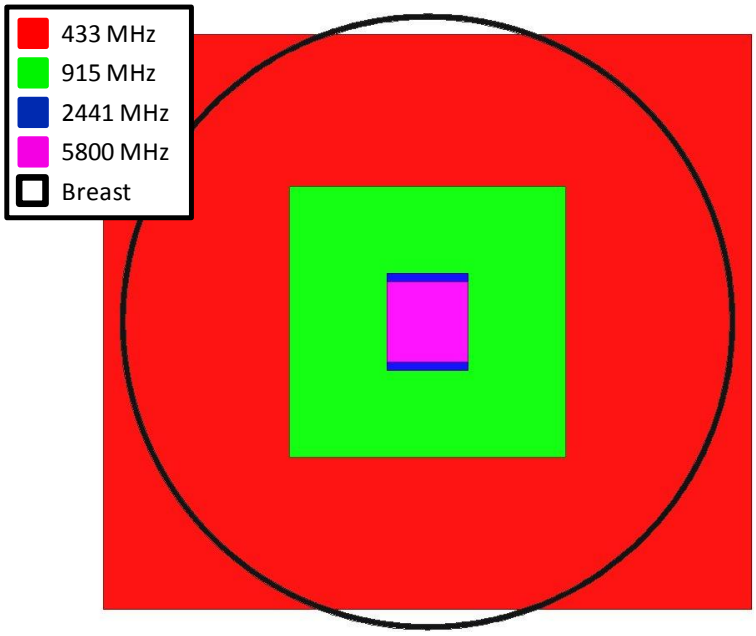

Figure 5.16 Scale Comparison of Patch Antennas Relative to 34B Breast Diameter

5.2.1.3 Refining Elements

Size reductions in antennas may conventionally be achieved by shrinking the effective wavelength required of the antenna or by increasing the effective electrical length. A simple method of decreasing the effective wavelength of an antenna is increasing the permittivity of the substrate or superstrate [125]. The effective electrical length may be increased by adding elements such as shorting pins to the antenna or changing the shape altogether [125].

For 433 MHz, the required size of the antenna is too large for a straightforward miniaturization. The Implantable and Body-Centric Antennas Research and Education Laboratory (ICARE) recently published a letter describing the leaky-wave antenna (LWA) shown in Figure 5.17(a) designed for operation from 360-540 MHz with a physical envelope of only $10 \times 12 \times 1.5$ mm^3 [126]. A classical LWA consists of a slit cut along the length of a waveguide that radiates power along the entire length of the slot [127]. This LWA operates on a partially reflective surface or screen (PRS) design principle. The substrate is excited as a parallel-plate waveguide region with power leaking from the slot cut into the top conductor. A high-permittivity superstrate (human skin) acts as a PRS to increase the wave number of the radiated wave. To accommodate the need for the high-permittivity superstrate without adding bulk to the geometry, a theoretical fluid matching the dielectric properties of skin replaces the silicone oil bolus. The antenna is simulated on the rectangular layered model with dimensions shown in Table 5.7. Return loss is shown in Fig. 5.17(b). Vertical cross-sections of SAR are shown in Figure 5.18, and horizontal cross-sections at 0 mm, 1 mm, 5 mm, and 10 mm from the skin to breast tissue barrier are shown in Figure 5.19. While the excellent size

and impedance bandwidth show great promise for this antenna, the SAR unfortunately degrades to less than 50 $mW \cdot kg^{-1}$ at a depth of 5 cm, making this the worst candidate in terms of energy deposition. An examination of the radiation pattern may indicate this results because the antenna directs most of its energy horizontally with a null near the *z*-axis.

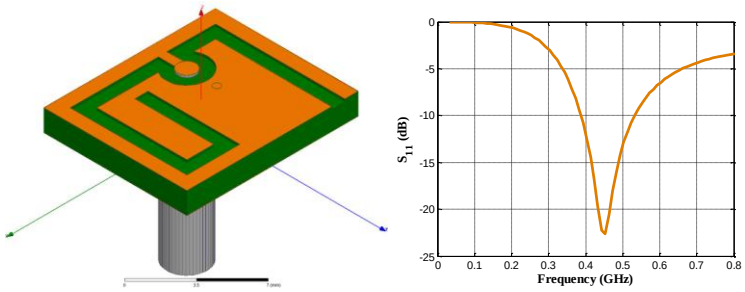

(a) (b)

Figure 5.17 Very Small, Low Frequency Leaky Wave Antenna

(a) Antenna Model
(b) S_{11} versus Frequency

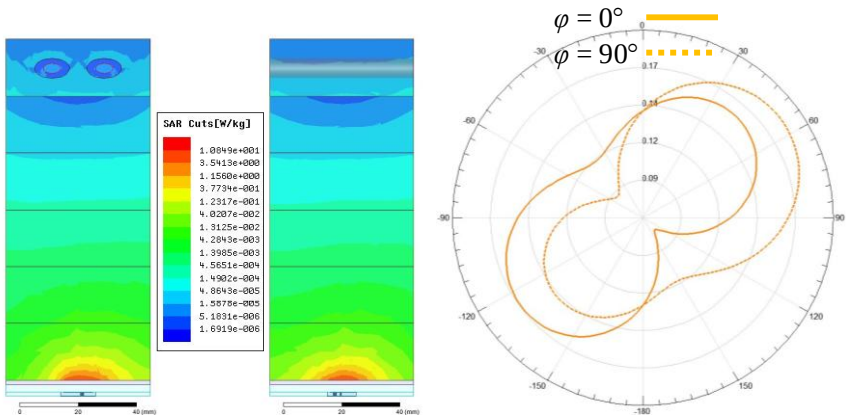

(a) (b) (c)

Figure 5.18 Leaky-Wave Antenna SAR and Radiation Pattern at 433 MHz

(a) SAR in the *xz*-plane
(b) SAR in the *xy*-plane
(c) Radiation Pattern

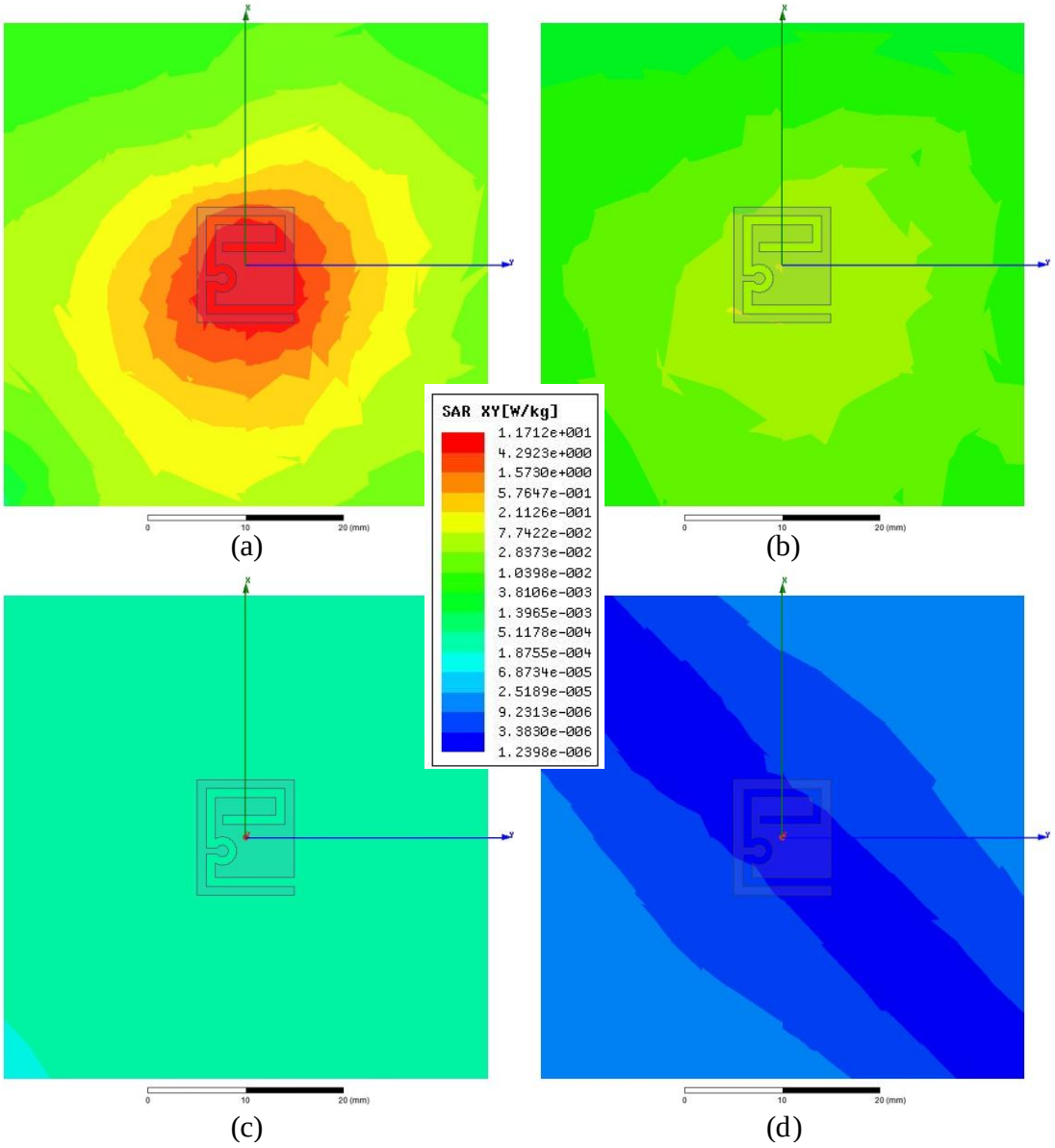

Figure 5.19 Leaky-Wave Antenna SAR: Horizontal Cross-Sections at 433 MHz

(a) 0 mm
(b) 1 mm
(c) 5 mm
(d) 10 mm

The effective wavelength in a dielectric is inversely proportional to the square root of the permittivity. Given that the optimized 915 MHz patch is only about three times as large as the 2.4 GHz antenna, substantially increasing the substrate permittivity

of the 915 MHz antenna may permit an effective size reduction. In Rogers RO3010, the wavelength is reduced by a factor of 3.2; therefore, achieving an additional requires a material with relative permittivity of at least 90. Ceramics often fill the need for such high-permittivity dielectrics. Kyocera K0140 (ε_r = 141, tan δ = 0.00028, D = 3900 kg·m^{-3}) may offer up to a 75% reduction in the size of the antenna on RO3010. Introducing a shorting pin between the patch and ground has also been shown to reduce the size of patch antennas in many cases [125]. Therefore, two further optimizations of patch antennas at 915 MHz are considered. A standard PSO with the parameters given in Table 5.8 is applied. For the antenna with the shorting pin, three additional dimensions must be considered: distance from the center of the patch to the feed along the width, D_{fy}, and distances from the center of the patch to the shorting pin, D_{sx} and D_{sy}. The new dimensional constraints are defined in Table 5.9.

The optimized design along with the required iterations and fitness are listed in Table 5.10. Figure 5.20(a) compares the fitness over all iterations. Figure 5.20(b) shows the return loss. The radiation patterns shown in Figure 5.21 reveal that the 915 MHz patch on the ceramic substrate still directs most of its energy into the tissue while the shorted patch has a more distorted field.

Table 5.7 Single Element Model Dimensions

Optimization	433, LWA	915, K0140	915, Short
L_{sample} (mm)	50	204	204
W_{sample} (mm)			
$L_{substrate}$ (mm)	12	40	40
$W_{substrate}$ (mm)	10		
$h_{substrate}$ (mm)	1.28		
h_{bolus} (mm)	2.50		
h_{skin} (mm)	1.55		
h_{breast} (mm)	100.00		
h_{muscle} (mm)	20.00		
$d_{maj,cortical}$ (mm)	12.00		
$d_{min,cortical}$ (mm)	7.00		
$d_{maj,cancellous}$ (mm)	6.00		
$d_{min,cancellous}$ (mm)	3.50		

Table 5.8 PSO Parameters for 915 MHz Patch Antenna Optimization

Particles	**k**	**V_{max}**	**c_1**	**c_2**	**ω**
21	6	0.5	1.4962	1.4962	[0.9, 0.5]
ω_{method}	**$Iterations_{Max}$**	**Threshold**	**Tolerance**	**Pop. Init.**	**Boundary Condition**
Linear	200	-15	10^{-2}	Random	Damping (Ceramic) Invisible (Short)

Table 5.9 PSO Position Constraints

Optimization (MHz)	L (mm)	W (mm)	D_{fx} (mm)	D_{fy} (mm)	D_{sx} (mm)	D_{sy} (mm)
915, Ceramic	[5, 20]		[0, 10]	-	-	-
915, Short	[10, 20]		[0, 10]		[-10, 10]	

Table 5.10 Optimized Antenna Dimensions and Optimization Details

Optimization (MHz)	L (mm)	W (mm)	D_{fx} (mm)	D_{fy} (mm)	D_{sx} (mm)	D_{sy} (mm)	Fitness (dB)	Iterations	Unique Evaluations
915, Ceramic	13.72	10.12	1.32	-	-	-	-16.3191	190	3832
915, Short	17.69	16.27	5.27	7.64	4.33	6.80	-15.4854	50	1050

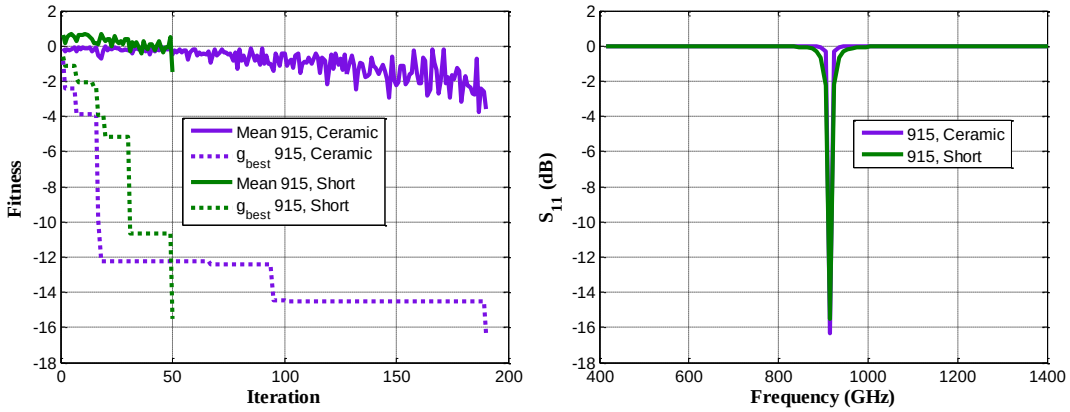

(a) (b)

Figure 5.20 915 MHz Antenna Optimization Results

(a) Comparison of Mean Fitness to g_{best}
(b) Return Loss

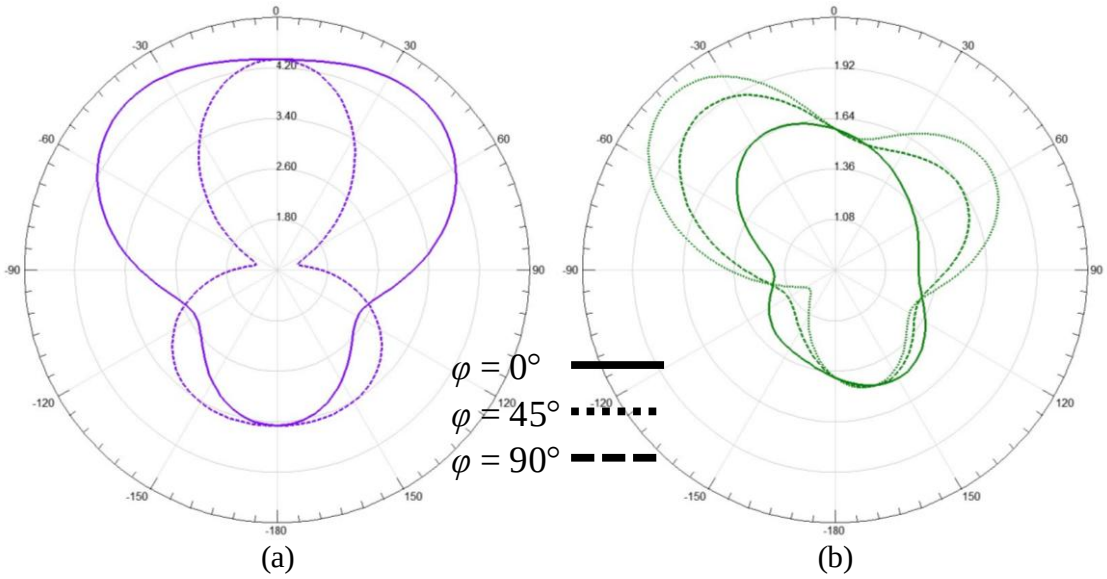

Figure 5.21 Radiation Patterns of Optimized 915 MHz Antennas

(a) Ceramic
(b) Shorted

5.2.1.4 Antenna Selection

The following criteria guide the selection of an antenna for a hyperthermia applicator array.

1. To allow space for multiple antennas in an array, the antenna must occupy less than a quarter of the surface area of a U.S. size 34B breast, which means the area of the antenna must be less than approximately 5,103 mm^2.
2. The antenna should facilitate transmission at the maximum power level permitted by the FCC or ECC. To qualify for the maximum level of +36 dBm (4 W), a transmitter must employ frequency hopping over at least 50–75 channels [114]. The antenna must therefore provide sufficient bandwidth for such operation.
3. The antenna should present suitable SAR levels at a depth of 5–6 cm.

A quick glance at the scale comparison in Figure 5.16 eliminates the 433 MHz patch from consideration. The second largest antenna, the 915 MHz patch on RO3010, has an area of 2551.5 mm^2. Therefore, it satisfies the requirement, and by extension the remaining elements do as well.

Regulatory agencies have designated the spectrum from 433.05–434.79 MHz, 902–928 MHz, 2.4–2.4835 GHz, and 5.725–5.875 GHz. Observation of the bandwidth in the return loss plots reveals that only the 433 MHz LWA and 2.441 and 5.8 GHz patch antennas occupy the available bandwidth to satisfy the first requirement.

The third criteria could be defined more explicitly, but in this case, the subjective term *suitable* conveys the idea of the best relative to all choices. Given that the SAR distribution of an array will likely differ quite a bit from a single element, this seems appropriate. From the SAR cross-sections in the *xy*-plane, the maximum levels of the LWA, 2.4 GHz patch, and 5.8 GHz patch fall below 50 $mW \cdot kg^{-1}$, 1000 $mW \cdot kg^{-1}$, and 120 $mW \cdot kg^{-1}$, respectively. With this information, the 2.4 GHz patch antenna emerges as the best choice.

5.2.2 Array Optimization

5.2.2.1 Model Configuration

To ease the transition to an anatomically accurate model, a simplified geometry of skin, dielectrically-homogeneous breast tissue, and muscle is constructed as shown in Figure 5.22. The skin and bolus maintain the thickness of the rectangular model, while the breast tissue approximates a hemisphere of radius 57 mm. Ribs are excluded from this model because their contributions are negligible since they are embedded in the much more conductive muscle. Initially, the 2.4 GHz patch antenna is applied as

designed in the previous section with a rectangular substrate and ground (Figure 5.23) to validate the performance of the flat patch warped to conform to the spherical surface. An examination of the return loss (Figure 5.24) reveals the insignificant influence of the new geometry on the antenna's frequency response. However, the radiation pattern (Figure 5.25(a)) shows that much of energy is reflected from the breast (likely by the chest wall). In an attempt to capture some of this energy the substrate and ground are extended to fully surround the surface of the breast. Again the alteration has only a minor effect on the frequency response (Figure 5.24), but the antenna now primarily radiates into the breast (Figure 5.25(b)). A comparison of the cross-sectional SAR distribution for each ground configuration in Figure 5.26 indicates that the fully encased breast also has a higher minimum SAR.

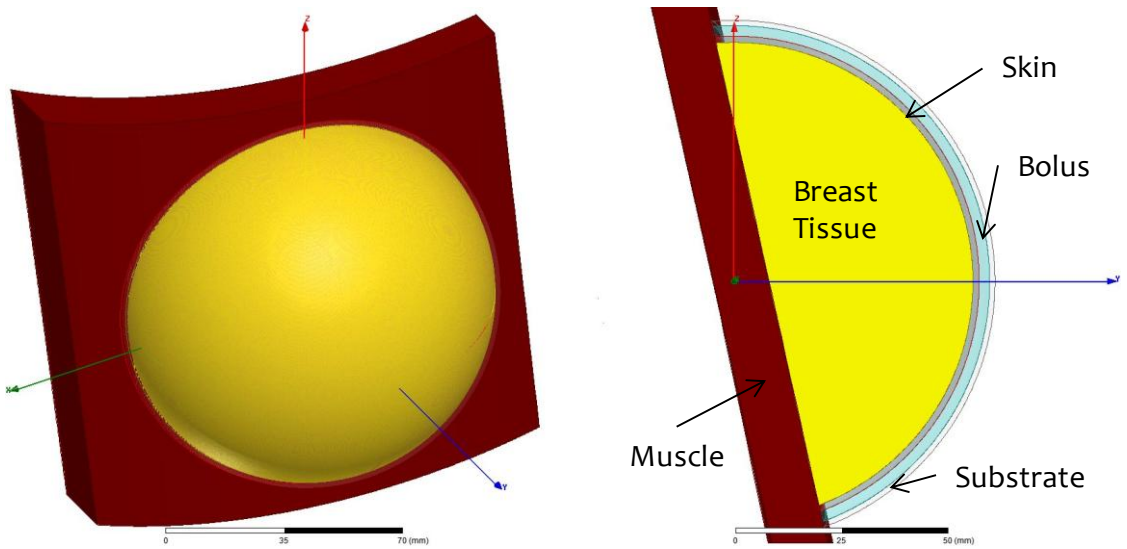

(a) (b)

Figure 5.22 Simplified Breast Model

(a) Isometric View
(b) Cross-Section

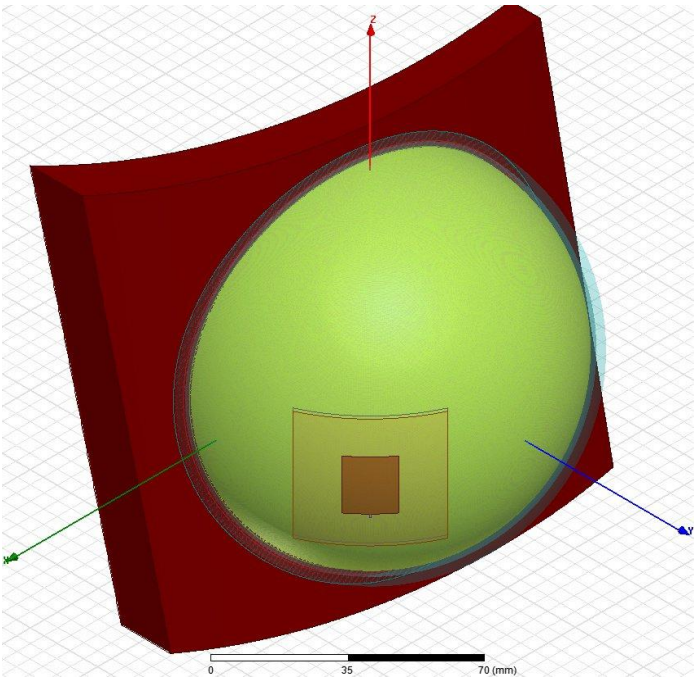

Figure 5.23 2.441 GHz Patch Antenna on Simplified Breast Model

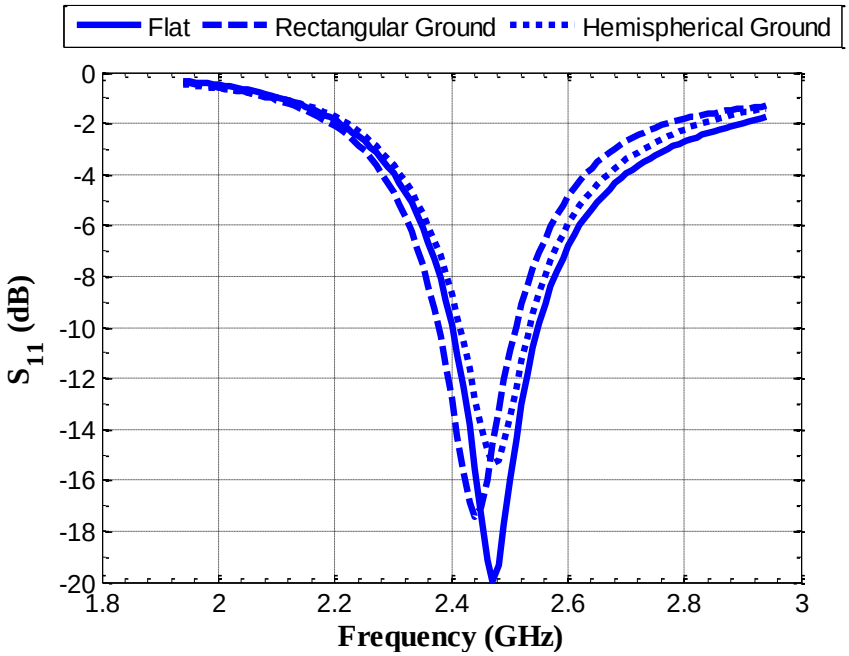

Figure 5.24 Return Loss Comparison of 2.441 GHz Element on Different Models

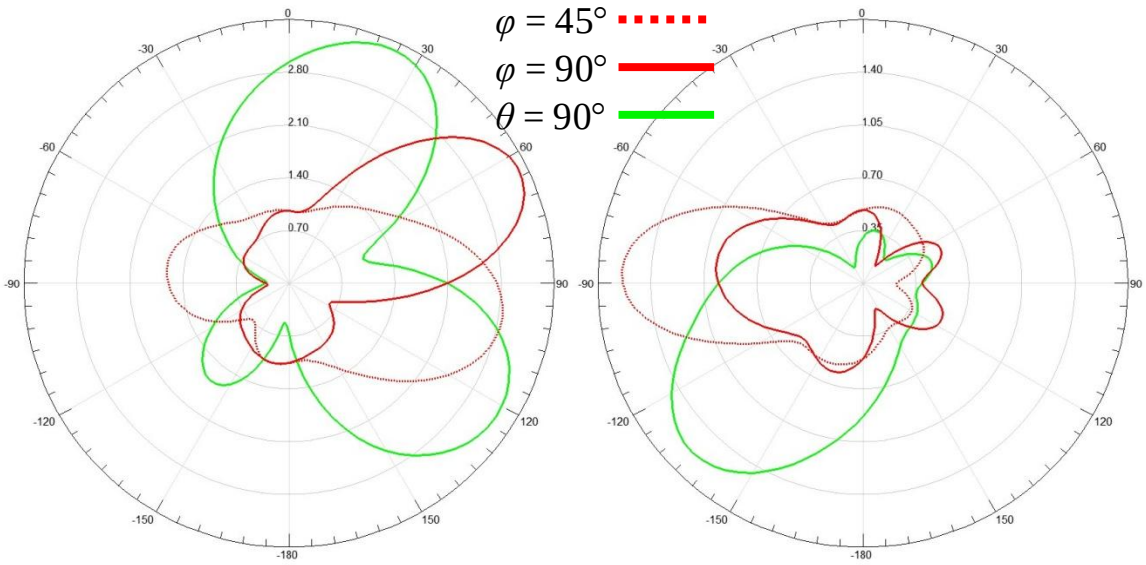

(a) (b)

Figure 5.25 Rectangular versus Hemispherical Ground Plane Radiation Patterns

(a) Rectangular Ground
(b) Hemispherical Ground

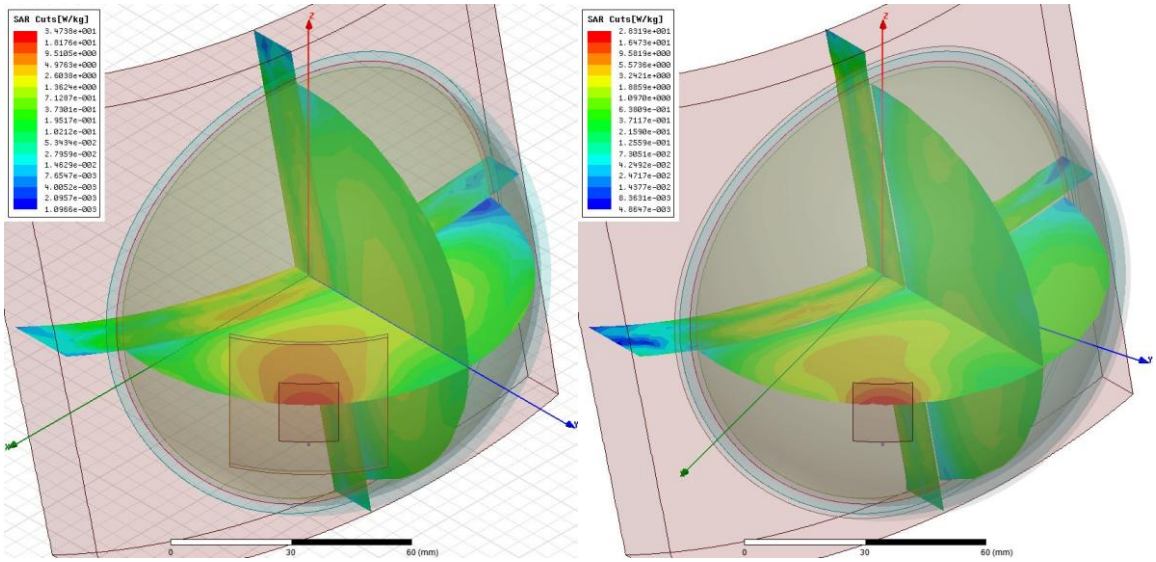

(a) (b)

Figure 5.26 Rectangular versus Hemispherical Ground Plane SAR Cross-Sections

(a) Rectangular Ground
(b) Hemispherical Ground

5.2.2.2 Array Configuration

Any pattern may define an antenna array with the most straightforward being a uniformly spaced linear grid. In this section, two variations of an array grid are explored. The first attempts to maximize the number of elements applied to the breast with 4 rows of elements, spaced by 27° horizontally and 30° vertically, for a total of 22 elements (Figure 5.27). In a more spartan configuration the second array employs a 3 × 3 grid of elements offset by 45° (Figure 5.28).

Although no specific details about the frequency response of individual elements may be gleaned from the plots of all of the S-parameters in Figures 5.29 and 5.30, some important information stands out. In the twenty-two-element array, at least 9 of the elements occupy bandwidth entirely outside of the ISM spectrum; all of the elements in the second array cover at least half of the band. Both arrays suffer a bit from high mutual coupling between some elements, but this appears more severe in the larger array and likely contributes to the number of elements whose resonance has shifted out-of-band.

The SAR distributions arrays demonstrate fewer differences than the frequency response. On the surface of the breast tissue, the minimum and maximum SAR range from about 2 $W \cdot kg^{-1}$ to 60 $W \cdot kg^{-1}$, respectively, for both arrays as shown in Figure 5.31. Both arrays also concentrate their energy in the center of the breast as seen in the cross-sections (Figure 5.32) and the view of the rear chest wall (Figure 5.33). In a bid for independence, the contributions of individual antennas are more apparent for the smaller array on both the surface and the cross-section. Radiation patterns are provided in Figure 5.34 as a baseline for comparison to the optimized arrays in the next section.

Given the large number of elements operating the efficiency of energy delivery is likely to suffer, and will place undue burden on any system supplying a signal to the elements. With little variance in the SAR between the arrays, using fewer elements simplifies the problem. Based on these factors, the best candidate for optimization is the 3 × 3 array.

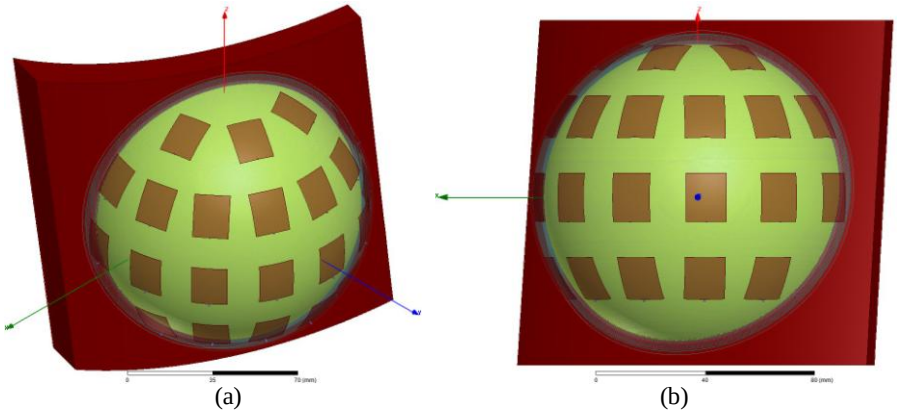

Figure 5.27 Twenty-two-Element Array on Simplified Breast Model

(a) Isometric View
(b) Front View

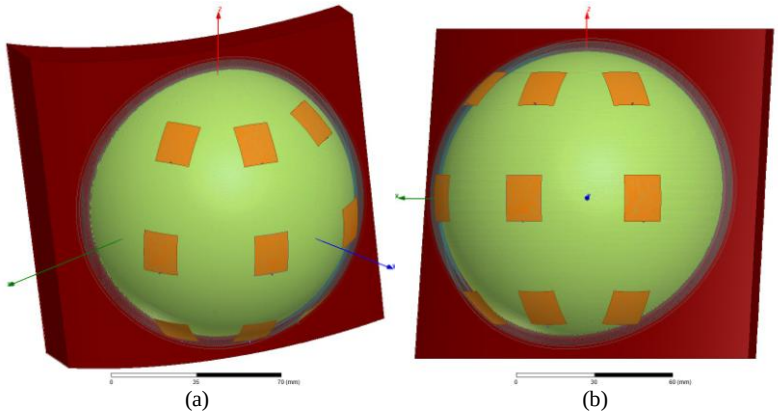

Figure 5.28 Nine-Element Array on Simplified Breast Model

(a) Isometric View
(b) Front View

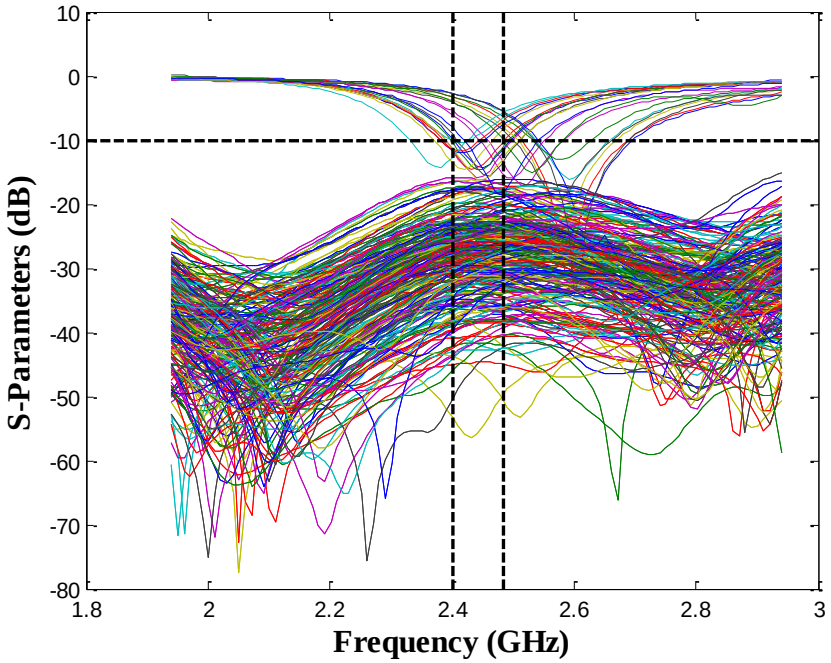

Figure 5.29 S-Parameters of Twenty-two-Element Array

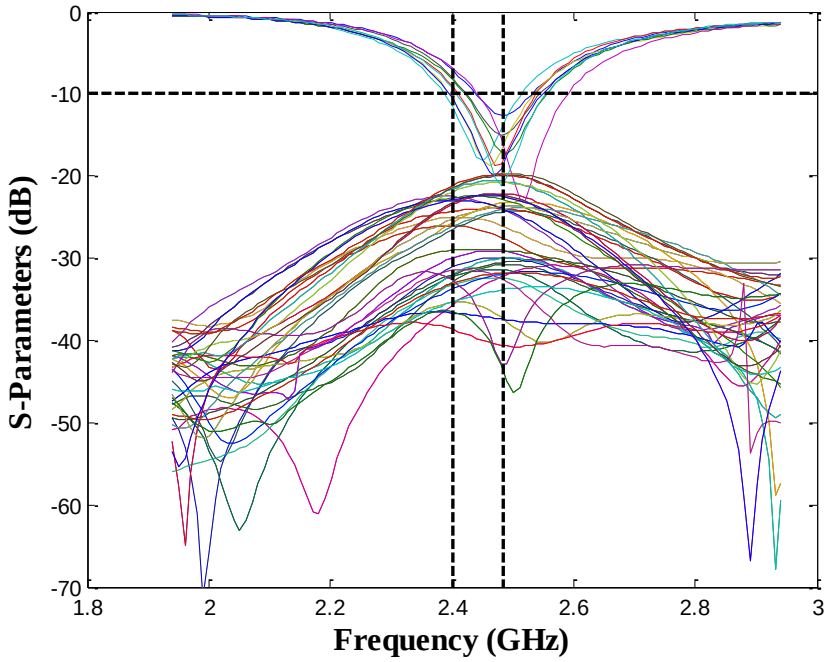

Figure 5.30 S-Parameters of Nine-Element Array

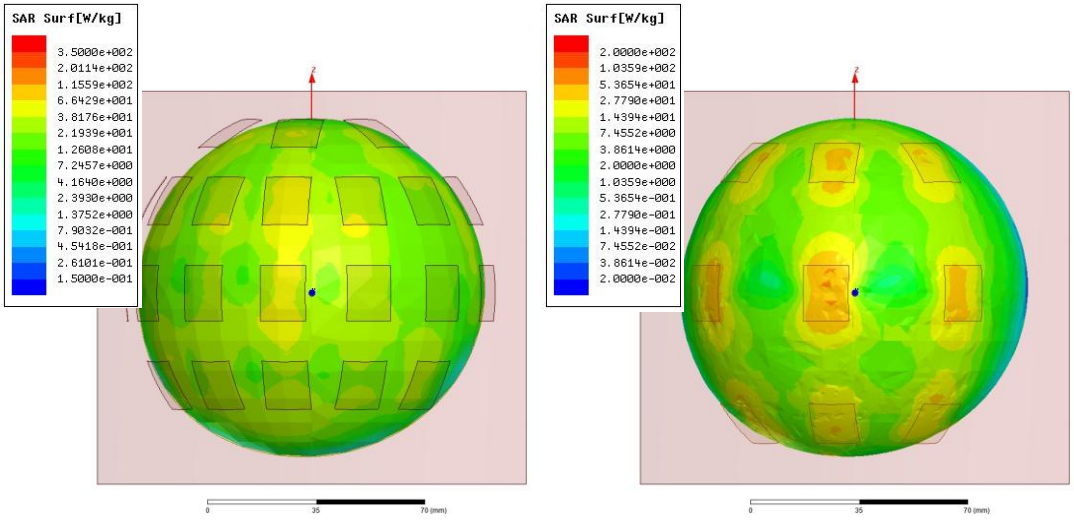

(a) (b)

Figure 5.31 Comparison of SAR for Array Variations on Breast Tissue Surface

(a) Twenty-two Elements
(b) Nine Elements

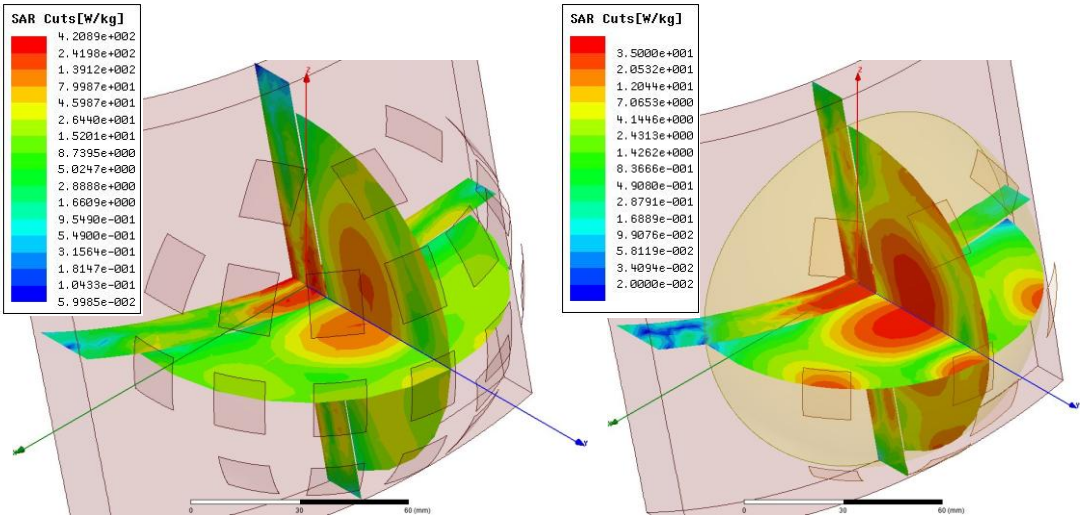

(a) (b)

Figure 5.32 Comparison of SAR for Array Variations on Central Cross-Sections

(a) Twenty-two Elements
(b) Nine Elements

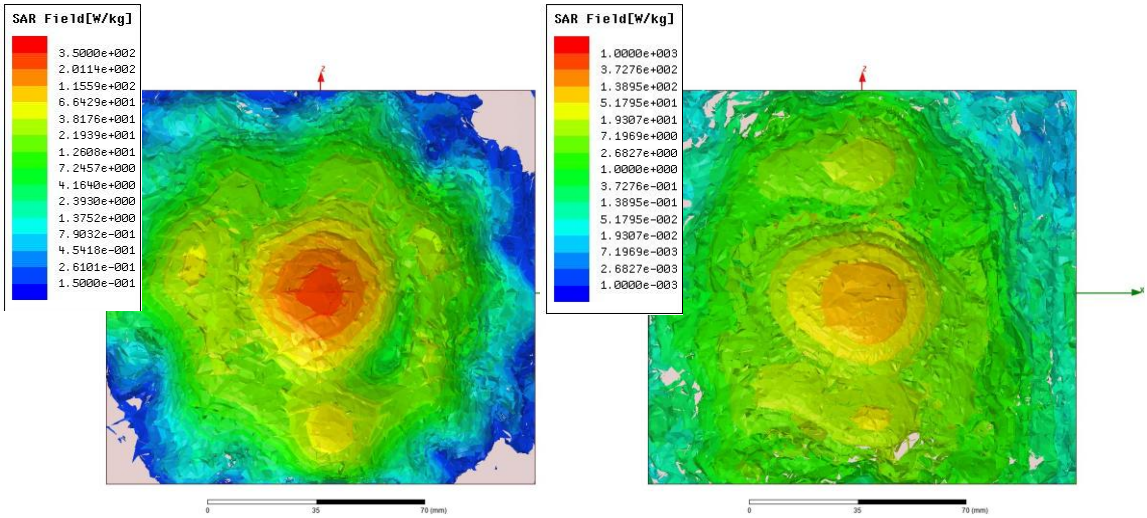

(a) (b)

Figure 5.33 Comparison of SAR for Array Variations on Rear Chest Wall

(a) Twenty-two Elements
(b) Nine Elements

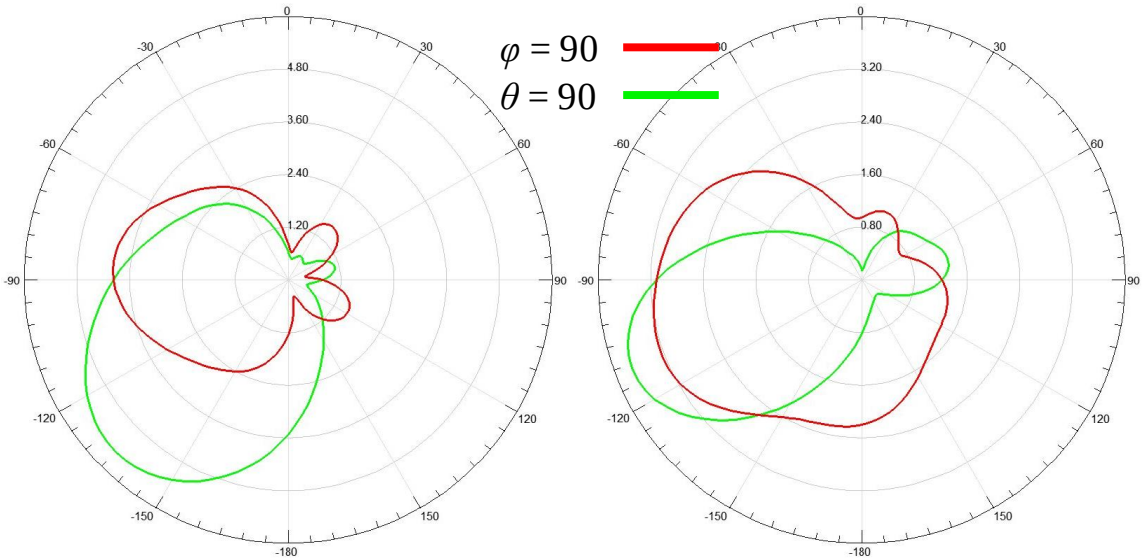

(a) (b)

Figure 5.34 Comparison of Radiation Patterns for Array Variations

(a) Twenty-two Elements
(b) Nine Elements

5.2.2.3 Optimization Configuration

To optimize the SAR distribution in the breast tissue, a standard PSO with the parameters listed in Table 5.11 is used. To accomplish the goal of homogeneous distribution, the SAR is sampled at 278 points throughout the breast tissue at 5.7 mm radial, 30° azimuth, and 20° elevation intervals. To steer the electric field, the phase of the input signal at each port is varied, while the power remains constant at 1 W per channel. The phase is allowed to range from -270° to 270°.

Table 5.11 PSO Parameters for SAR Optimization

Particles	**k**	**V_{max}**	**c_1**	**c_2**	**ω**
21	7	0.5	1.4962	1.4962	[0.9, 0.5]
ω method	**$Iterations_{Max}$**	**Threshold**	**Tolerance**	**Pop. Init.**	**Boundary Condition**
Linear	200	-1	10^{-2}	Random	Damping

While the explicitly-stated primary goal is uniform SAR distribution, an implicit goal is large uniform SAR value. When most people consider uniformity among a population, *average* is probably a word that immediately springs to mind, but optimizing strictly for some target mean obviously will not necessarily have any influence on uniformity. So perhaps the mode should be considered. If the objective function minimizes the difference between the mode and the mean, then it seems reasonable to expect the SAR values to be relatively similar at all points. However, if the fitness only rewards the difference, the problem could quickly be solved by reducing the power at all ports to zero. The mean and mode would be zero, but the SAR would also be zero. Therefore it is imperative to also reward a large typical SAR value. Based on the values

seen in the initial simulations, SAR values on the order of 10–50 $W \cdot kg^{-1}$ should be expected. Simply comparing the mean to the difference could allow a large average value to overwhelm the difference. Weighting the mean may mitigate some of these issues. If the reward for the mean is sufficiently small, then it only becomes a contributing factor when the difference approaches zero. Thus first considered function is

$$fit_1 = \left|\overline{\|SAR\|} - \text{mode}(\|SAR\|)\right| - 0.1 \times \overline{SAR}. \tag{5.6}$$

SAR represents the entire set of data points. When calculating the difference, the SAR values are rounded to the nearest integer to bin real numbers into groups of whole numbers to enhance the contribution of the mode by eliminating small differences.

Although minimizing the difference between the statistically typical value and the most commonly occurring value may indicate similar values throughout the volume, it does not address the issue of local hotspots. So perhaps it could be beneficial to minimize the difference between the maximum and the mode as given by the function

$$fit_2 = |\max(\|SAR\|) - \text{mode}(\|SAR\|)| - 0.1 \times \overline{SAR}. \tag{5.7}$$

After some consideration, it becomes obvious that relying on the mode as an indicator of similarity may prove unwise. In a set of 277 unique numbers, the mode only comprises two values; therefore, (5.5) and (5.6) may be skewed by a disproportionately small portion of the set. Therefore, it may be useful to determine the percentage of points that fall within some specific distance of the mean as given by

$$fit_3 = -(\sum(|\overline{SAR} - SAR| < 0.1 \times \overline{SAR})/N_{SAR}) - 0.01 \times \overline{SAR} \tag{5.8}$$

where N_{SAR} is the number of elements in the set *SAR*. The weight for the mean of the SAR is reduced to 0.01. Since the first term will always fall in the interval [-1, $-N_{SAR}^{-1}$], any mean value greater than 10 would dominate (5.7) if the weight remain 0.1.

5.2.2.4 Optimization Results

The array SAR is minimized according to each of the fitness functions described in the previous section, resulting in the optimized element phases given in Table 5.12. Only the optimization using fit_1 reaches the threshold as shown in Figure 5.35, which compares the mean to best fitness across all iterations. Optimization with fit_2 appears to have very nearly stagnated after just over 100 iterations, but the mean value of fit_3 is clearly still decreasing as the procedure terminates at the maximum number of iterations. Figure 5.36 displays the "view" of the best particle from the perspective of the fitness function. As the ultimate goal of this optimization is to reduce the SAR value at all sampled points to a single value, an ideal histogram of the SAR in the breast tissue should contain a single peak equal to the number of sampled points. Figures 5.37 (a), (c), and (e) present histograms of each set of points in Figure 5.36. As anticipated, fit_3 clusters more points to the mean than, and eliminates more high values than fit_1. The array optimized by fit_2 deftly removes the outlying high values as designed, but fails to reward a single value over others. The first fitness function does manage to reward a higher mean, but likely as a result of the inclusion of many high values. Calculations of the SAR on an expanded set of 35,131 points (Figures 5.37 (b), (d), (f)) show very little difference between the first and second solutions, but validate the effectiveness of fit_3 in maximizing the homogeneity of SAR.

On the breast tissue surface, SAR varies little between the three phase configurations aside from the location of the "warmest" patches. Unfortunately, all three solutions still show surface hot spots (Figure 5.38). The SAR distributions seen on the cross-sections of the model in Figures 5.39 and 5.40 bear out the expectations set forth by Figure 5.37. The first two configurations have much larger regions of lower than average SAR than the third, and the first produces more high SAR areas. Interestingly, the radiation patterns shown in Figure 5.41 indicate that much of the energy in the second configuration travels from rather than through the model; this may explain the elimination of higher SAR values by fit_2. Based on the SAR analysis, fit_3 best embodies the prescribed goals of this experiment, and although it is far from ideal, the third configuration is the best solution found.

Table 5.12 Optimized Antenna Element Phases

Port*	1_0	1_1	1_2	2_0	2_1	2_2	3_0	3_1	3_2	Fitness
fit_1	24°	7°	14°	22°	264°	-136°	-89°	218°	131°	-1.0969
fit_2	28°	43°	24°	-71°	-252°	-182°	-180°	-206°	-17°	7.0142
fit_3	-212°	194°	-192°	58°	90°	69°	-40°	177°	95°	-0.3698

* Ports are numbered from the lower left as *m_n*, where *m* is the row and *n* is the column.

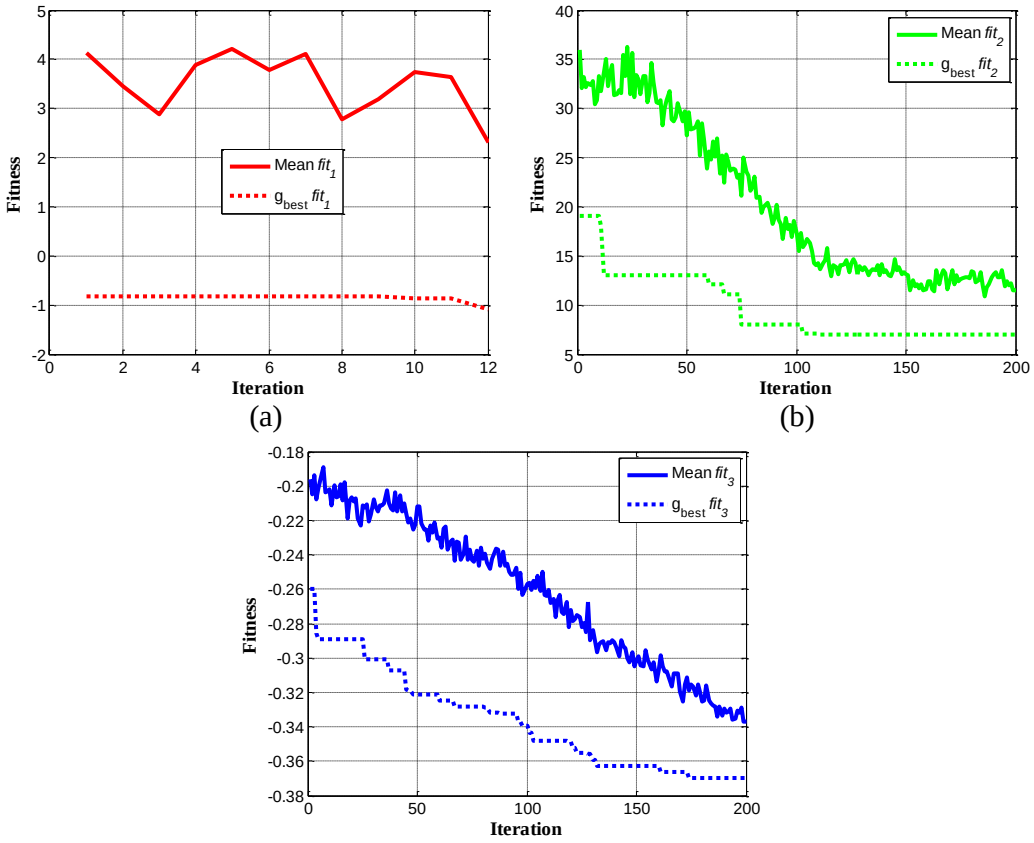

Figure 5.35 Comparison of Mean Fitness to g_{best} for SAR Optimization

(a) fit_1
(b) fit_2
(c) fit_3

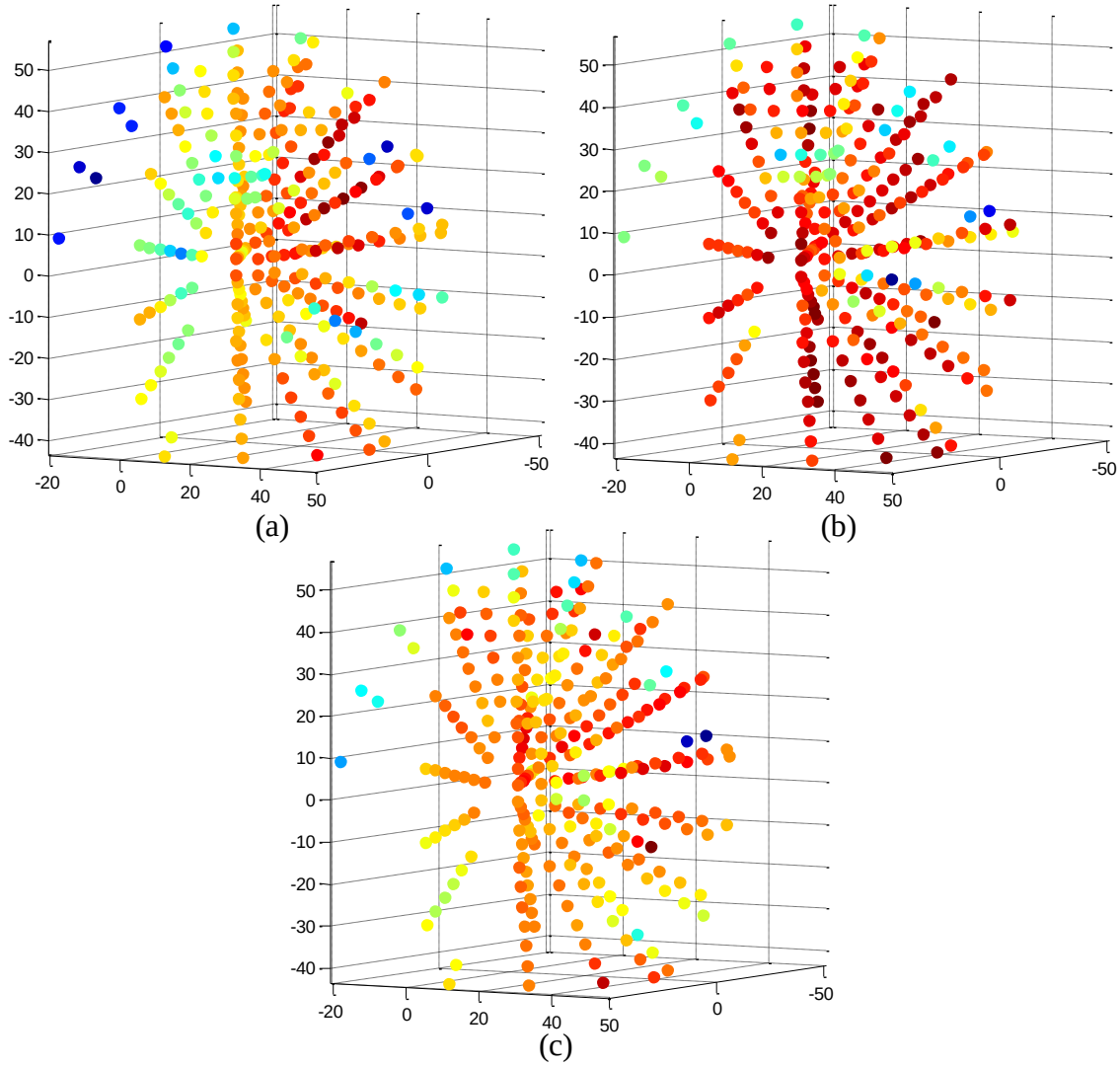

Figure 5.36 Point Clouds of Optimized Array SAR Values

(a) fit_1
(b) fit_2
(c) fit_3

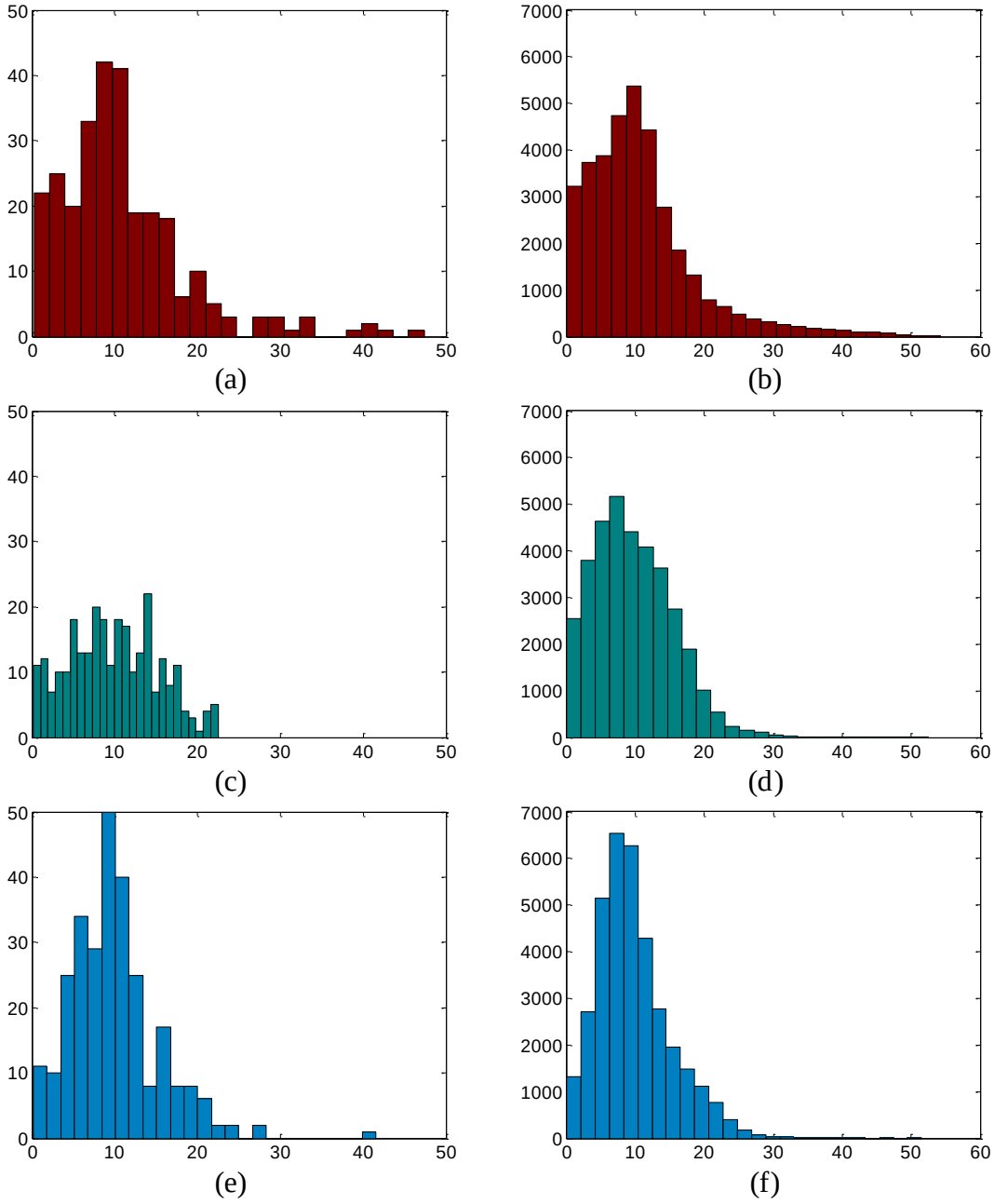

Figure 5.37 Histograms of Optimized Array SAR Values

(a) fit_1, Optimization Points
(b) fit_1, Expanded Points
(c) fit_2, Optimization Points
(d) *fit2*, Expanded Points
(e) fit_3, Optimization Points
(f) fit_3, Expanded Points

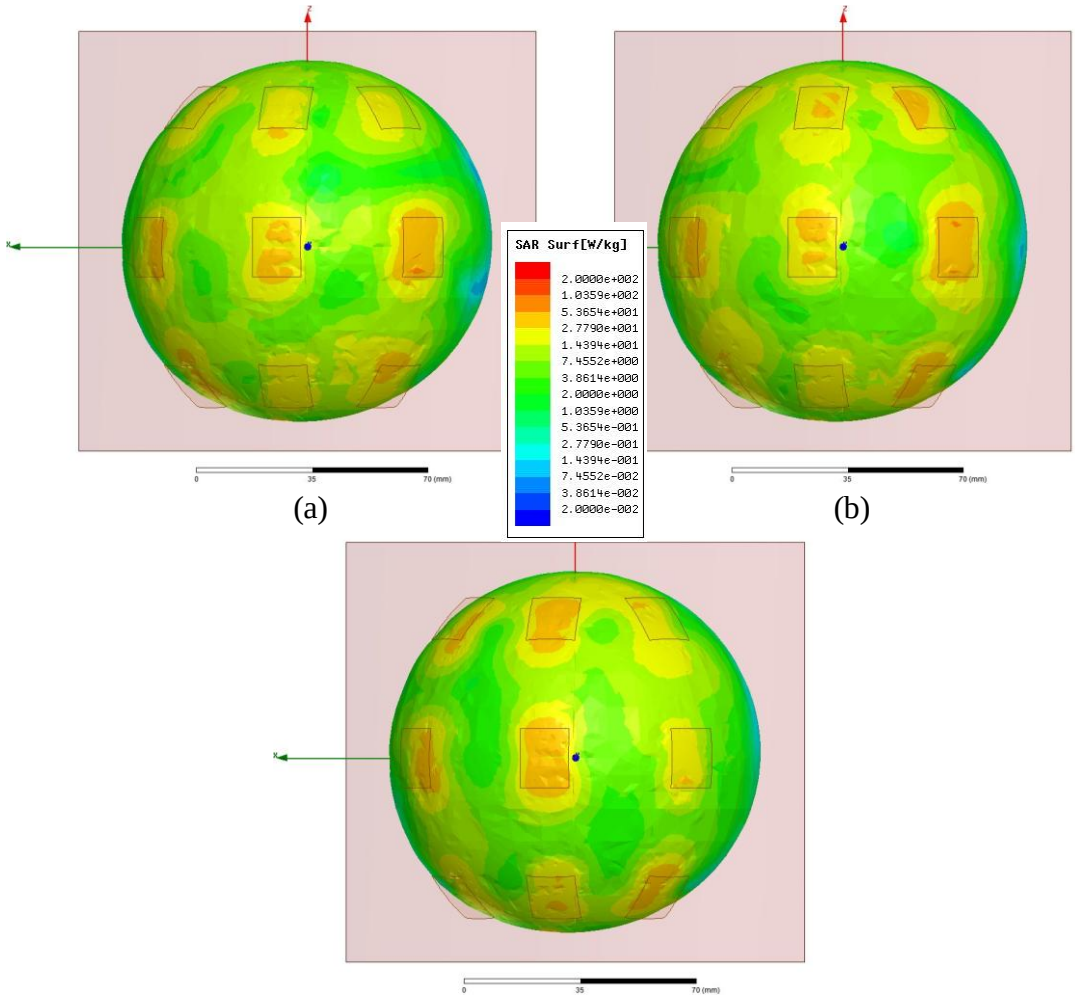

(a) (b)

(c)

Figure 5.38 Comparison of Optimized SAR on Breast Tissue Surface

(a) fit_1
(b) fit_2
(c) fit_3

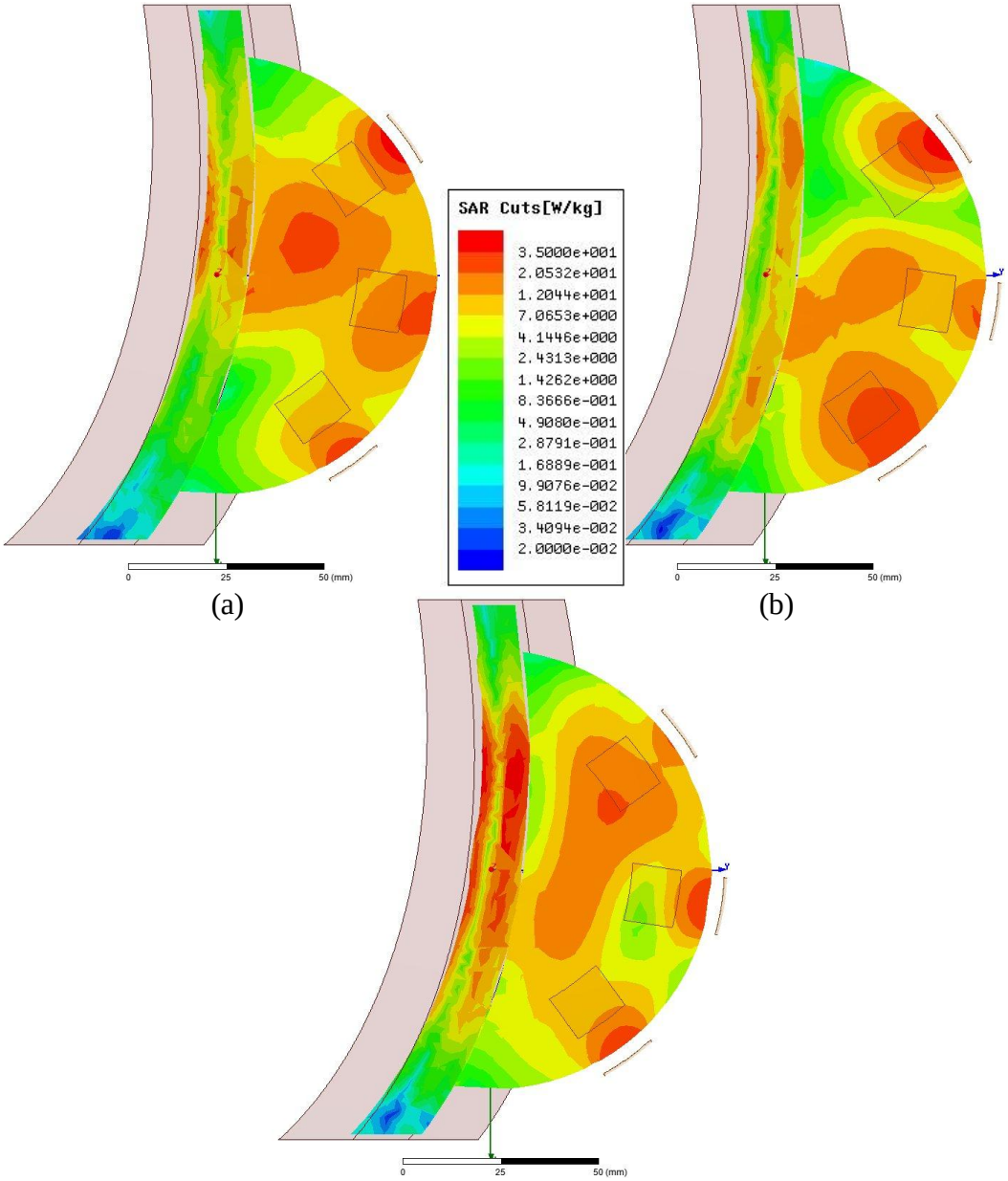

Figure 5.39 Comparison of Optimized SAR on a Horizontal Cross-Section

(a) fit_1
(b) fit_2
(c) fit_3

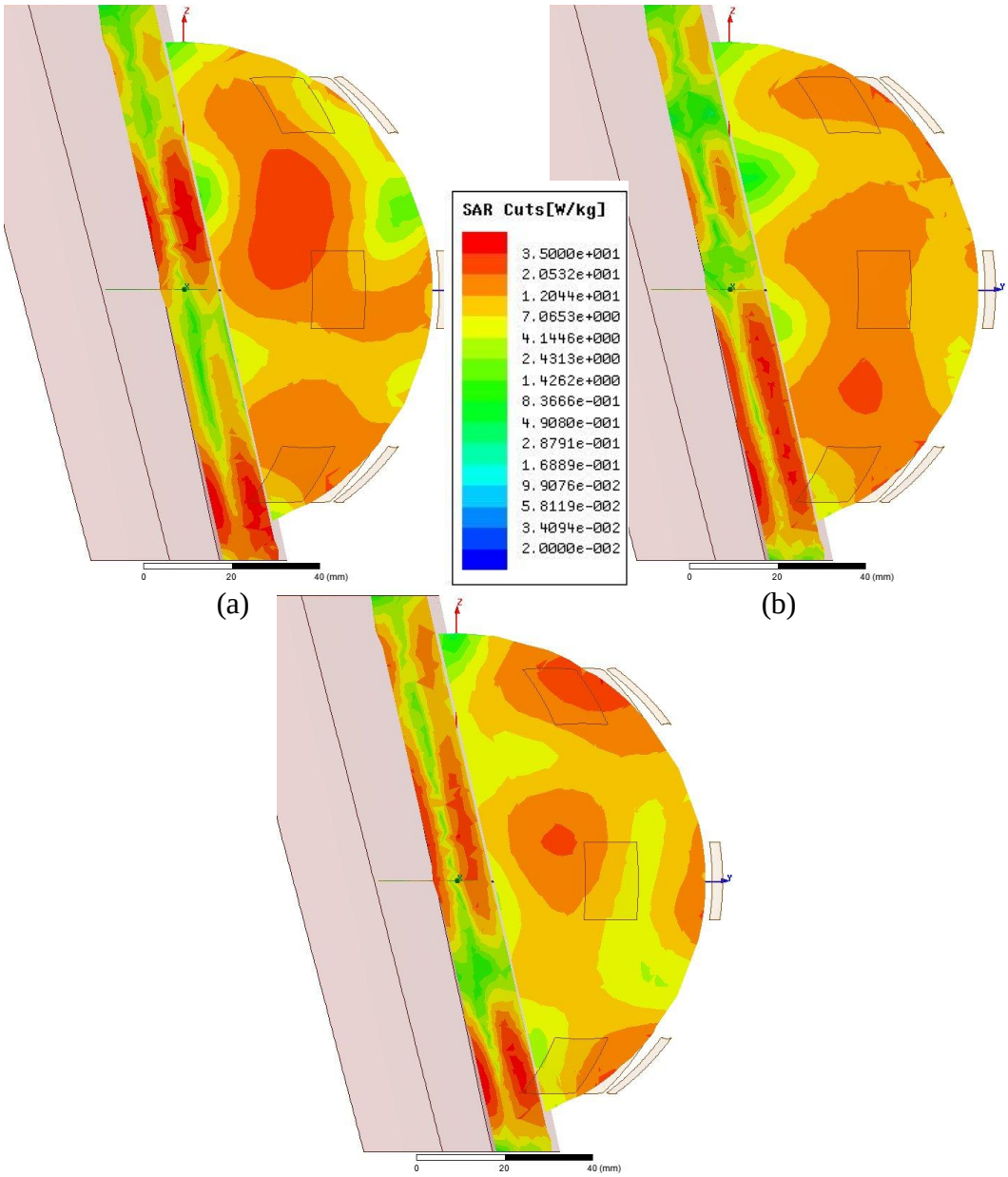

Figure 5.40 Comparison of Optimized SAR on a Vertical Cross-Section

(a) fit1
(b) fit2
(c) fit3

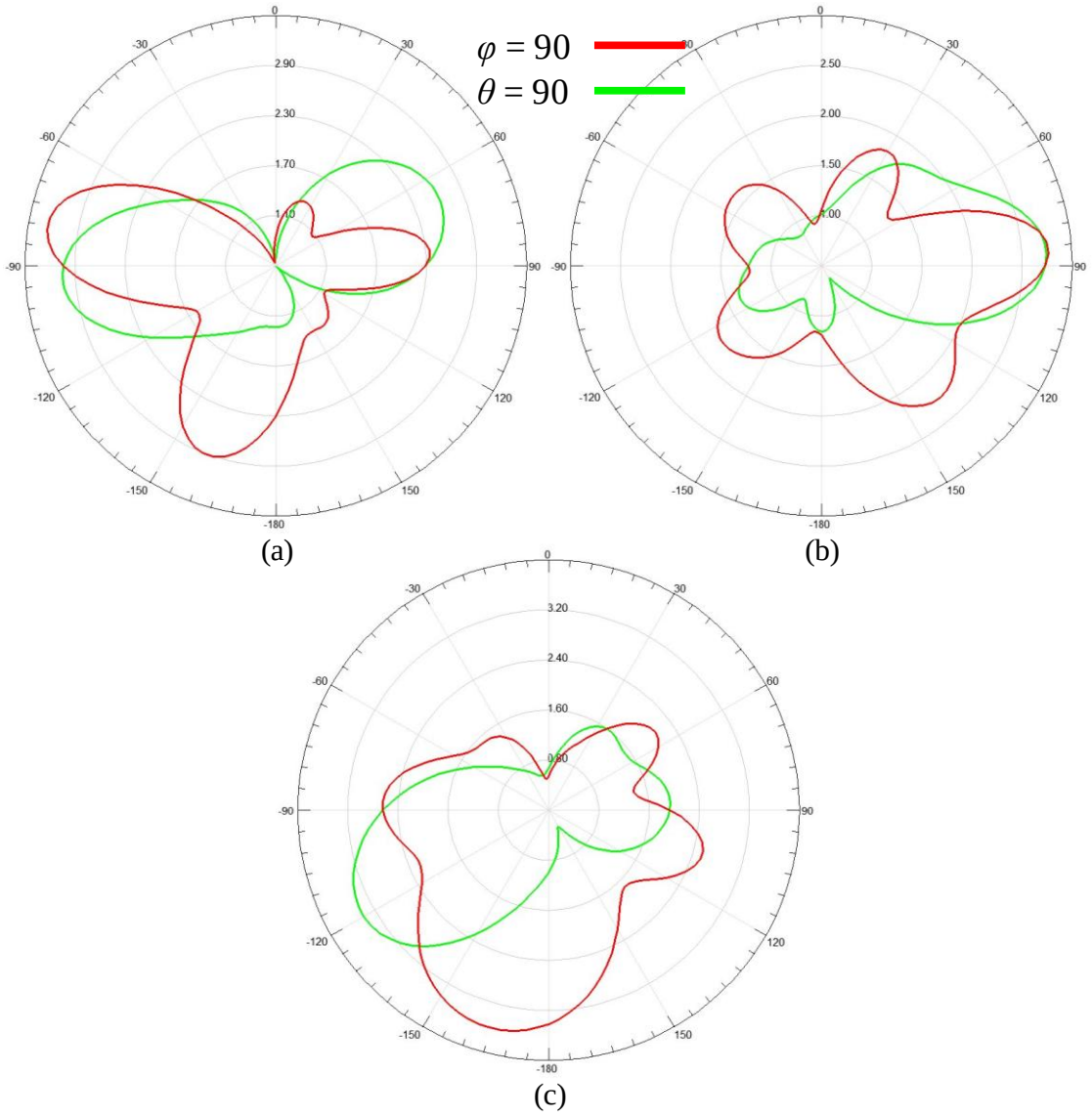

Figure 5.41 Radiation Patterns of Optimized Arrays

(a) fit_1
(b) fit_2
(c) fit_3

5.2.2.5 Optimized Array Applied to Heterogeneous Breast Model

While the uniform breast tissue model provides a convenient test platform, it is not truly representative of a human breast in which glandular and fibrous tissues constitute substantially more than 15% at least some regions. As the normal types 1 and

2 breast tissue described in [119]–[121] represent a mixture of adipose, glandular, and fibrous tissues, inserting a vaguely representative shape of the region of breast most likely to contain these elements into the homogeneous model should provide a somewhat reasonable approximation of their influence on antenna behavior. A consultation of Figure 5.1 reveals that ligaments and gland lobules mingle with adipose throughout the breast with a primary concentration near the center. To approximate these regions, cones of type 1 (0–30% adipose) and type 2 (31-84% adipose) are introduced to the homogeneous model as shown in Figure 5.42. The type 1 cone (pink) has upper and lower radii of 9.525 mm and 19.95 mm, respectively, and a height of 18.24 mm. The type 2 cone (blue) mates to the bottom of the type 1 cone, and has a lower radius of 28.5 mm with a height of 22.8 mm. The total height of the cones and the diameter of the largest cone correspond to approximately 36% and 50% of the breast diameter, respectively.

To evaluate the effects of the presence of the higher permittivity tissues, the array optimized by fit_3 in the previous section is applied to the heterogeneous model. The frequency response (Figure 5.43) indicates that at least one element has shifted nearly entirely out-of-band, but overall the antennas are relatively undisturbed. However, the previously homogeneous SAR distribution has been broken into a highly absorptive central region with the clear influence of individual elements visible near the surface as shown in Figures 5.44 and 5.45. Additionally most of the radiated field points away from the breast rather than toward it (Figure 5.46). Unfortunately these results do not ultimately satisfy the goals of the optimization, but they do provide a path forward.

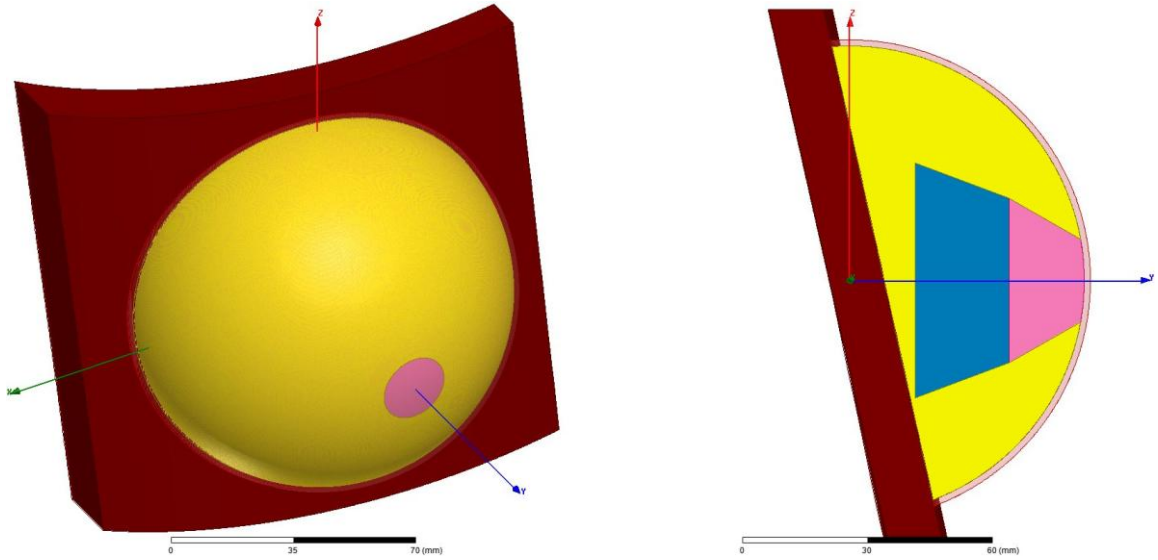

(a) (b)

Figure 5.42 Breast Model with Glandular and Fibrous Tissues Included

(a) Isometric View
(b) Vertical Cross-Section Showing Breast Tissue Types 1 (Pink) and 2 (Blue)

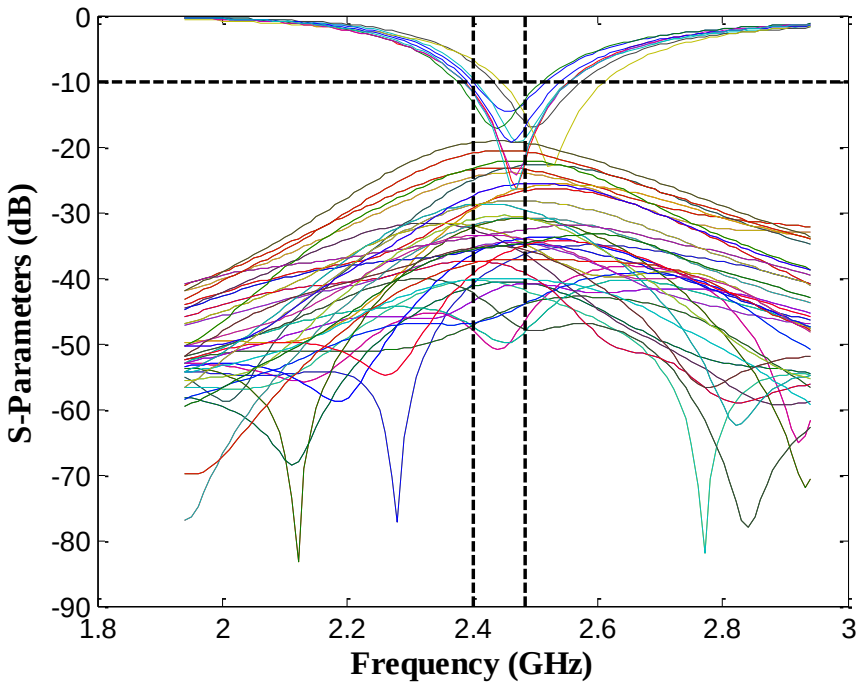

Figure 5.43 S-Parameters of Nine-Element Array on Heterogeneous Model

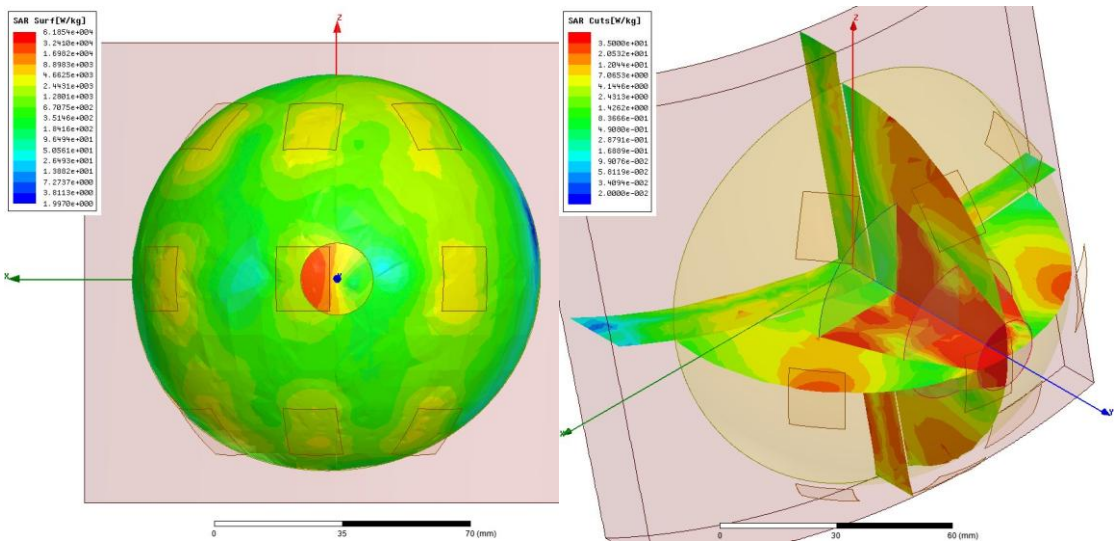

(a) (b)

Figure 5.44 SAR of Nine-Element Array on Heterogeneous Model

(a) SAR on Surface of Breast Tissue
(b) SAR on Cross-Sections

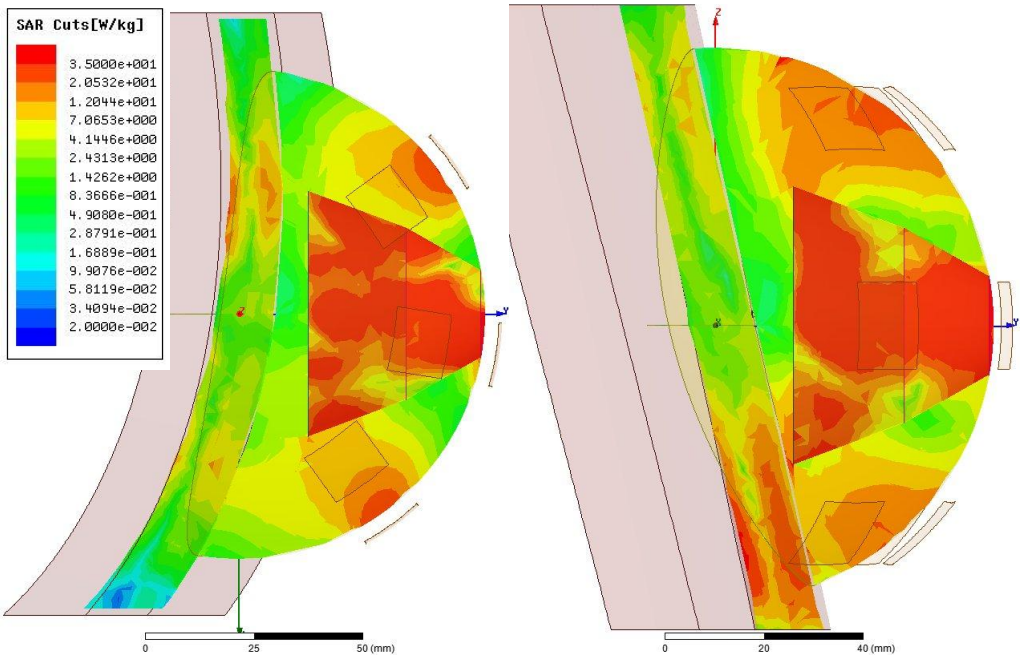

(a) (b)

Figure 5.45 SAR of Nine-Element Array on Multi-Tissue Model Cross-Sections

(a) Horizontal
(b) Vertical

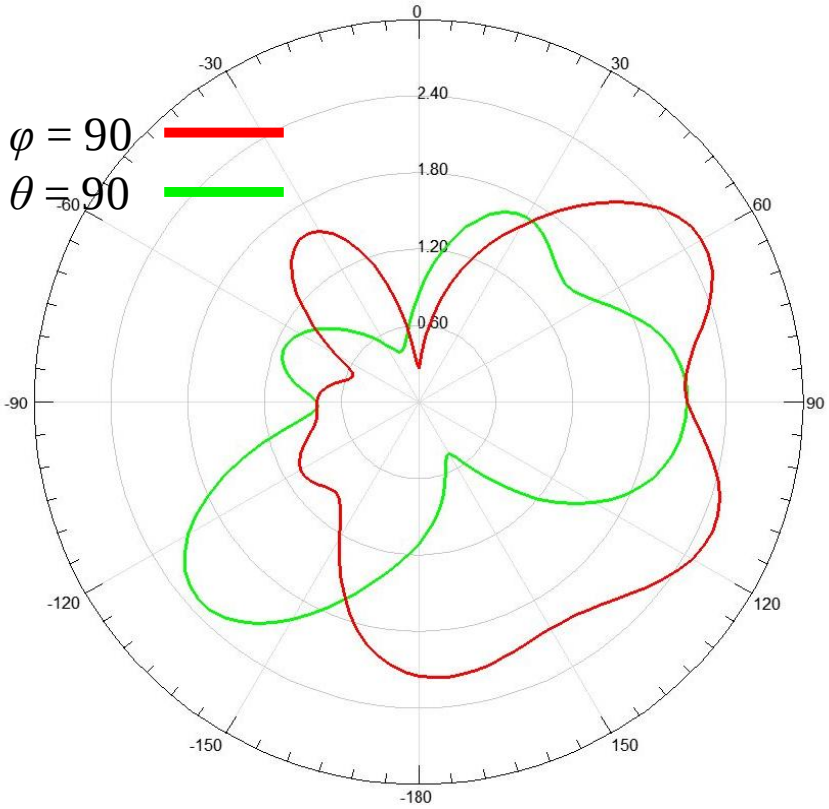

Figure 5.46 Radiation Pattern of Nine-Element Array on Heterogeneous Model

CHAPTER VI

CONCLUSIONS AND FUTURE WORK

6.1 Conclusions

Given the proper conditions, antennas applied in medicine can offer improved quality of life to patients. Implantable medical devices such as pacemakers and glucose monitors rely on antennas to harmlessly communicate important information to the patient and his physicians. However, the same (or at least very similar) antennas can also be used in the destruction of cancer. This dissertation has explored designing antennas for both applications through optimization.

While many optimization techniques exist, this paper investigates particle swarm optimization and a few of its variants (Meta PSO, Modified Meta PSO, and Stabilized Modified Meta PSO) due to their successes in antenna optimization in the literature. A series of benchmarks is performed to determine the effectiveness of each defining parameter. The only concrete resolutions from the testing are that Modified Meta PSO should generally be avoided, and that over a large enough set of data, individual parameters influence the performance of the optimizer very little.

Miniaturization of electronic components opens the way for increasingly complex devices in smaller packages. In turn many new applications for implants are becoming feasible, and all of them will require communication links. Unfortunately, the wonder of the human body introduces a wonderfully non-trivial array of complications that an

antenna designer must overcome. Implanted antennas must compensate for the frequency- and temperature-dependent nature of their environment. A dual-band serpentine planar inverted-F antenna is optimized for subcutaneous implantation for the MedRadio and Industrial, Scientific, and Medical spectra to complement the implantable transceivers that use one band for communication and the other for low-powered wakeup signals. Measurements of the fabricated antenna embedded in gel designed to mimic the dielectric properties of skin reveal excellent performance relative to the simulations.

Growing interest in the adjuvant application of hyperthermia in cancer treatment stems from the mounting evidence that radiation (the non-ionizing kind) assists radiation (the ionizing kind) and chemotherapy. Increasing the temperature of tumors can increase blood perfusion and receptivity to cancer-destroying drugs. Unfortunately current systems require patients to remain confined during administration of microwave heating for continuous temperature monitoring and due high power requirements. Chapter V investigates the possibility of using a lower-powered antenna array in the shape of a relatively comfortable garment to allow patients some freedom during treatment. Seven antennas are optimized for operation in the unlicensed 433, 915, 2400, and 5800 MHz on a layered cubic model representative of the tissues found in the human breast. Based on its excellent bandwidth and acceptably high induced specific absorption rate (SAR), a rectangular patch antenna tuned for a center frequency of 2.441 GHz is selected to create a nine-element array organized in a 3 × 3 grid with 45° radial separation between the elements. The array is arranged on a hemi-spherical model containing layers of skin, dielectrically homogeneous breast tissue, and muscle. The phase difference between the antenna feeds is then optimized to deliver uniform SAR levels throughout the breast

tissue. The optimized configuration is then simulated on a model containing heterogeneous breast tissues. While the SAR distribution is relatively homogeneous in the homogeneous model, the heterogeneous tissue introduces large disturbances in the antenna's near-field, resulting in higher levels of SAR in the fibrous and glandular tissues than the adipose tissue. Unfortunately the solution described in this dissertation could not be used for adjuvant hyperthermia in the absence of temperature monitoring and calibration for an individual.

6.2 Future Work

The hyperthermia study in Chapter V offers cautious optimism that at least partially fulfills the stated goals could be designed with more work. First, the array should be optimized for the heterogeneous model, and the electromagnetic simulation process should be coupled to a thermal solver to verify temperatures. Second, the power level for each port should be optimized alongside the phase difference. Third, breast phantoms should be fabricated to validate the simulations. Finally, other array configurations such as concentric rings should be considered for optimization once the data gained from the measurements has been incorporated.

REFERENCES

[1] J.A. Warren, R.D. Dreher, R.V. Jaworski, J.J. Putzke, and R.J. Russie, "Implantable cardioverter defibrillators," *Proceedings of the IEEE* , vol.84, no.3, pp.468-479, Mar 1996.

[2] F. Nebeker, "Golden accomplishments in biomedical engineering," *Engineering in Medicine and Biology Magazine, IEEE* , vol.21, no.3, pp. 17- 47, May/Jun 2002.

[3] "Medical Implant Communications Service (MICS) federal register," Rules and Regulations, vol. 64, no. 240, pp. 69 926–69 934, Dec. 1999.

[4] P. Soontornpipit, C.M. Furse, and Y.C. Chung, "Design of implantable microstrip antenna for communication with medical implants," *IEEE Transactions on Microwave Theory and Techniques*, vol.52, no.8, pp. 1944- 1951, Aug. 2004.

[5] J. Kim and Y. Rahmat-Samii, "Implanted antennas inside a human body: simulations, designs, and characterizations," *IEEE Transactions on Microwave Theory and Techniques*, vol.52, no.8, pp. 1934- 1943, Aug. 2004.

[6] C. Gabriel, S. Gabriel, and E. Corthout, "The dielectric properties of biological tissues: I. Literature survey," *Physics in Medicine and Biology*, vol. 41, pp. 2231–2249, 1996.

[7] S. Gabriel, R. W. Lau, and C. Gabriel, "The dielectric properties of biological tissues: II. Measurements in the frequency range 10 Hz to 20 GHz," *Physics in Medicine and Biology*, vol. 41, pp. 2251–2269, 1996.

[8] S. Gabriel, R. W. Lau, and C. Gabriel, "The dielectric properties of biological tissues: III. Parametric models for the dielectric spectrum of tissues," *Physics in Medicine and Biology*, vol. 41, pp. 2271–2293, 1996.

[9] T. Karacolak, A.Z. Hood, and E. Topsakal, "Design of a dual-band implantable antenna and development of skin mimicking gels for continuous glucose monitoring," *IEEE Transactions on Microwave Theory and Techniques*, vol.56, no.4, pp.1001-1008, April 2008.

[10] T. Karacolak and E. Topsakal, "Electrical properties of nude rat skin and design of implantable antennas for wireless data telemetry," *2008 IEEE MTT-S International Microwave Symposium Digest*, pp. 907-910, 15-20 June 2008.

[11] T. Yilmaz, T. Karacolak, and E. Topsakal, "Characterization and testing of a skin mimicking material for implantable antennas operating at ISM band (2.4 GHz-2.48 GHz)," *IEEE Antennas and Wireless Propagation Letters*, vol.7, pp.418-420, 2008.

[12] P. Wust, B. Hildebrandt, G. Sreenivasa, B. Rau, J. Gellermann, H. Riess, R. Felix, and P.M. Schlag, "Hyperthermia in combined treatment of cancer," *The Lancet Oncology*, vol. 3, pp. 487-497, Aug. 2002.

[13] A.Y. Cheung and J. Al-Atrash, "Microwave hyperthermia for cancer therapy," *IEE Proceedings*, vol. 134, no. 6, pp. 493-522, June 1987.

[14] B. Hildebrand, P. Wust, O. Ahlers, A. Dieing, G. Sreenivasa, T. Kerner, R. Felix, and H. Riess, "The cellular and molecular basis of hyperthermia," *Critical Reviews in Oncology/Hematology*, vol. 43, no. 1 , pp. 33-56, July 2002.

[15] J.H. Breasted, *The Edwin Smith Surgical Papyrus*. Chicago, 1930.

[16] R.D. Issels, "Hyperthermia adds to chemotherapy," *European Journal of Cancer*, vol. 44, no. 17, pp. 2546-2554, Nov. 2008.

[17] R. Colombo, A. Salonia, L.F. Da Pozzo, R. Naspro, M. Freschi, R. Paroni, M. Pavone-Macaluso, and P. Rigatti, "Combination of intravesical chemotherapy and hyperthermia for the treatment of superficial bladder cancer: preliminary clinical experience," *Critical Reviews in Oncology/Hematology*, vol. 47, no. 2, pp. 127-139, Aug. 2003.

[18] J. van der Zee, D.G. González, G.C. van Rhoon, J.D.P. van Dijk, W.L.J. van Putten, and A.A.M. Hart, "Comparison of radiotherapy alone with radiotherapy plus hyperthermia in locally advanced pelvic tumours: a prospective, randomised, multicentre trial," *The Lancet*, vol. 355, pp. 1119-1125, Apr. 2000.

[19] R. Colombo, L.F. Da Pozzo, A. Lev, M. Freschi, G. Gallus, and P. Rigatti, "Neoadjuvant combined microwave induced local hyperthermia and topical chemotherapy versus chemotherapy alone for superficial bladder cancer," *The Journal of Urology*, vol. 155, no. 4, pp. 1227-1232, Apr. 1996.

[20] A.G. van der Heijden, L.A. Kiemeney, O.N. Gofrit, O. Nativ, A. Sidi, Z. Leib, R. Colombo, R. Naspro, M. Pavone, J. Baniel, F. Hasner, and J.A. Witjes, "Preliminary european results of local microwave hyperthermia and chemotherapy treatment in intermediate or high risk superficial transitional cell carcinoma of the bladder," *European Urology*, vol. 46, no. 1, pp. 65-72, July 2004.

[21] R.J.M. Lammers, J.A. Witjes, B.A. Inman, I. Leibovitch, M. Laufer, O. Nativ, and R. Colombo, "The role of a combined regimen with intravesical chemotherapy and hyperthermia in the management of non-muscle-invasive bladder cancer: a systematic review," *European Urology*, vol. 60, no. 1, pp. 81-93, July 2011.

[22] H.I. Robins, W.H. Dennis, R.A. Steeves, and P.M. Sondel, "A proposal for the addition of hyperthermia to treatment regimens for acute and chronic leukemia," *Journal of Clinical Oncology*, vol. 2, no. 9, pp. 1050-1056, Sep. 1984.

[23] P. K. Sneed, P.R. Stauffer, M.W. McDermott, C.J. Diederich, K.R. Lamborn, M.D. Prados, S. Chang, K.A. Weaver, L. Spry, M.K. Malec, S.A. Lamb, B. Voss, R.L. Davis, W.M. Wara, D.A. Larson, T.L. Phillips, and P.H. Gutin, "Survival benefit of hyperthermia in a prospective randomized trial of brachytherapy boost ± hyperthermia for glioblastoma multiforme," *International Journal of Radiation Oncology*Biology*Physics*, vo. 40, no. 2, pp. 287-295, Jan. 1998.

[24] Y. Kinashi, S.I. Masunaga, M. Suzuki, K. Ono, T. Ohnishi, "Hyperthermia enhances thermal-neutron–induced cell death of human glioblastoma cell lines at low concentrations of 10b," *International Journal of Radiation Oncology*Biology*Physics*, vol. 40, no. 5, pp. 1185-1192, Mar. 1998.

[25] J. Dragovic, H.G. Seydel, T. Sandhu, A. Kolosvary, and J. Blough, "Local superficial hyperthermia in combination with low-dose radiation therapy for palliation of locally recurrent breast carcinoma," *Journal of Clinical Oncology*, vol. 7, no. 1, pp. 30-35, Jan. 1989.

[26] C.C. Vernon, J.W. Hand, S.B. Field, D. Machin, J.B. Whaley, J. van der Zee, W.L.J. van Putten, G.C. van Rhoon, J.D.P. van Dijk, D.G. González, F. Liu, P. Goodman, and M. Sherar, "Radiotherapy with or without hyperthermia in the treatment of superficial localized breast cancer: Results from five randomized controlled trials," *International Journal of Radiation Oncology*Biology*Physics*, vol. 35, no. 4, pp. 731-744, July 1996.

[27] T.M. Zagar, K.A. Higgins, E.F. Miles, Z. Vujaskovic, M.W. Dewhirst, R.W. Clough, L.R. Prosnitz, and E.L. Jones, "Durable palliation of breast cancer chest wall recurrence with radiation therapy, hyperthermia, and chemotherapy," *Radiotherapy and Oncology: Journal of the European Society for Therapeutic Radiology and Oncology*, vol. 97, no. 3, pp. 535-540, Dec. 2010.

[28] E.L Jones, L.R Prosnitz, M.W Dewhirst, P.K Marcom, P.H Hardenbergh, L.B Marks, and D.M Brizel, "Tumor oxygenation during concurrent hyperthermia, taxol, and radiation therapy for locally advanced breast cancer," *International Journal of Radiation Oncology*Biology*Physics*, vol. 48, no. 3, Supplement 1, p. 197, 2000.

[29] Z Vujaskovic, J.M Poulson, K.L Blackwell, E.L Jones, E.L Rosen, T.V Samulski, D.M Brizel, M.W Dewhirst, and L.R Prosnitz, "Neoadjuvant chemotherapy and hyperthermia improve tumor reoxygenation in patients with locally advanced breast carcinoma," *International Journal of Radiation Oncology*Biology*Physics*, vol. 54, no. 2, Supplement, p. 218, Oct. 2002.

[30] T. Feyerabend, G.J. Wiedemann, B. Jäger, H. Vesely, B. Mahlmann, and E. Richter, "Local hyperthermia, radiation, and chemotherapy in recurrent breast cancer is feasible and effective except for inflammatory disease," *International Journal of Radiation Oncology*Biology*Physics*, vol. 49, no. 5, pp. 1317-1325, Apr. 2001.

[31] Z Vujaskovic, E.L Jones, L.R Prosnitz, P.K Marcom, P.H Hardenbergh, L.B Marks, T.V Samulski, D.M Brizel, M.W Dewhirst, "Concurrent chemotherapy, hyperthermia and radiotherapy improve reoxygenation in locally advanced breast cancer," *International Journal of Radiation Oncology*Biology*Physics*, vol. 57, no. 2, p. S357, Oct. 2003.

[32] D.S. Yoo, Z. Vujaskovic, L.R. Prosnitz, L.B. Marks, K.L. Blackwell, M.W. Dewhirst, and E.L. Jones, "2026: Hyperthermia Augments Local Response to Doxil Chemotherapy in Breast Cancer Patients," *International Journal of Radiation Oncology*Biology*Physics*, vol. 66, no. 3, pp. S223-S224, Nov. 2006.

[33] T.M. Zagar, K. Higgins, M. Edward, Z. Vujaskovic, M. Dewhirst, R. Clough, and E. Jones, "Long-term palliation of breast cancer chestwall recurrence with radiation therapy, hyperthermia, and chemotherapy," *International Journal of Radiation Oncology*Biology*Physics*, vol. 75, no. 3, p. S505, Nov. 2009.

[34] M. Sherar, F. Liu, M. Pintilie, W. Levin, J. Hunt, R. Hill, J. Hand, C. Vernon, G. van Rhoon, J. van der Zee, D.G. Gonzalez, J. van Dijk, J. Whaley, and D. Machin, "Relationship between thermal dose and outcome in thermoradiotherapy treatments for superficial recurrences of breast cancer: Data from a phase III trial," *International Journal of Radiation Oncology*Biology*Physics*, vol. 39, no. 2, pp. 371-380, Sept. 1997.

[35] E. Jones, D. Brizel, M. Dewhirst, A. Alvarez, A. Berchuck, D. Clarke-Pearson, G. Rodriquez, J. Soper, and L. Prosnitz, "Phase I/II results using concurrent hyperthermia, radiotherapy, and chemotherapy for cervix cancer," *International Journal of Radiation Oncology*Biology*Physics*, vol. 51, no. 3, Supplement 1, pp. 63-64, Nov. 2001.

[36] M. Franckena, L.J.A. Stalpers, P.C.M. Koper, R.G.J. Wiggenraad, W.J. Hoogenraad, J.D.P. van Dijk, C.C. Wárlám-Rodenhuis, J.J. Jobsen, G.C. van Rhoon, and J. van der Zee, "Long-term improvement in treatment outcome after radiotherapy and hyperthermia in locoregionally advanced cervix cancer: an update of the dutch deep hyperthermia trial," *International Journal of Radiation Oncology*Biology*Physics*, vol. 70, no. 4, pp. 1176-1182, Mar. 2008.

[37] M. Franckena, L.C. Lutgens, P.C. Koper, C.E. Kleynen, E.M. van der Steen-Banasik, J.J. Jobsen, J.W. Leer, C.L. Creutzberg, M.F. Dielwart, Y. van Norden, R.A.M. Canters, G.C. van Rhoon, and J. van der Zee, "Radiotherapy and hyperthermia for treatment of primary locally advanced cervix cancer: results in 378 patients," *International Journal of Radiation Oncology*Biology*Physics*, vol. 73, no. 1, pp. 242-250, Jan. 2009.

[38] R.D. Issels, S. Abdel-Rahman, C.-M. Wendtner, M.H. Falk, V. Kurze, H. Sauer, U. Aydemir, W. Hiddemann, "Neoadjuvant chemotherapy combined with regional hyperthermia (RHT) for locally advanced primary or recurrent high-risk adult soft-tissue sarcomas (STS) of adults: long-term results of a phase II study," *European Journal of Cancer*, vol. 37, no. 13, pp. 1599-1608, Sept. 2001.

[39] A. Ressel, O. Schmitt, C. Weiss, and T. Feyerabend, "Therapeutic outcome and side-effects after radiotherapy, chemotherapy and/or hyperthermia treatment of head and neck tumour xenografts," *European Journal of Cancer*, vol. 38, no. 4, pp. 594-601, Mar. 2002.

[40] K. Riehemann, O. Schmitt, and E.-M. Ehlers, "The effects of thermochemotherapy using cyclophosphamide plus hyperthermia on the malignant pleural mesothelioma in vivo," *Annals of Anatomy*, vol. 187, no. 3, pp. 215-223, July 2005.

[41] M. van Vulpen, B.W. Raaymakers, J.J.W. Lagendijk, J. Crezee, A.A.C. de Leeuw, J.R.A. van Moorselaar, C.M. Ligtvoet, and J.J. Battermann, "Three-dimensional controlled interstitial hyperthermia combined with radiotherapy for locally advanced prostate carcinoma—a feasibility study," *International Journal of Radiation Oncology*Biology*Physics*, vol. 53, no. 1, pp. 116-126, May 2002.

[42] M.S. Anscher, C. Lee, H. Hurwitz, D. Tyler, L.R. Prosnitz, P. Jowell, G. Rosner, T. Samulski, and M.W. Dewhirst, "A pilot study of preoperative continuous infusion 5-fluorouracil, external microwave hyperthermia, and external beam radiotherapy for treatment of locally advanced, unresectable, or recurrent rectal cancer," *International Journal of Radiation Oncology*Biology*Physics*, vol. 47, no. 3, pp. 719-724, June 2000.

[43] J. Van Der Zee and J. Overgaard, “Hyperthermia classic commentary: ‘Hyperthermia as an adjuvant to radiation therapy of recurrent or metastatic malignant melanoma. A multicentre randomized trial by the European Society for Hyperthermic Oncology’ J. Overgaard, D. González González, M.C.C.H. Hulshof, G. Arcangeli, O. Dahl, O. Mella & S.M. Bentzen, International Journal of Hyperthermia 1996;12:3–20,” *International Journal of Hyperthermia*, vol. 25, no. 5, pp. 335-337, Aug. 2009.

[44] J. Overgaard, D.G. Gonzalez, M.C.C.H. Hulshof, G. Arcangeli, O. Dahl, O. Mella, and S.M. Bentzen, “Hyperthermia as an adjuvant to radiation therapy of recurrent or metastatic malignant melanoma. A multicentre randomized trial by the European Society for Hyperthermic Oncology,” *International Journal of Hyperthermia*, vol. 25, no. 5, pp. 323-334, Aug. 2009.

[45] M. Aktas, D. de Jong, J.J. Nuyttens, J. van der Zee, D.H.M. Wielheesen, E. Batman, C.W. Burger, and A.C. Ansink, “Concomitant radiotherapy and hyperthermia for primary carcinoma of the vagina: A cohort study,” *European Journal of Obstetrics & Gynecology and Reproductive Biology*, vol. 133, no. 1, pp. 100-104, July 2007.

[46] C. Müller, “Eine neüe Behandlungsmethode bösartiger Geschwülste,” *Münchener Medizinische Wochenschrift*, vol. 28, pp. 1490-1493, 1910.

[47] S.L. Warren, “Preliminary study of the effect of artificial fever upon hopeless tumor cases,” *American Journal of Roentgenology*, vol. 33, p. 75, 1935.

[48] K.D. Paulsen, J.W. Strohbehn, and D.R. Lynch, "Theoretical electric field distributions produced by three types of regional hyperthermia devices in a three-dimensional homogeneous model of man," *IEEE Transactions on Biomedical Engineering*, vol. 35, no. 1, pp. 36-45, Jan. 1988.

[49] M.J. Hagmann, "Optimization of helical coil applicators for hyperthermia," *IEEE Transactions on Microwave Theory and Techniques*, vol. 36, no. 1, pp. 148-150, Jan. 1988.

[50] C.-Q. Wang and O.P. Gandhi, "Numerical simulation of annular phased arrays for anatomically based models using the FDTD method," *IEEE Transactions on Microwave Theory and Techniques*, vol. 37, no. 1, pp. 118-126, Jan. 1989.

[51] K.M. Jones, J.A. Mechling, J.W. Strohbehn, and B.S. Trembly, "Theoretical and experimental SAR distributions for interstitial dipole antenna arrays used in hyperthermia," *IEEE Transactions on Microwave Theory and Techniques*, vol. 37, no. 8, pp. 1200-1209, Aug. 1989.

[52] C.M. Furse and M.F. Iskander, "Three-dimensional electromagnetic power deposition in tumors using interstitial antenna arrays," *IEEE Transactions on Biomedical Engineering*, vol. 36, no. 10, pp. 977-986, Oct. 1989.

[53] J.T. Loane, III and S.-W. Lee, "Gain optimization of a near-field focusing array for hyperthermia applications," *IEEE Transactions on Microwave Theory and Techniques*, vol. 37, no. 10, pp. 1629-1635, Oct. 1989.

[54] K.J. Kim, W.C. Choi, and Y.J. Yoon, "Array structure for uniform heat distribution with modified dipole elements," *2012 IEEE International Workshop on Antenna Technology (iWAT)*, pp. 358-361, 5-7 March 2012.

[55] E. Zastrow, S.C. Hagness, B.D. Van Veen, and J.E. Medow, "Time-Multiplexed Beamforming for Noninvasive Microwave Hyperthermia Treatment," *IEEE Transactions on Biomedical Engineering*, vol. 58, no. 6, pp. 1574-1584, June 2011.

[56] J.W. Hand, "Electromagnetic techniques in cancer therapy by hyperthermia," *IEE Proceedings A Physical Science, Measurement and Instrumentation, Management and Education - Reviews*, vol. 128, no. 9, pp. 593-601, Dec. 1981.

[57] J. Robinson and Y. Rahmat-Samii, "Particle swarm optimization in electromagnetics," *IEEE Transactions on Antennas and Propagation*, vol. 52, no. 2, pp. 397- 407, Feb. 2004.

[58] P. Soontornpipit, C.M. Furse, and Y.C. Chung, "Miniaturized biocompatible microstrip antenna using genetic algorithm," *IEEE Transactions on Antennas and Propagation*, vol.53, no.6, pp. 1939-1945, June 2005.

[59] N. Jin and Y. Rahmat-Samii, "Advances in Particle Swarm Optimization for Antenna Designs: Real-Number, Binary, Single-Objective and Multiobjective Implementations," *IEEE Transactions on Antennas and Propagation*, vol. 55, no. 3, Mar. 2007.

[60] Z. Bayraktar, P.L. Werner, and D.H. Werner, "The Design of Miniature Three-Element Stochastic Yagi-Uda Arrays Using Particle Swarm Optimization," *IEEE Antennas and Wireless Propagation Letters*, vol. 5, no. 1, pp. 22-26, Dec. 2006.

[61] S. Selleri, M. Mussetta, P. Pirinoli, R.E. Zich, and L. Matekovits, "Some insight over new variations of the particle swarm optimization method," *IEEE Antennas and Wireless Propagation Letters*, vol. 5, no. 1, pp. 235-238, Dec. 2006.

[62] S.M. Mikki and A.A. Kishk, "Quantum particle swarm optimization for electromagnetics," *IEEE Transactions on Antennas and Propagation*, vol. 54, no. 10, pp. 2764-2775, Oct. 2006.

[63] J.J. Liang, A.K. Qin, P.N. Suganthan, and S. Baskar, "Comprehensive learning particle swarm optimizer for global optimization of multimodal functions," *IEEE Transactions on Evolutionary Computation*, vol. 10, no. 3, pp. 281-295, June 2006.

[64] S. Genovesi, A. Monorchio, R. Mittra, and G. Manara, "A sub-boundary approach for enhanced particle swarm optimization and its application to the design of artificial magnetic conductors," *IEEE Transactions on Antennas and Propagation*, vol. 55, no. 3, pp. 766-770, Mar. 2007.

[65] S. Selleri, M. Mussetta, P. Pirinoli, R.E. Zich, and L. Matekovits, "Differentiated Meta-PSO methods for array optimization," *IEEE Transactions on Antennas and Propagation*, vol. 56, no. 1, pp. 67-75, Jan. 2008.

[66] J. C. Callaghan, and W. G. Bigelow, "An electrical artificial pacemaker for standstill of the heart," *Annals of Surgery*, vol. 134, no. 1, pp. 8-17, July 1951.

[67] F. Nebeker, "Golden accomplishments in biomedical engineering," *IEEE Engineering in Medicine and Biology Magazine*, vol. 21, no. 3, pp. 17-47, May/June 2002.

[68] M. Mirowski, "Termination of malignant ventricular arrhythmias with an implanted automatic defibrillator in human beings," *New England Journal of Medicine*, vol. 303, p. 322, 1980.

[69] K. Takahata, A. DeHennis, K.D. Wise, and Y.B. Gianchandani, "Stentenna: a micromachined antenna stent for wireless monitoring of implantable microsensors," *Proceedings of the 25th Annual International Conference of the IEEE Engineering in Medicine and Biology Society, 2003.*, vol.4, pp. 3360-3363, 17-21 Sept. 2003.

[70] R.N. Simons, D.G. Hall, and F.A. Miranda, "Spiral chip implantable radiator and printed loop external receptor for RF telemetry in bio-sensor systems," *2004 IEEE Radio and Wireless Conference*, pp. 203- 206, 19-22 Sept. 2004.

[71] R.N. Simons and F.A. Miranda, "Radiation characteristics of miniature silicon square spiral chip antenna for implantable bio-MEMS sensors," *2005 IEEE Antennas and Propagation Society International Symposium*, vol.1B, pp. 836-839, 2005.

[72] R.N. Simons, F.A. Miranda, J.D. Wilson, and R.E. Simons, "Wearable wireless telemetry system for implantable bio-MEMS sensors," *28th Annual International Conference of the IEEE Engineering in Medicine and Biology Society, 2006*, pp. 6245-6248, Aug. 30, 2006-Sept. 3, 2006.

[73] K. Kuwana, T. Dohi, Y. Hashimoto, K. Matsumoto, and I. Shimoyama, "Implantable telemetry capsule for monitoring arterial oxygen saturation and heartbeat," *30th Annual International Conference of the IEEE Engineering in Medicine and Biology Society, 2008.*, pp. 3204-3207, 20-25 Aug. 2008.

[74] D.S. Gamini and P.N. Shastry, "Design and measurements of implantable chip radiator and external receptor for wireless blood pressure monitoring system," *IEEE MTT-S International Microwave Symposium Digest, 2009.*, pp. 1681-1684, 7-12 June 2009.

[75] J. Kim and Y. Rahmat-Samii, "An implanted antenna in the spherical human head: SAR and communication link performance," *IEEE Topical Conference on Wireless Communication Technology, 2003.*, pp. 202-203, 15-17 Oct. 2003.

[76] E. Topsakal, T. Karacolak, J.E. Gaxiola-Sosa, K. Entesari, R. Cooper, J. Butler, and S. Fisher, "Low-power long-term implantable wireless telemetry for monitoring of physiological signals," *2011 XXXth URSI General Assembly and Scientific Symposium*, pp. 1-2, 13-20 Aug. 2011.

[77] Zarlink Semiconductor, "Medical implantable RF transceiver," ZL70101 datasheet, Oct. 2006.

[78] T. Karacolak, R. Cooper, J. Butler, S. Fisher, and E. Topsakal, "In vivo verification of implantable antennas using rats as model animals," *IEEE Antennas and Wireless Propagation Letters*, vol. 9, pp. 334-337, 2010.

[79] A.Z. Hood and E. Topsakal, "Particle swarm optimization for dual-band implantable antennas," *2007 IEEE Antennas and Propagation Society International Symposium*, pp. 3209-3212, 9-15 June 2007.

[80] C.J. Sanchez-Fernandez, O. Quevedo-Teruel, J. Requena-Carrion, L. Inclan-Sanchez, E. Rajo-Iglesias, and M.N.M. Kehn, "Dual-band implantable antenna based on short-circuited SRR," *Proceedings of the Fourth European Conference on Antennas and Propagation (EuCAP), 2010*, pp. 1-4, 12-16 April 2010.

[81] C.J. Sanchez-Fernandez, O. Quevedo-Teruel, J. Requena-Carrion, L. Inclan-Sanchez, and E. Rajo-Iglesias, "Dual-band microstrip patch antenna based on short-circuited ring and spiral resonators for implantable medical devices," *IET Microwaves, Antennas & Propagation*, vol.4, no.8, pp. 1048-1055, Aug. 2010.

[82] F. Merli, L. Bolomey, E. Meurville, and A.K. Skrivervik, "Dual band antenna for subcutaneous telemetry applications," *2010 IEEE Antennas and Propagation Society International Symposium (APSURSI)*, pp.1-4, 11-17 July 2010.

[83] F. Merli, L. Bolomey, J.F. Zurcher, E. Meurville, and A.K. Skrivervik, "Versatility and tunability of an implantable antenna for telemedicine," *Proceedings of the 5th European Conference on Antennas and Propagation (EUCAP)*, pp. 2487-2491, 11-15 April 2011.

[84] F. Merli, L. Bolomey, J. Zurcher, G. Corradini, E. Meurville, and A.K. Skrivervik, "Design, realization and measurements of a miniature antenna for implantable wireless communication systems," *IEEE Transactions on Antennas and Propagation*, vol.59, no.10, pp. 3544-3555, Oct. 2011.

[85] C.L. Chang, F.J. Huang, C.M. Lee, W.C. Ma, C.H. Luo, and H.Y. Huang, "Novel triple-band biotelemetry system with miniaturized antenna for implantable sensing applications," *2010 IEEE Sensors*, pp. 104-107, 1-4 Nov. 2010.

[86] C.K. Chou, "Application of electromagnetic energy in cancer treatment," *IEEE Transactions on Instrumentation and Measurement*, vol. 37, no. 4, pp. 547-551, Dec. 1988.

[87] P. Wust, H. Stahl, K. Dieckmann, S. Scheller, J. Löffel, H. Riess, J. Bier, V. Jahnke, and R. Felix, "Local hyperthermia of N2/N3 cervical lymph node metastases: Correlation of technical/thermal parameters and response," *International Journal of Radiation Oncology*Biology*Physics*, vol. 34, no. 3, pp. 635-646, Feb. 1996.

[88] D.E. Thrall, D.M. Prescott, T.V. Samulski, G.L. Rosner, D.L. Denman, R.L. Legorreta, R.K. Dodge, R.L. Page, J.M. Cline, J. Lee, B.C. Case, S.M. Evans, J.R. Oleson, and M.W. Dewhirst, "Radiation plus local hyperthermia versus radiation plus the combination of local and whole-body hyperthermia in canine sarcomas," *International Journal of Radiation Oncology*Biology*Physics*, vol. 34, no. 5, pp. 1087-1096, Mar. 1996.

[89] A. Dietsch, J.-C. Camart, J.-P. Sozanski, B. Prevost, B. Mauroy, and M. Chivé, "Microwave thermochemotherapy in the treatment of the bladder carcinoma—electromagnetic and dielectric studies—clinical protocol," *IEEE Transactions on Biomedical Engineering*, vol. 47, no. 5, pp. 633-641, May 2000.

[90] M.D. Sapozink, F.A. Gibbs, Jr., M.J. Egger, and J.R. Stewart, "Abdominal Regional Hyperthermia With an Annular Phased Array," *Journal of Clinical Oncology*, vol. 4, no. 5, pp. 775-783, May 1986.

[91] C. DeSantis, R. Siegel, P. Bandi, and A. Jemal, "Breast cancer statistics, 2011," *CA: A Cancer Journal for Clinicians*, vol. 61, no. 6, pp. 408-418, Nov/Dec 2011.

[92] American Cancer Society. Cancer Facts & Figures 2012 [Online]. Available: http://www.cancer.org/Research/CancerFactsFigures/CancerFactsFigures/cancer-facts-figures-2012

[93] K. Engin, "Biological rationale and clinical experience with hyperthermia," *Controlled Clinical Trials*, vol. 17, no. 4, pp. 316-342, Aug. 1996.

[94] J.H. Holland, *Adaptation in Natural and Artificial Systems*. Ann Arbor, MI: The University of Michigan Press, 1975.

[95] R.L. Haupt, "An Introduction to Genetic Algorithms for Electromagnetics," *IEEE Antennas and Propagation Magazine*, vol. 37, no. 2, Apr. 1995.

[96] D.S. Weile and E. Michielssen, "Genetic Algorithm Optimization Applied to Electromagnetics: A Review," *IEEE Transactions on Antennas and Propagation*, vol. 45, no. 3, pp. 343-353, Mar. 1997.

[97] J.M. Johnson and Y. Rahmat-Samii, "Genetic Algorithms in Engineering Electromagnetics," *IEEE Antennas and Propagation Magazine*, vol. 39, no. 4, Aug. 1997.

[98] J. Kennedy and R.C. Eberhart, "Particle swarm optimization," in *Proceedings of the IEEE International Conference on Neural Networks*, vol. IV, Perth, Australia, 1995, pp. 1942-1948.

[99] P. Miller, "Swarm Theory," *National Geographic*, vol. 212, pp. 129-147, July 2007.

[100] T.D. Seeley, "Research Interests," 2005. [Online]. Available: http://www.nbb.cornell.edu/Faculty/seeley/research2.html [Accessed Sept. 27, 2007].

[101] T.D. Seeley and S.C. Buhrman, "Nest-site Selection in Honey Bees: How Well do Swarms Implement the "Best-of-*N*" Decision Rule?" *Behavioral Ecology and Sociobiology*, vol. 49, no. 5, pp. 416-427, Apr. 2001.

[102] J. Kennedy, "Methods of Agreement: Inference Among the EleMentals," in *Proceedings of the 1998 IEEE ISIC/CIRA/ISAS Joint Conference*, Gaithersburg, Maryland, pp. 883-887, 14-17 Sep. 1998.

[103] J. Kennedy and R.C. Eberhart, *Swarm Intelligence*. San Francisco: Morgan Kaufmann, 2001.

[104] D.H. Wolpert and W.G. Macready, "No Free Lunch Theorems for Optimization," *IEEE Transactions on Evolutionary Computation*, vol. 1, no. 1, pp. 67-82, Apr. 1997.

[105] J. Kennedy and W.M. Spears, "Matching Algorithms to Problems: An Experimental Test of the Particle Swarm and Some Genetic Algorithms on the Multimodal Problem Generator," in *Proceedings of the 1998 IEEE International Conference on Evolutionary Computing*, Anchorage, Alaska, pp. 78-83, 4-9 May 1998.

[106] R. Hassan, B. Cohanim, O. de Weck, and G. Venter, "A Comparison of Particle Swarm Optimization and the Genetic Algorithm," in *Proceedings of the 1st AIAA Multidisciplinary Design Optimization Specialist Conference*, Austin, Texas, 18-21 Apr. 2005.

[107] A. Carlisle and G. Dozier, "An Off-The-Shelf PSO," in *Proceedings of the Workshop on Particle Swarm Optimization*, pp. 1–6, Indianapolis, IN, 2001.

[108] M. Clerc, *Particle Swarm Optimization*. Wiley, 2010.

[109] R.C. Eberhart and Y. Shi, "Comparing Inertia Weights and Constriction Factors in Particle Swarm Optimization," in *Proceedings of the 2000 Congress on Evolutionary Computation*, vol. 1, pp. 84–88, La Jolla, CA, 16–19 July 2000.

[110] Y. Shi and R.C. Eberhart, "Parameter Selection in Particle Swarm Optimization," *Evolutionary Programming VII: 7th International Conference*, pp. 591-600, San Diego, CA, 25–27 March 1998.

[111] Y. Shi and R.C. Eberhart, "A Modified Particle Swarm Optimizer," in *Evolutionary Computation Proceedings, 1998*, pp. 69–73, Anchorage, AK, 4–9 May 1998.

[112] W. Weng, F. Yang, and A. Elsherbeni, "Integration of Taguchi's Method and Particle Swarm Optimization for Electromagnetic Global Optimization," The Second European Conference on Antennas and Propagation, Edinburgh, UK, Nov. 2007.

[113] S.M. Mikki and A.A. Kishk, "Hybrid Periodic Boundary Condition for Particle Swarm Optimization," *IEEE Transactions on Antennas and Propagation*, vol. 55, no. 11, pp. 3251–3256, Nov. 2007.

[114] United States Code of Federal Regulations, Title 47, Part 15.

[115] D.H. McCunn, "Bra Underwire Charts." [Online]. Available: http://deofsf.com/Resources/Bra-Underwire-Charts.pdf [Accessed May 8, 2013].

[116] J.T. Hansen, "Thorax," in *Netter's Clinical Anatomy*, *2*nd ed. Philadelphia, PA: Saunders, 2010, p. 79.

[117] E.S. deParedes, *Atlas of Mammography*, *3*rd ed. LWW, 2007.

[118] A. Sutradhar and M.J. Miller, "In Vivo Measurement of Breast Skin Elasticity and Breast Skin Thickness," *Skin Research and Technology*, vol. 19, no. 1, pp. 191–199, Feb. 2013.

[119] M. Lazebnik *et al.*, "A Large-Scale Study of the Ultrawideband Microwave Dielectric Properties of Normal Breast Tissue Obtained from Reduction Surgeries," *Physics in Medicine and Biology*, vol. 52, pp. 2637–2656, 2007.

[120] M. Lazebnik *et al.*, "A Large-Scale Study of the Ultrawideband Microwave Dielectric Properties of Normal, Benign and Malignant Breast Tissues Obtained from Cancer Surgeries," *Physics in Medicine and Biology*, vol. 52, pp. 6093–6115, 2007.

[121] M. Lazebnik *et al.*, "Highly Accurate Debye Models for Normal and Malignant Breast Tissue Dielectric Properties at Microwave Frequencies," *IEEE Microwave and Wireless Components Letters*, vol. 7, no. 12, pp. 822–824, Dec. 2007.

[122] T. Juang *et al.*, "Construction of a Conformal Water Bolus Vest Applicator for Hyperthermia Treatment of Superficial Skin Cancer," in *Proceedings of the 26th Annual International Conference of the IEEE Engineering in Medicine & Biology Society*, pp. 3467–3470, San Francisco, CA, 1–5 Sept. 2004.

[123] K. Arunachalam *et al.*, "Design of a Water Coupling Bolus with Improved Flow Distribution for Multielement Superficial Hyperthermia Applicators," *International Journal of Hyperthermia*, vol. 25, no. 7, pp. 554–565, 2009.

[124] P.R. Stauffer *et al.*, "Radiation Patterns of Dual Concentric Conductor Microstrip Antennas for Superficial Hyperthermia," *IEEE Transactions on Biomedical Engineering*, vol. 45, no. 5, May 1998.

[125] R. Garg *et al.*, *Microstrip Antenna Design Handbook*. Boston: Artech House, 2001.

[126] M. Asili, R. Green, S. Seran, and E. Topsakal, "A Small Implantable Antenna for MedRadio and ISM Bands," *IEEE Antennas and Wireless Propagation Letters*, vol. 11, pp. 1683–1685, 2012.

[127] D.R. Jackson and A.A. Oliner, "Leaky-Wave Antennas," in *Modern Antenna Handbook*, C.A. Balanis, Ed. Hoboken, NJ: Wiley, pp. 325–367, 2007.